

Seismic Retrofitting Project

Simplified Calculations for the Structural Analysis of Earthen Historic Sites

Research Report

Paulo B. Lourenço, João M. Pereira,
and Daniel Torrealva

In collaboration with Maria Pia Ciocci,
Federica Greco, Giorgos Karanikoloudis,
and Claudia Cancino



Seismic Retrofitting Project

Simplified Calculations for the Structural Analysis of Earthen Historic Sites

Paulo B. Lourenço, João M. Pereira,
and Daniel Torrealva

In collaboration with Maria Pia Ciocci, Federica Greco,
Giorgos Karanikoloudis, and Claudia Cancino

THE GETTY CONSERVATION INSTITUTE
LOS ANGELES
TECMINHO – UNIVERSITY OF MINHO
GUIMARÃES
PONTIFICIA UNIVERSIDAD CATÓLICA DEL PERÚ
LIMA

© 2021 J. Paul Getty Trust, TecMinho – University of Minho, and Pontificia Universidad Católica del Perú

Getty Conservation Institute
1200 Getty Center Drive, Suite 700
Los Angeles, CA 90049-1684
United States
Telephone (+1) 310 440-7325
Fax (+1) 310 440-7702
E-mail: gciweb@getty.edu
www.getty.edu/conservation

TecMinho – University of Minho
Campus de Azurém
Alameda da Universidade
P-4800-058 Guimarães
Portugal
Phone (+351) 253 510-590
Fax (+351) 253 510-591
E-mail: tecm@tecminho.uminho.pt
www.tecminho.uminho.pt

Pontificia Universidad Católica del Perú
Avenida Universitaria 1801
San Miguel, Lima 15088
Peru
Phone (+51) 626-2000
E-mail: vri@pucp.edu.pe
<https://www.pucp.edu.pe>

ISBN: 978-1-937433-70-3 (online resource)
ISBN: 978-1-937433-69-7 (print on demand)

The Getty Conservation Institute (GCI) works to advance conservation practice in the visual arts, broadly interpreted to include objects, collections, architecture, and sites. It serves the conservation community through scientific research, education and training, model field projects, and the broad dissemination of the results of both its own work and the work of others in the field. And in all its endeavors, it focuses on the creation and dissemination of knowledge that will benefit professionals and organizations responsible for the conservation of the world's cultural heritage.

Founded in 1990, TecMinho is a private non-profit association, having had as sponsors the University of Minho and the Association of Municipalities of Vale do Ave, Portugal. Its basic mission is to be an interface of the University of Minho, promoting its connection to society, especially in the areas of science and technology, and contributing to regional development by improving the competitiveness of organizations and increasing the skills of individuals.

Pontificia Universidad Católica del Perú (PUCP) is a diverse academic community inspired by ethical, democratic, and Catholic principles. It provides a well-rounded education, including civic, humanistic, and scientific components, which together enhance knowledge through research and innovation at the international level. It promotes the creation and dissemination of art and culture, acknowledging the multicultural nature of the country, while committing to human and sustainable development.

Cover: Team members of the Seismic Retrofitting Project studying the temporary stabilization for Ica Cathedral, Peru. Photograph Scott Warren © 2011, J. Paul Getty Trust.

Getty Conservation Institute



Contents

Project Participants	v
CHAPTER 1	
Introduction	1
The Seismic Retrofitting Project	2
Objectives	3
CHAPTER 2	
Material Properties	5
Overview of Masonry Structures	5
Masonry Quality Index	7
CHAPTER 3	
Blueprint Assessment	12
In-Plane Indexes	12
<i>Wall Area Ratio</i>	12
<i>Area to Weight Ratio</i>	13
<i>Base Shear Ratio</i>	14
<i>Proposed Approach for Simplified In-plane Assessment</i>	15
Application Examples	17
<i>European Churches</i>	17
<i>New Zealand Churches after the 2010–11 Canterbury Earthquakes</i>	19
CHAPTER 4	
Limit Macro-Block Assessment	22
Limit Equilibrium Analysis	22
Linear Kinematic Analysis	24
Nonlinear Kinematic Analysis	25
<i>Estimation of the Capacity Curve (SDOF)</i>	25
Safety Verification	27
<i>Linear Kinematic Analysis (Force Control)</i>	28
<i>Nonlinear Kinematic Analysis (Displacement Control)</i>	29

Application Example: Design of Buttresses for the Church of Kuñotambo, Peru	30
<i>Kinematic Mechanism 1: Unstrengthened State</i>	34
<i>Kinematic Mechanism 2: Strengthened State</i>	37
CHAPTER 5	
Simplified Finite Element Modeling Approaches for Seismic Assessment	44
Summary of Available Types of Finite Element Analysis	44
Simplified Finite Element Analysis	46
<i>Verification of Structural Safety Using the Areas of Stress Concentration</i>	47
<i>Verification of Structural Safety Using the Vibration Modes</i>	47
Examples of Simplified Finite Element Analysis	48
<i>Application Example: The Church of Kuñotambo, Peru</i>	48
<i>Application Example: Partial Substructure Analysis of Ica Cathedral, Peru</i>	49
CHAPTER 6	
Examples of Design Calculations	53
Seismic Assessment of Casa Arones, Cusco, Peru	53
Strengthening Proposal for Ica Cathedral, Peru	56
CHAPTER 7	
Conclusions and Recommendations	61
References	63

Project Participants

Seismic Retrofitting Project—Modeling Phase

PROJECT DIRECTORS

Claudia Cancino

Senior Project Specialist, Getty Conservation Institute, Los Angeles

Paulo B. Lourenço

Professor, University of Minho, Portugal

PARTICIPANTS

Alberto Barontini

Research Assistant, University of Minho, Portugal

Maria Pia Ciocci

Research Assistant, University of Minho, Portugal

Federica Greco

Research Assistant (2015–2016), University of Minho, Portugal

Graduate Intern (2016–17), Getty Conservation Institute, Los Angeles

Giorgos Karanikoloudis

Research Assistant, University of Minho, Portugal

Elena Macchioni

Associate Project Specialist, Getty Conservation Institute, Los Angeles

Susan Macdonald

Head, Buildings and Sites Department, Getty Conservation Institute, Los Angeles

João M. Pereira

Postdoctoral Research Associate, University of Minho, Portugal

Valerio Sabbatini

Graduate Intern (2019–20), Getty Conservation Institute, Los Angeles

Daniel Torrealva Professor

Pontificia Universidad Católica del Perú, Lima

Introduction

The structural analysis of historic masonry constructions is a complex task for a number of reasons: (a) geometric data are missing, as well as information about the inner core of the structural elements being analyzed; (b) the process of characterization of the mechanical properties of the materials used is difficult and expensive; (c) there is great variability in the mechanical properties due to workmanship and use of natural materials; (d) long construction periods have resulted in significant changes to the constitution of the structural elements; (e) the construction sequence and existing damage to the structure are unknown; and (f) regulations and codes are nonapplicable. Moreover, the behavior of the connections between the different masonry elements (walls, arches, and vaults) and between the masonry elements and timber elements (roofs and floors) is usually unknown.

When dealing with existing constructions, information about their structure is essential, as is the conceptual definition of different knowledge levels and consequent confidence factors for assessment. European code (EC8 2004) applies confidence factors (FC) to mean material property values, which are determined as a function of the knowledge levels (KL). The KL depend on the number of tests and inspections performed on the existing building. In the rational definition of KL of historic masonry buildings, however, it should be noted that in most real-world cases, (a) no construction drawings, structural designs, or test reports are available; (b) the structure was built in the absence of design regulations, conforming—in the best-case scenario—to a “rule of art” (Vitruvius 2005) to which no simulation of design can be applied; and (c) the direct experimental measurement of material parameters often is not feasible or, if technically and economically feasible for monumental buildings, is not entirely reliable (Sheppard 1985; Chiostrini, Galano, and Vignoli 2003; Magenes and Penna 2009).

The Italian standard (NTC 2018) defines specific criteria for masonry regarding the different KL. A complete geometric survey is required, and information regarding structural details should specifically address the following:

- quality of connections between vertical walls;
- quality of connections between floor/roof and walls;
- presence of ring beams or other tying devices;
- presence of structurally efficient architraves/lintels above openings;
- presence of elements which can equilibrate horizontal thrusts;
- presence of structural or non-structural elements of high vulnerability; and
- typology of masonry (stone or brick, regular or irregular units, single-leaf or multi-leaf, with or without transversal ties)

Three categories are defined regarding the quantification of material parameters: (1) limited in situ investigations, (2) extensive in situ investigations, and (3) exhaustive in situ investigations (NTC 2018). In the first category, the mechanical properties of the material are estimated after visual inspections. Here, plaster is removed in selected areas in

order to assess the masonry bond (or texture) and the connection between orthogonal walls. A visual inspection is conducted through the thickness of the wall to determine the internal level of connection between the leaves and the ability of the wall to behave monolithically through the thickness. From this, a qualitative evaluation is made of the mortar consistency. This assessment of the typology and quality of the material, supported by historical analysis, is then used to help quantify the mechanical parameters reported in a reference table (see chap. 4), which was compiled based on the experimental data available on common typologies.

In the second category, extensive in situ investigations, the visual inspections described in the previous level are carried out extensively and systematically with superficial and internal samples for every type of masonry present. Tests using double flat jacks and tests for characterization of the mortar (type of binding agent, type of aggregate, binding agent/aggregate ratio, etc.) and possibly of the stone and/or brick (physical and mechanical characteristics) are required to verify the correspondence of the masonry to the typology defined in the reference table. A test for every type of masonry present in the building is required. Nondestructive testing procedures (sonic tests, sclerometer tests, penetrometer test for mortar, thermography, ground penetrating radar, etc.) may be utilized as complements to the tests (NTC 2018).

Finally, exhaustive in situ investigations serve to obtain direct quantitative information on the material strength. Apart from the visual inspections of the internal samples and the tests administered in the first and second levels, a further series of experimental tests must be carried out, in both quantity and quality, in order to estimate the mechanical characteristics of the masonry. The tests generally include diagonal compression tests on panels or combined tests of vertical compression and shear. Nondestructive testing methods can be used in combination but not as a substitute (NTC 2018). The results must be utilized with reference to the values reported in the reference tables available in the literature.

The Seismic Retrofitting Project

During the 1990s, the Getty Conservation Institute (GCI) carried out a major research and laboratory testing program, the Getty Seismic Adobe Project (GSAP), which investigated the performance of historic adobe structures during earthquakes and developed cost-effective retrofit methods aimed at substantially preserving the authenticity of these buildings. Results of this research have been disseminated in a series of publications in both English and Spanish (Tolles, Kimbro, and Ginell 2002).

In 2006, the GCI's Earthen Architecture Initiative convened two programs: the Getty Seismic Adobe Project Colloquium and the symposium "New Concepts in Seismic Strengthening of Historic Adobe Structures." The first program, held April 11–13 at the Getty Center, focused on implementation of the GSAP. Papers presented at the colloquium, as well as the main conclusions of its roundtable discussions, were published as part of the colloquium proceedings (Hardy, Cancino, and Ostergren 2009). The participants concluded that the GSAP methodology was excellent and effective. However, the methodology's reliance on high-tech materials and professional expertise was a deterrent to its wider implementation.

The following year, in August 2007, an earthquake with a moment magnitude (M_w) of 8.0 and VII–VIII maximum local Modified Mercalli Intensity (MMI) occurred off the coast of Pisco, Peru. There were 519 deaths and 1,366 injuries recorded, with a total of 650,000

people affected and 80,000 dwellings damaged. From October 28 to November 2, 2007, a rapid assessment to better understand the failure of fifteen historic earthen sites in the area was performed by a multidisciplinary team of national and international experts convened by the GCI in response to a request from the Instituto Nacional de Cultura del Perú (Peruvian National Institute of Culture), which is now the Ministerio de Cultura del Perú (Ministry of Culture of Peru). The team's findings were later published (Cancino 2011).

Following these results and the conclusions of the GSAP colloquium, in 2009 the GCI initiated the Seismic Retrofitting Project (SRP), with the objective of adapting GSAP techniques to better match the equipment, materials, and technical skills available in many countries with earthen sites. Using four Peruvian historic earthen buildings representing typologies across Latin America, the GCI—in collaboration with the Ministerio de Cultura del Perú, the Escuela de Ciencias e Ingeniería of the Pontificia Universidad Católica del Perú (PUCP; School of Science and Engineering, Pontifical Catholic University of Peru), and the University of Minho—is designing, testing, and implementing seismic retrofitting techniques and maintenance programs with locally available materials that will improve the structural performance and safety of earthen buildings while minimizing loss of historic fabric. The Department of Architecture and Civil Engineering at the University of Bath and the Department of Civil, Environmental and Geomatic Engineering at University College London also partnered with the SRP from 2010 to 2012 and from 2013 to 2014, respectively.

From 2015 until 2017, the University of Minho used modeling as a method to understand the structural behavior of the SRP building prototypes and validate the retrofitting techniques later designed for them. Not only is the application of this method quite innovative, but it also has advanced the field of structural analysis of earthen structures and is worth publishing.

Objectives

The present document is intended to help engineering professionals who work in the assessment and analysis of historic earthen structures using simplified calculations. Other reports in the Getty's SRP series related to structural analysis are *Seismic Retrofitting Project: Recommendations for Advanced Modeling of Historic Earthen Sites* (Lourenço and Pereira 2018) and *Seismic Retrofitting Project: Modeling of Prototype Buildings* (Lourenço et al. 2019).

Following this introductory chapter are six additional sections. Chapter 2 gathers information on the mechanical properties of masonry. Due to the nature of the materials, the scatter in terms of mechanical properties is considerable. This chapter summarizes the available reported and standardized mechanical properties for adobe masonry. A qualitative method in the form of a quality index that can be related to these properties is also discussed.

Chapter 3 presents a simplified approach to seismic assessment of masonry structures for different simplified geometric indexes. These simple geometric data consider local seismic hazard (such as peak ground acceleration, or PGA) and can be used as an initial (very fast) screening technique to help prioritize further studies with respect to seismic vulnerability. This technique can be implemented without visiting the buildings, therefore resulting in low accuracy. It is expected that these geometric indexes can detect cases of

serious vulnerability and define priority of study. The employment of these techniques is highlighted using application examples.

In chapter 4, assessment of local collapse mechanisms of masonry structures using limit analysis with macro-blocks is discussed. A thorough explanation is provided of all the steps required to perform the analysis, design, and safety verifications, followed by a detailed example.

Chapter 5 explains how to use simplified finite element modeling (FEM) to assess masonry structures. A summary of available analysis types is given, as well as methods for assessing structural safety. Examples are provided to aid understanding.

Chapter 6 presents case studies of design calculations and prescribed interventions that consider the methods of analysis and intervention techniques covered in the preceding chapters. These are not intended to be applied to similar buildings without going through the analysis process previously described.

Finally, chapter 7 posits conclusions and recommendations regarding simplified calculations for the structural analysis of historic earthen sites and reviews the main issues in the overall assessment of such topics.

Material Properties

Being composed of units and mortar, the nature of masonry materials allows several different combinations of the constituent materials, unit arrangement, shape and dimension, perforation, slenderness ratio, strength, and so forth (Zilch and Schatz 2001). The result is a scatter of reference values as seen in the literature. This chapter gathers these available sources of information and presents a qualitative analysis in the form of a quality index that can be related to the mechanical properties of masonry.

Overview of Masonry Structures

As stated, masonry is a heterogeneous material composed of units and mortar. The mechanical properties of masonry are greatly dependent on the physical and mechanical properties of these components. Eurocode 6 (EC6 2005) establishes the following relationship to determine the characteristic compressive strength, f_c , of masonry as a composite (eq. 2.1):

$$f_c = K f_{bc}^{0.7} f_{mc}^{0.3} \quad (2.1)$$

Here, K is a constant that depends on the combination of unit and mortar (e.g., for dimensioned stone units, K is 0.45), f_{bc} is the compressive strength of a masonry unit, and f_{mc} is the compressive strength of masonry mortar. This value should be multiplied by 1.2 to obtain the average value in the absence of more information.

Some normative documents (e.g., NZSEE 2017) suggest some reference values for the mechanical properties of both mortar and brick, defining different classes according to visual inspections and hand tests (table 2.1). The Italian code, first with ordinance OPCM 3431 (2005) and later with technical building code NTC (2018), prescribes a range of values for the mechanical properties of different types of masonry (tables 2.2 and 2.3).

TABLE 2.1.
Strength parameters for mortar and brick according to NZSEE (2017).

	Hardness	Probable compressive strength, f_c (MPa)	Probable tensile strength, f_t (MPa)	Probable cohesion, c (MPa)
Brick	Soft (scratches with aluminum pick)	14.0	1.7	-
	Medium (scratches with 10-cent copper coin)	26.0	3.1	-
	Hard (does not scratch with above tools)	35.0	4.2	-
Mortar	Very soft (raked out by finger pressure)	0.0–1.0	-	0.1
	Soft (scratches easily with fingernails)	1.0–2.0	-	0.3
	Medium (scratches with fingernails)	2.0–5.0	-	0.5
	Hard (scratches using aluminum pick)	To be established from testing	-	0.7
	Very hard (does not scratch with above tools)	To be established from testing	-	To be established from testing

TABLE 2.2.

Reference values of the mechanical parameters (minimum to maximum) for different types of masonry, as prescribed by OPCM 3431 (2005).

Masonry typology	f_c (MPa)	τ (MPa)	E (MPa)	G (MPa)	ρ kg/m ³
	min-max	min-max	min-max	min-max	
Irregular stone masonry (pebbles, erratic, and irregular stones)	0.60–0.90	0.020–0.032	690–1050	115–175	1900
Uncut stone masonry with facing walls of limited thickness and infill core	1.10–1.55	0.035–0.051	1020–1440	170–240	2000
Cut stone masonry with good bonding	1.50–2.00	0.056–0.074	1500–1980	250–330	2100
Soft stone masonry (tuff, limestone, etc.)	0.80–1.20	0.028–0.042	900–1260	150–210	1600
Dressed rectangular stone masonry	3.00–4.00	0.078–0.098	2340–2820	390–470	2200
Full brick masonry with lime mortar	1.80–2.80	0.060–0.092	1800–2400	300–400	1800
Masonry in half-filled brick blocks with cement mortar	3.80–5.00	0.240–0.320	2800–3600	560–720	1500
Hollow brick masonry (perforations < 45%)	4.60–6.00	0.300–0.400	3400–4400	680–880	1200
Hollow brick masonry with dry perpendicular joints (perforations < 45%)	3.00–4.00	0.100–0.130	2580–3300	430–550	1100
Concrete block masonry (perforations between 45% and 65%)	1.50–2.00	0.095–0.125	2200–2800	440–560	1200
Masonry in half-filled concrete blocks	3.00–4.40	0.180–0.240	2700–3500	540–700	1400

f_c – average compressive strength of masonry
 τ – average shear strength of masonry
 E – average value of Young's modulus
 G – average value of shear modulus
 ρ – average value of specific mass

TABLE 2.3.

Reference values of the mechanical parameters (minimum to maximum) for different types of masonry, as prescribed by NTC (2018).

Masonry typology	f_c (MPa)	τ (MPa)	E (MPa)	G (MPa)	ρ kg/m ³
	min-max	min-max	min-max	min-max	
Rubble stone masonry (pebbles, erratic, and irregular stone)	1.0–1.8	0.020–0.032	690–1050	230–350	1900
Irregular stone masonry with external leaves of limited thickness and infill	2.0–3.0	0.035–0.051	1020–1440	340–480	2000
Regular stone masonry with good bond	2.6–3.8	0.056–0.074	1500–1980	500–660	2100
Soft stone masonry (tuff, calcarenite, etc.)	1.4–2.4	0.028–0.042	900–1260	300–420	1600
Dressed rectangular stone masonry	6.0–8.0	0.090–0.120	2400–3200	780–940	2200
Solid brick masonry with lime mortar	2.4–4.0	0.060–0.092	1200–1800	400–600	1800
Perforated brick (< 40%) masonry with cement mortar	5.0–8.0	0.240–0.320	3500–5600	875–1400	1500
Perforated brick (< 45%) masonry	4.0–6.0	0.300–0.400	3600–5400	1080–1620	1200
Perforated brick (< 45%) masonry with unfilled perpendicular joints	3.0–4.0	0.100–0.130	2700–3600	810–1080	1100
Concrete and lightweight concrete block masonry (voids: 45%–65%)	1.5–2.0	0.095–0.125	1200–1600	300–400	1200
Concrete block (< 45%) masonry	3.0–4.4	0.180–0.240	2400–3520	600–880	1400

f_c – average compressive strength of masonry
 τ – average shear strength of masonry
 E – average value of Young's modulus
 G – average value of shear modulus
 ρ – average value of specific mass

TABLE 2.4.
Default lower-bound masonry properties (ASCE 41-06 2006).

Property	Masonry condition		
	Good	Fair	Poor
Compressive strength (MPa)	6.21	4.14	2.07
Young's modulus	$550 f_c$	$550 f_c$	$550 f_c$
Flexural tensile strength (MPa)	0.14	0.07	0.00
Shear strength (MPa)			
Masonry with a running bond lay-up	0.19	0.14	0.09
Fully grouted masonry with a lay-up other than running bond	0.19	0.14	0.09
Partially grouted or ungrouted masonry with a lay-up other than running bond	0.08	0.06	0.03

These values can be adjusted, taking into consideration factors such as quality of the mortar, thickness of the joints, presence of regular masonry courses, transverse elements (through stones, headers, or other connections), or an excessively thick inner core. The American standard (ASCE 41-06 2006) defines default lower-bound properties for masonry according to its condition (table 2.4).

Young's modulus E is usually associated with compressive strength f_c by $E = af_c$, with a wide range of variation in multiplier a , which, according to Tomazevic (1999), is between 200 and 1000. In ASCE 41-06 (2006), the recommended relationship for existing masonry is $E = 550f_c$, whereas in Eurocode 6 (2005) the recommended relationship for modern masonry is $E = 1000f_c$.

A level of uncertainty accompanies the relationship between tensile and compressive strength of masonry (Angelillo, Lourenço, and Milani 2014). The flexural strength of masonry, as stated in Eurocode 6 (EC6 2005), ranges from $f_{xk1} = 0.05\text{--}0.20$ MPa for a plane failure parallel to bed joints to $f_{xk2} = 0.10\text{--}0.40$ MPa for a plane failure perpendicular to bed joints, whereas in ASCE 41-06 (2006) the expected tensile strength varies from 0.00 to 0.14 MPa.

Masonry Quality Index

Knowledge of the mechanical properties of masonry is of primary interest in the assessment of existing buildings, particularly when implementation of in situ or laboratory tests is not possible. Technicians may only perform a visual analysis of the masonry and refer to literature data to estimate the mechanical properties of the masonry.

The Masonry Quality Index (MQI) is a method proposed by Antonio Borri and Alessandro De Maria that already has been integrated into the normative of the Italian region of Umbria (Regione dell'Umbria 2003) and refined over the years (Borri and De Maria 2009; Borri et al. 2015). It consists of evaluating the presence, partial presence, or absence of certain characteristics in the masonry that, if executed during the construction of a wall, provide a good behavior and ensure compactness and a monolithic response. The examination of seven parameters is required, as indicated in equation 2.2 and the list below, and the final MQI can be calculated according to this equation (Borri et al. 2015):

$$MQI = SM(SD + SS + WC + HJ + VJ + MM) \quad (2.2)$$

where

- SM criteria for stone/brick mechanical properties and conservation state (table 2.5);
- SD criteria for stone/brick dimensions (table 2.6);
- SS criteria for stone/brick shape (table 2.7);
- WC criteria for wall leaf connections (table 2.8);
- HJ criteria for horizontality of bed joints (table 2.9);
- VJ criteria for stagger properties of vertical joints (table 2.10); and
- MM criteria for mortar properties (table 2.11).

Examination of these parameters requires in-depth knowledge of historical construction methods due to the demands placed upon the engineer to classify each parameter under three possible conditions: Fulfilled (F), Partially Fulfilled (PF), and Not Fulfilled (NF) (Borri and De Maria 2009).

TABLE 2.5.
Criteria for stone/brick mechanical properties and conservation state (SM) (Borri et al. 2015).

Condition	Description
NF – Not Fulfilled	<ul style="list-style-type: none"> • Degraded/damaged elements (> 50% of actual number of elements) • Hollow bricks (solid < 30%) • Mud bricks • Unfired bricks
PF – Partially Fulfilled	<ul style="list-style-type: none"> • Presence of degraded/damaged elements ($\geq 10\%$, $\leq 50\%$) • Hollow bricks ($55\% \geq \text{solid} \geq 30\%$) • Sandstone or tuff elements
F – Fulfilled	<ul style="list-style-type: none"> • Undamaged elements of degraded/damaged elements (< 10%) • Solid fired bricks • Hollow bricks (solid > 55%) • Concrete blocks • Hard stone

TABLE 2.6.
Criteria for stone/brick dimensions (SD) (Borri et al. 2015).

Condition	Description
NF – Not Fulfilled	<ul style="list-style-type: none"> • Presence of more than 50% of elements with large dimension (< 20 cm) • Brick bond pattern made of only head joints
PF – Partially Fulfilled	<ul style="list-style-type: none"> • Presence of more than 50% of elements with large dimension (20–40 cm) • Co-presence of elements of different dimensions
F – Fulfilled	<ul style="list-style-type: none"> • Presence of more than 50% of elements with large dimension (> 40 cm)

TABLE 2.7.
Criteria for stone/brick shape (SS) (Borri et al. 2015).

Condition	Description
NF – Not Fulfilled	<ul style="list-style-type: none"> • Rubble, rounded, or pebble stonework (predominant) on both masonry leaves
PF – Partially Fulfilled	<ul style="list-style-type: none"> • Co-presence of rubble, rounded, or pebble stonework and barely cut or perfectly cut stones and bricks on both masonry leaves • One masonry leaf made of perfectly cut stones or bricks • Masonry made of irregular (rubble, rounded, pebble) stonework, but with presence of pinning stones
F – Fulfilled	<ul style="list-style-type: none"> • Barely cut stones or perfectly cut stones on both masonry leaves (predominant) • Brickwork

TABLE 2.8.
Criteria for wall leaf connections (WC) (Borri et al. 2015).

Condition	Description (qualitative analysis)
NF – Not Fulfilled	<ul style="list-style-type: none"> • Small stones compared to wall thickness • No headers
PF – Partially Fulfilled (Double-leaf walls)	<ul style="list-style-type: none"> • Wall thickness larger than stone larger dimension • Limited number of headers
F – Fulfilled	<ul style="list-style-type: none"> • Wall thickness similar to stone larger dimension • Systematic presence of headers

TABLE 2.9.
Criteria for horizontality of bed joints (HJ) (Borri et al. 2015).

Condition	Description
NF – Not Fulfilled	<ul style="list-style-type: none"> • Bed joints not continuous
PF – Partially Fulfilled (Double-leaf walls)	<ul style="list-style-type: none"> • Only one wall leaf with continuous bed joints
F – Fulfilled	<ul style="list-style-type: none"> • Bed joints continuous • Stone masonry wall with brick courses (distance between courses < 60 cm)

TABLE 2.10.
Criteria for stagger properties of vertical joints (VJ) (Borri et al. 2015).

Condition	Description (qualitative analysis)
NF – Not Fulfilled	<ul style="list-style-type: none"> • Aligned vertical joints • Aligned vertical joints for at least two large stones • Solid brick wall made of only headers
PF – Partially Fulfilled	<ul style="list-style-type: none"> • Partially staggered vertical joints (vertical joints between two bricks are not placed in the middle of the adjacent upper and lower bricks)
F – Fulfilled	<ul style="list-style-type: none"> • Properly staggered vertical joints (vertical joints between two bricks are placed in the middle of the adjacent upper and lower bricks)

TABLE 2.11.
Criteria for mortar properties (MM) (Borri et al. 2015).

Condition	Description
NF – Not Fulfilled	<ul style="list-style-type: none"> • Very weak mortar, dusty mortar with no cohesion • No mortar (rubble or pebble stonework) • Large bed joints made of weak mortar (thickness comparable to stone/brick thickness) • Porous stones/bricks with weak bonding to mortar
PF – Partially Fulfilled	<ul style="list-style-type: none"> • Medium-quality mortar, with bed joints not largely notched • Masonry made of irregular (rubble) stonework and weak mortar, but with presence of pinning stones
F – Fulfilled	<ul style="list-style-type: none"> • Good-quality and nondegraded mortar, regular bed joint thickness or large bed joint thickness made of mortar of very good quality • Masonry made of large perfectly cut stones with no mortar or very thin bed joint thickness

The first parameter, SM, considers the conservation state and the mechanical properties of brick or stone. For unfired or mud bricks with very low strength, the outcome is generally NF; for masonry made of tuff and sandstone (or soft stone in general), the assumed outcome is PF. From this point, six further parameters may contribute to a reduction factor, allowing the index to represent the actual condition of the masonry. All criteria are based on qualitative analysis. However, for two of the parameters, WC and VJ, a quantitative criterion related to measurements taken on a wall section or leaf surface has been proposed (Borri et al. 2015).

Because a single wall panel can be subjected to varying loading conditions (fig. 2.1) and not all parameters influence the response of the panel in a similar manner depending on the loading conditions, the MQI (eq. 2.2, above) can lead to three different values according to the loading direction (Borri et al. 2015). Evidence shows that these parameters affect the quality of masonry; therefore, different weights (of values between 0 and 3) should be assigned to these parameters. The values of the weights were deduced from previous work (Mastrodicasa 1978; Giuffrè 1999) and are based on evidence from case studies and experimental evaluations. Table 2.12 shows results for vertical loading.

FIGURE 2.1.
Diagram showing loading conditions on a single wall panel: vertical static load (V), out-of-plane static and dynamic loads (O), and in-plane dynamic load (I).

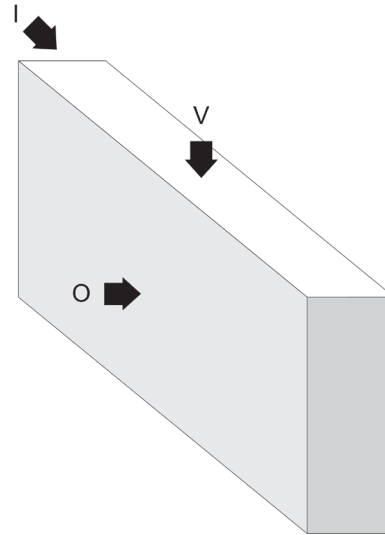


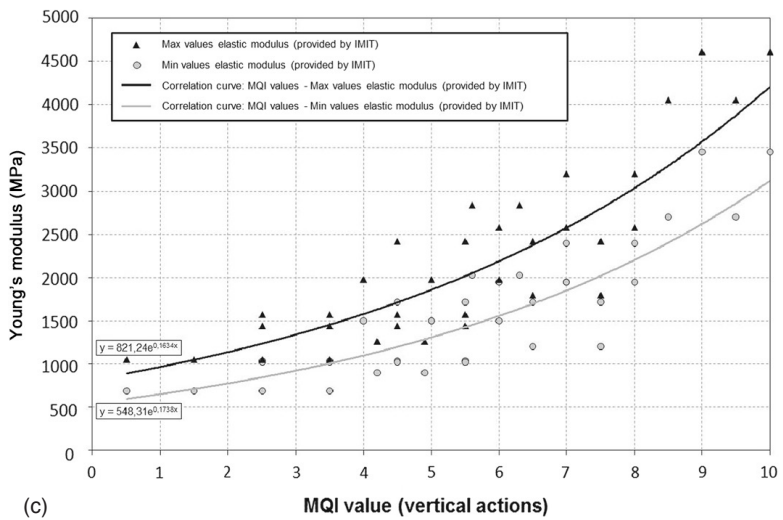
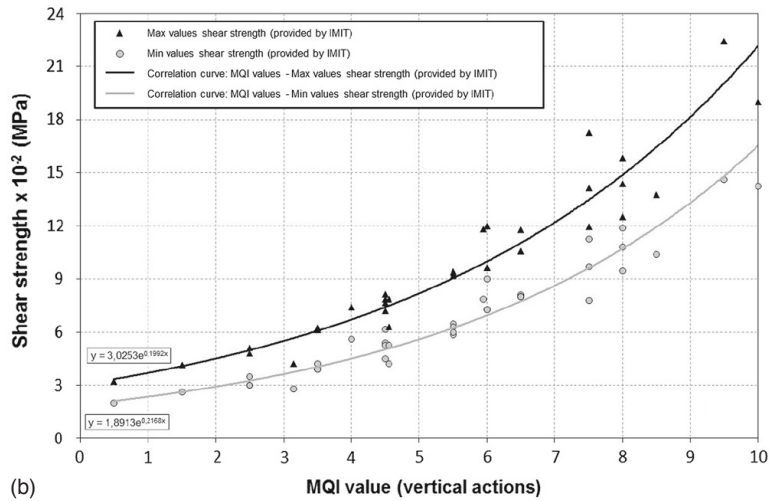
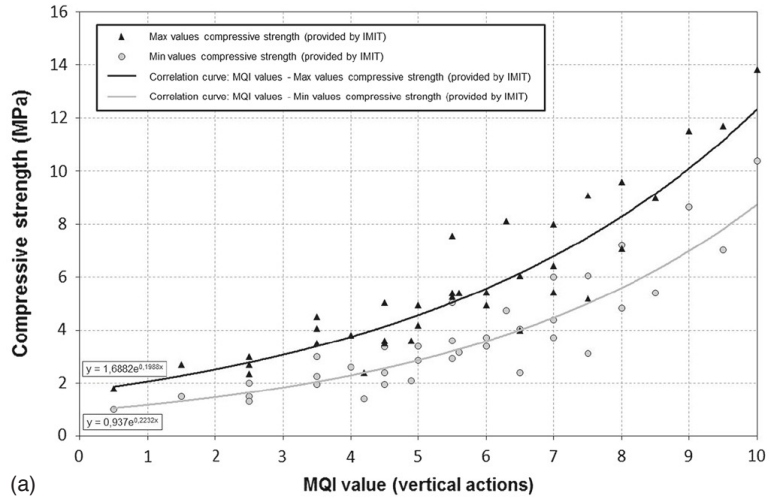
TABLE 2.12.
Parameters for combining vertical loading influence (Borri et al. 2015).

	Vertical loading (V)		
	NF	PF	F
HJ	0	1	2
WC	0	1	1
SS	0	1.5	3
VJ	0	0.5	1
SD	0	0.5	1
MM	0	0.5	2
SM	0.3	0.7	1

The MQI can be used to obtain an estimation of the mechanical parameters of existing buildings through correlation procedures. In an example, Borri et al. (2015) used the Italian code (NTC 2018) and experimental studies (Borri et al. 2011; Corradi et al. 2014; Borri, Castori, and Corradi 2014) to establish a relationship between the MQI and the mechanical properties of the existing masonry. Figure 2.2 shows the relationship obtained for compressive strength, shear strength, and Young's modulus of masonry as a function of the MQI for vertical loading conditions (V).

Despite the good correlation obtained, Borri et al. (2015) state that this index was only compared and correlated with some Italian masonry typologies. Some variations are expected when considering differences in the behavior of historic mortars, stone shapes, and way of assemblage. However, if enough data are available, it is possible to introduce adjustments in the weights for the qualitative analysis of the MQI.

FIGURE 2.2.
Graphs showing values of mechanical properties of existing masonry buildings as a function of MQI values: (a) compressive strength; (b) shear strength; and (c) Young's modulus. Source: Adapted from Borri et al. 2015.



Blueprint Assessment

Structural analysis of masonry structures encompasses several different approaches; a comprehensive review is given in Lourenço and Pereira (2018). The approach proposed by Lourenço and Roque (2006) involves a much simpler, faster, and lower-cost procedure and is based on a simplified geometric approach for immediate screening of a large number of buildings at risk. The objectives are to compare simple geometric data considering local seismic hazard (e.g., PGA) and to evaluate the possibility of adopting simple indexes (a numerical indicator deduced from observations and used to express a process or condition) related to geometric data as a first (very fast) screening technique to help prioritize further studies with respect to seismic vulnerability. This simplified process can be used without visiting the buildings, therefore resulting in low accuracy. It is expected that the geometric indexes can detect cases of serious vulnerability and can define priority of study.

The application of a simplified process of analysis usually requires that the structure is regular and symmetrical, that the floors act as rigid diaphragms, and that the dominant collapse mode is in-plane shear failure of the walls (Meli 1998). In general, the latter two conditions are not verified by historic masonry structures, meaning that the simplified process should be understood not as a quantitative safety assessment but merely as a simple indicator of possible seismic performance of the building. The in-plane indexes considered for a simplified process of analysis are (a) wall area ratio, (b) area to weight ratio, and (c) base shear ratio (Lourenço and Roque 2006). These are discussed below.

In-Plane Indexes

The three indexes manipulate the geometric values of the structural walls and produce a scalar. Because the indexes measure different quantities, their use with a large sample of buildings strengthens their applicability. As stated above, a more rigorous assessment of the actual safety conditions of a building is necessary in order to determine quantitative values and define remedial measures if necessary.

Wall Area Ratio

The index used to assess the safety of historic constructions is wall area ratio, the ratio between the area of the earthquake-resistant walls in each main direction (transversal x and longitudinal y) and the total in-plan area of the building. According to Eurocode 8 (EC8 2004), walls should only be considered earthquake resistant if their thickness is greater than 0.35 m and the ratio between height and thickness is lower than 9. The first index, $\gamma_{1,i}$, reads in equation 3.1 as:

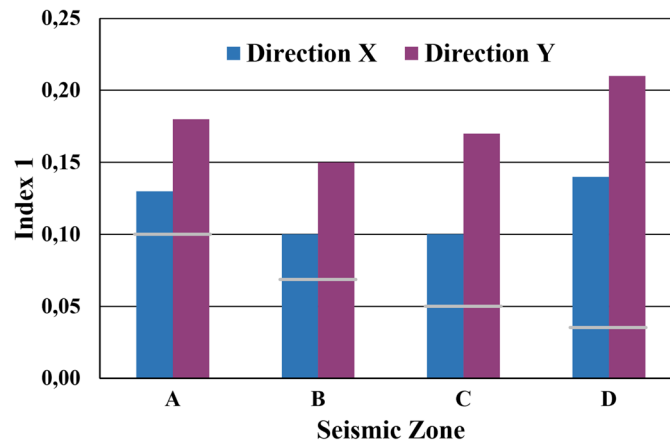
$$\gamma_{1,i} = A_{wi}/S \quad [-] \quad (3.1)$$

where A_{wi} is the in-plan area of earthquake-resistant walls in direction i and S is the total in-plan area of the building.

The nondimensional index $\gamma_{1,i}$ is the simplest one, being associated with base shear strength. Special attention is required when using this index, as it ignores the slenderness ratio of the walls and the weight of the construction. Eurocode 8 (EC8 2004) recommends values up to 5%–6% for regular structures with rigid floor diaphragms, which do not apply to earthen buildings. In cases of high seismicity, a minimum value of 10% seems to be recommended for historic masonry buildings (Meli 1998). For the sake of simplicity, high-seismicity cases can be assumed to be those where the design ground acceleration for rocklike soils is larger than 0.2 g (Lourenço and Roque 2006).

Lourenço and Roque (2006) applied these indexes to a total of fifty-eight Portuguese churches. They found that index $\gamma_{1,i}$ indicated an unexpected variation for the churches, because the average values exhibited minor differences according to seismicity (fig. 3.1), contrary to the expected dependency ($\gamma_{1,A} > \gamma_{1,B} > \gamma_{1,C} > \gamma_{1,D}$; note that seismicity zone A > seismicity zone D). On average, the adopted criterion was not debased. The authors concluded that the cases involving a deficient earthquake resistance along the transversal direction of the church nave (direction x) required further investigation.

FIGURE 3.1. Bar graph showing average results for index $\gamma_{1,i}$, according to orthogonal directions. Gray lines indicate the threshold; seismicity zone A > seismicity zone D. Source: Lourenço and Roque 2006.



Area to Weight Ratio

The index $\gamma_{2,i}$ provides the area to weight ratio between the in-plan area of the earthquake-resistant walls in each main direction (transversal x and longitudinal y) and the total weight of the building. Equation 3.2 reads:

$$\gamma_{2,i} = A_{wi}/G \quad [L^2F^{-1}] \quad (3.2)$$

where A_{wi} is the in-plan area of earthquake-resistant walls in direction i and G is the quasi-permanent vertical action.

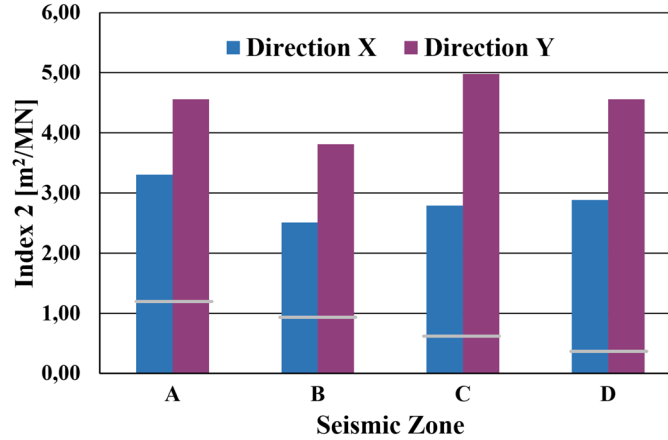
This index is associated with the horizontal cross-section of the building, per unit of weight. The height (i.e., mass) of the building is thus considered; however, a major disadvantage is that the index is dimensional, meaning that it must be analyzed for fixed units. In cases of high seismicity, a minimum value of 1.2 m²/MN seems to be recommended for historic masonry buildings (Meli 1998).

Lourenço and Roque (2006) also applied these indexes to the fifty-eight churches. They found that index $\gamma_{2,i}$, although being inversely proportional to the height of the buildings, presented a situation similar to that of index 1. Again, the calculated values were independent of the seismic zone, which is partly associated with the fact that the height of the

buildings does not decrease as seismicity increases (fig. 3.2). The fact that not a single building debased the criterion proposed by Meli (1998) seems to indicate that the threshold might need revision and conflicts with index 1. New thresholds are proposed below for all indexes.

FIGURE 3.2.

Bar graph showing average results for index $\gamma_{2,p}$ according to orthogonal directions. Gray lines indicate the threshold; seismicity zone A > seismicity zone D. Source: Lourenço and Roque 2006.



Base Shear Ratio

Base shear ratio provides a safety value with respect to the shear safety of the construction. The total base shear for seismic loading ($V_{Sd,base} = F_E$) can be estimated based on an analysis of horizontal static loading equivalent to the seismic action ($F_E = \beta \times G$), where β is an equivalent seismic static coefficient related to design ground acceleration. The shear strength of the structure ($V_{Rd,base} = F_{Rd}$) can be estimated from the contribution of all earthquake-resistant walls (eq. 3.3):

$$F_{Rd,i} = \sum A_{wi} \times f_{vk} \quad (3.3)$$

where, according to Eurocode 6 (EC6 2005) (eq. 3.4):

$$f_{vk} = f_{vk0} + 0.4\sigma_d \quad (3.4)$$

where f_{vk0} is the cohesion, which can be assumed equal to a low value or zero in the absence of more information; σ_d is the design value of the normal stress; and 0.4 represents the tangent of a constant friction angle ϕ , equal to 22° , a value demonstrated to be adequate for masonry walls.

In equation 3.5, index 3, γ_3 , reads:

$$\gamma_{3,i} = F_{Rd,i} / F_E \quad [-] \quad (3.5)$$

If a zero cohesion is assumed ($f_{vk0} = 0$), $\gamma_{3,i}$ is independent of the building height, with equation 3.6 reading as follows:

$$\gamma_{3,i} = V_{Rd,i} / V_{Sd} = A_{wi} / A_w \times \tan \phi / \beta \quad (3.6)$$

But for a non-zero cohesion, which is most relevant for low-height buildings, $\gamma_{3,i}$ reads (eq. 3.7):

$$\gamma_{3,i} = V_{Rd,i} / V_{Sd} = A_{wi} / A_w \times [\tan \phi + f_{vk0} / (\gamma \times h)] / \beta \quad (3.7)$$

where A_{wi} is the in-plan area of earthquake-resistant walls in direction i ; A_w is the total in-plan area of earthquake-resistant walls; h is the average height of the building; γ is the volumetric masonry weight; ϕ is the friction angle of masonry walls; and β is an equivalent static

seismic coefficient. It is assumed that the normal stress in the walls is due only to their self-weight ($\sigma_d = \gamma \times h$). This seems reasonable and on the safe side for historic masonry buildings, which usually have very thick walls.

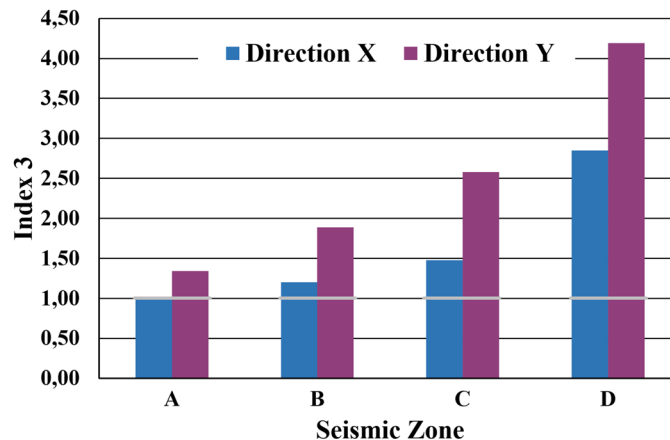
Equation 3.7 must be used carefully, since the contribution of the cohesion can be very large. For example, assuming three different heights of the building (h) and constant values for the tangent of the friction angle ($\tan \phi$) equal to 0.4, cohesion (f_{vko}) equal to 0.1 N/mm², and a volumetric weight (γ) of 20 kN/m³, the following can be calculated:

- for a height of 5.0 m, $\tan \phi + f_{vko}/(\gamma \times h)$ is equal to 1.4 with a contribution of the cohesion of 72%;
- for a height of 10.0 m, $\tan \phi + f_{vko}/(\gamma \times h)$ is equal to 0.9 with a contribution of the cohesion of 55%; and
- for a height of 20.0 m, $\tan \phi + f_{vko}/(\gamma \times h)$ is equal to 0.65 with a contribution of the cohesion of 38%.

This nondimensional index considers the seismicity of the zone, considered in β . The building will be safer with increasing ratio (earthquake-resistant walls/weight), meaning a larger relation (A_{wi}/A_w) and lower heights. For historic masonry buildings and typical action, a minimum value of $\gamma_{3,i}$ equal to one seems acceptable (Lourenço and Roque 2006).

Upon application of this approach to the fifty-eight churches, Lourenço and Roque (2006) found index $\gamma_{3,i}$ to exhibit increasing values with decreasing seismicity as a direct result of the constant values of indexes 1 and 2 (fig. 3.3). On average, index $\gamma_{3,i}$ was on the verge of violating the adopted criterion of zone A but was adequate for the other zones. Individually, 68% of churches in zone A and 9% of churches in zone B violated the adopted criterion. Like the previous indexes, almost all cases that might require further investigation showed a deficient earthquake resistance along the transversal direction of the church nave (direction x). Moreover, index 3 was clearly in conflict with the other two indexes, indicating that a new proposal for criteria violation is needed. It is important to mention that if a value of 0.10 N/mm² were adopted for the cohesion, all churches would fulfill the adopted criterion (Lourenço and Roque 2006).

FIGURE 3.3.
Bar graph showing average results for index $\gamma_{3,p}$ according to orthogonal directions. Gray lines indicate the threshold; seismicity zone A > seismicity zone D. Source: Lourenço and Roque 2006.



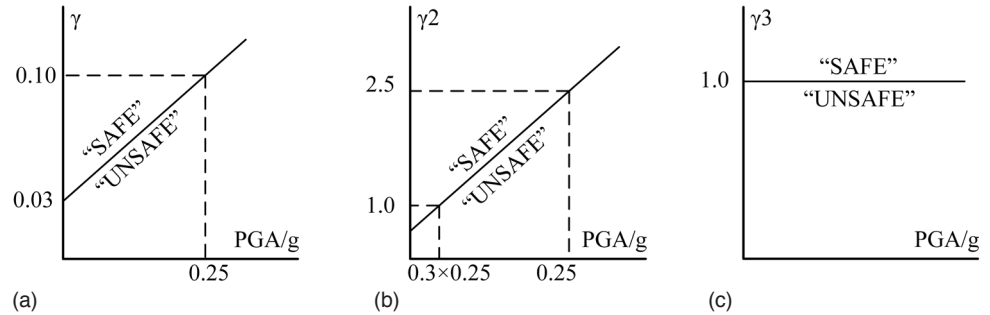
Proposed Approach for Simplified In-Plane Assessment

The three indexes depend linearly on the ratio (A_{wi}/A_w). This ratio provides direct information about the in-plan stiffness of the structure along each main direction. It is usually accepted that the sum of the relations (A_{wi}/A_w) for the two orthogonal directions can be

larger than the unit value, due to superposition of the areas in the two directions (Meli 1998). The indexes depend linearly also on the following quantities: (a) ratio between total area of earthquake-resistant walls and total in-plan area of the building (index 1); (b) height of the building (index 2); and (c) ratio between friction and equivalent seismic static coefficient (index 3).

Also of importance is that these indexes measure rather different quantities and cannot be directly compared. Index 2 is dimensional and should be used with care and, like index 1, is independent of design ground acceleration. Therefore, for buildings with identical safety, both indexes should increase as seismicity increases. Thus, seismicity is considered by assuming that the threshold value given previously is valid for a PGA value of 0.25 g and a linear correlation with the PGA is assumed, as illustrated in figure 3.4 (EC8 2004). In contrast, index 3 should be constant in different seismic zones, as it considers the effect of seismicity. This index format is close to the traditional safety approach adopted for structural design, being the threshold value equal to 1 (fig. 3.4).

FIGURE 3.4. Graphs showing assumed thresholds for the three in-plane indexes as a function of PGA: (a) index 1, (b) index 2, and (c) index 3. Note that index 2 is dimensional (m^2/MN), while indexes 1 and 3 are nondimensional. Source: Lourenço et al. 2013.



Index 1 is independent of the height, which is considered a major drawback. Therefore, only indexes 2 and 3 are further analyzed. The comparison between γ_2 and γ_3 is equivalent to comparing $1/h$ and $1/\beta$, or height and seismicity, if cohesion is ignored. These quantities clearly are not comparable and seem uncorrelated according to the results presented by Lourenço and Roque (2006). To take the value of the height (h) of the building into account, the following approach is suggested, assuming the criterion for γ_3 must be fulfilled. This results in a minimum value of $\gamma_{3,i,min}$ equal to the unit value. Based on equation 3.6, it is possible to obtain a minimum ratio of walls as follows (eq. 3.8):

$$\gamma_{3,i,min} = 1.0 \Leftrightarrow (A_{wi}/A_w)_{min} = \beta / \tan \phi \quad (3.8)$$

Having introduced this result in equation 3.2, the minimum value of $\gamma_{2,i,min}$ reads as follows (eq. 3.9):

$$\gamma_{2,i,min} = \beta / (\gamma \times h \times \tan \phi) \quad (3.9)$$

The proposed strategy is to adopt both index 2 and index 3 simultaneously, such that $\gamma_{2,i} > \gamma_{2,i,min}$ and $\gamma_{3,i} > 1.0$. It is stressed that (a) the first criterion is different than imposing a maximum height to the building, because the walls, the height, and the seismicity are involved in the inequality; and (b) the second criterion only considers the height of the building if cohesion is different than zero and therefore might yield unreliable results (Lourenço and Roque 2006).

Application Examples

This simplified screening approach was used to compare simple geometric data considering local seismic hazard and to determine whether indexes related to these data could be used as a first (very fast) technique to help define priorities for further studies with respect to seismic vulnerability. Detailed applications of this approach can be found in Lourenço and Roque (2006) and Lourenço et al. (2013). Two case studies are presented below: European churches (Portuguese, Spanish, and Italian); and New Zealand churches (in and around Christchurch). The latter study was used to validate the proposed thresholds with data from the 2010–11 earthquakes in the Canterbury region of New Zealand.

European Churches

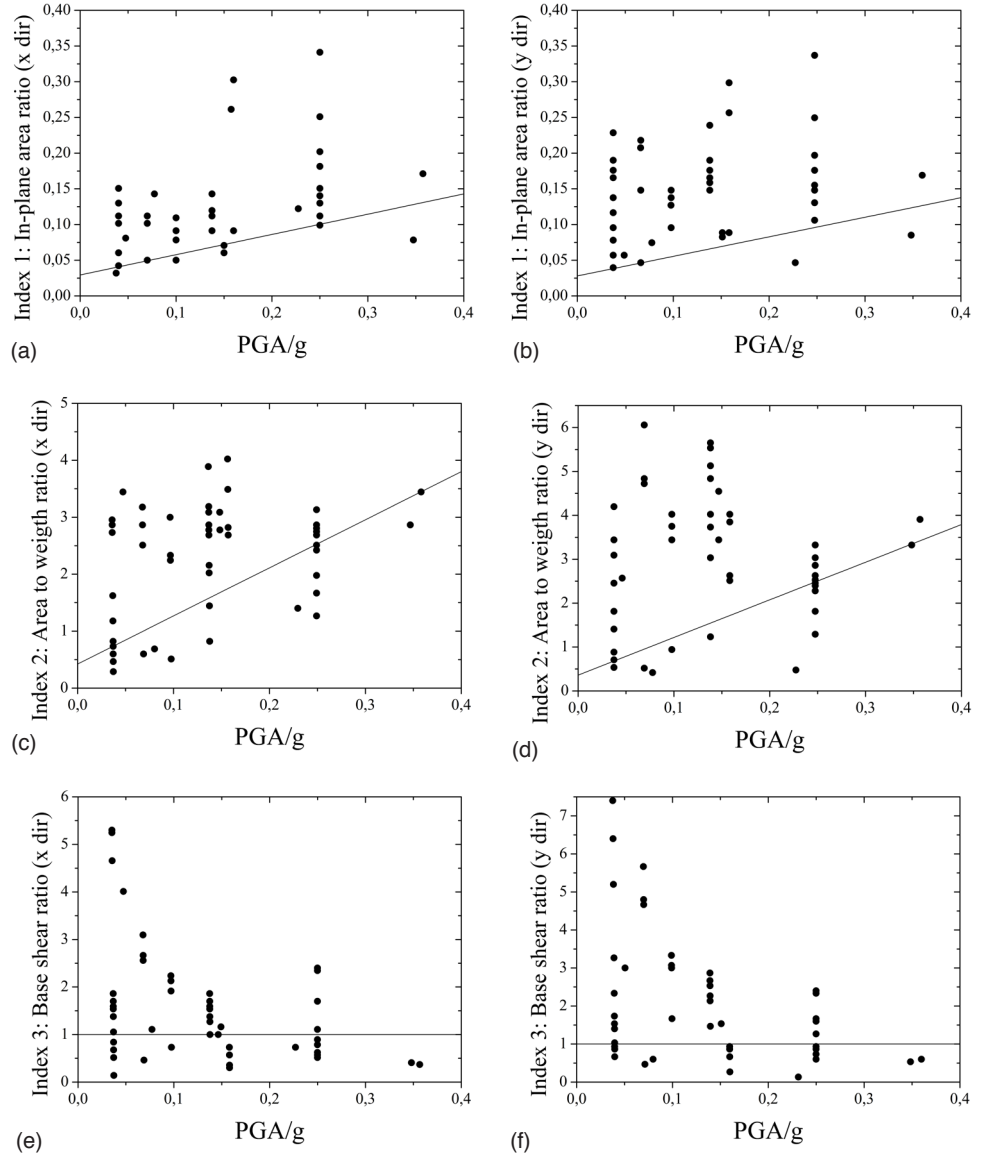
The methods were applied to a sample of forty-four Portuguese, Spanish, and Italian historic church buildings of clay brick, selected according to their seismic hazard and the availability of building construction information. For this analysis, it was assumed that all the masonry materials were similar, the volumetric weight of masonry was 20 kN/m^3 , the weight of the roofs was equal to 2.0 kN/m^3 , and the cohesion value was assumed equal to 0.05 N/mm^2 . The results (see fig. 3.4) are a function of the local parameter PGA, along with the threshold for each index, namely $\gamma_{1,i} \leq 10\%$, $\gamma_{2,i} \leq 2.5 \text{ m}^2/\text{MN}$, and $\gamma_{3,i} \leq 1.0$ for a PGA of 0.25 g (Lourenço et al. 2013).

In terms of average values, index 1 presents lower values in the transversal direction x of the church nave, which is expected due to the geometry of the church buildings, although Italian indexes are quite similar in both directions. Index 1 does not show a clear variation with seismicity, even if it tends to increase somewhat as seismicity increases. When a comparison is made using the proposed threshold, 25% of the churches debase the criterion in the x direction and 9% violate it in the y direction. This outcome means that the cases that require further investigation are mainly those with a deficient earthquake resistance along the transversal direction of the church nave (Lourenço et al. 2013).

Index 2, although inversely proportional to the height of the buildings, presents a situation similar to that of index 1. Again, the calculated values do not show a visible trend with respect to seismicity; however, an increase of index 2 can be associated with PGA increase. On average, index 2 also presents lower values in the x direction, again justified by the churches' geometry. As a result, this index is debased by 39% and 30% of the historic buildings in x and y directions, respectively. This index is mainly debased by the Spanish churches (Lourenço et al. 2013).

Index 3 shows an alarming decrease in variation with the PGA parameter. For moderate- and high-seismicity areas ($\text{PGA} > 0.15 \text{ g}$), index 3 is debased by all churches in both directions. Despite this, index 3 is not entirely fulfilled also for low-seismicity areas. As with indexes 1 and 2, index 3 presents lower values in the x direction. Individually, 41% and 32% of the churches debase index 3 in the x and y directions, respectively, which denotes a deficient earthquake resistance along both the transversal and longitudinal directions. Unexpectedly, this index assumes minimum values slightly lower than 0.15 in both directions, which is most likely associated with highly vulnerable structures that probably would not survive an earthquake. This index is mainly debased by the Italian churches (Lourenço et al. 2013).

FIGURE 3.5. Scatterplots showing the relationship between the three in-plane indexes and PGA: (a) index 1, direction x; (b) index 1, direction y; (c) index 2, direction x; (d) index 2, direction y; (e) index 3, direction x; and (f) index 3, direction y. Source: Lourenço et al. 2013.



To perform a preliminary screening and prioritize further studies in historic masonry structures in earthquake-prone countries, Lourenço et al. (2013) suggested identifying the historic buildings for which all in-plane indexes are debased or disrupted in at least one direction. An alternative approach would be to consider the simultaneous disruption of index 3 and either index 1 or 2. Both criteria show that deficient resistance to earthquake loading not only is associated with high seismicity, as for most of the Italian churches described above, but also can occur in moderate-seismicity areas, including the two Portuguese churches in the sample, or even in low-seismicity areas, such as most of the Spanish churches. Considering the first criterion, 18% of the sample requires remedial measures or, at least, more in-depth investigation. However, under the second criterion, almost half of the sample (43%) exhibits deficient earthquake resistance (Lourenço et al. 2013).

New Zealand Churches after the 2010–11 Canterbury Earthquakes

Following the series of quakes that struck New Zealand in 2010–11 in and around Christchurch in the region of Canterbury, the indexes related to the simplified analysis methods were calculated for the stone and clay brick churches studied in the affected area.

The objective was to validate the proposed thresholds for each of the three in-plane indexes (in-plane area ratio, area to weight ratio, and base shear ratio) using the PGA on each church during the quake that occurred on February 22, 2011. In applying the simplified analysis, it was assumed that all the masonry materials were similar, the volumetric weight of masonry was 20 kN/m^3 , the weight of the roofs was 2.0 kN/m^3 , and a cohesion value was equal to 0.05 N/mm^2 . Based on the network of seismographs (CRSMN 2003), it was possible to associate the PGA recorded at a given location with a nearby church (Lourenço et al. 2013).

After the Canterbury earthquake, a building safety evaluation process was carried out and each building was classified into one of three groups according to national regulations. The process overview and guidelines are reported in NZSEE (2009) and based on North American procedures developed by the Applied Technology Council (ATC-20 1989; ATC-20-2 1995). In addition to the new classification, a placard was placed at the main entrance to each structure, keyed to three color tags: green indicated no restrictions to use of the building; yellow meant that, due to safety concerns, use of the building was restricted to short periods of time and only for essential business; and red indicated the building was unsafe and reentry was prohibited. Heritage buildings were also assessed following the same guidelines (Lourenço et al. 2013).

Figure 3.6 shows the scatterplots of each index and the recorded horizontal PGA of the February 22 seismic event for clay brick churches, as well as the proposed thresholds (see fig. 3.4). The threshold for the first index is excellent, with all green-tagged churches above or near the line and only one yellow- and one red-tagged church incorrectly identified. Threshold results for indexes 2 and 3 are also acceptable. The x (or transverse) direction provides better results in all three indexes; this is the critical direction. The indexes are consistent even if they are not directly correlated. Index 3 exhibits the worst performance if cohesion is taken into consideration, with better results obtained for zero cohesion (see fig. 3.6; Lourenço et al. 2013).

Comparatively, the thresholds for the stone churches are not as good (fig. 3.7). For all indexes, and in both directions, green-tagged churches were subjected to a PGA equal or higher to 1.0 g under the threshold, and red-tagged churches were subjected to a PGA lower than 0.125 g above the threshold. This lack of homogeneity justifies the lack of agreement with the thresholds, as the seismic behavior of the stone churches is rather different. Monumental churches constructed of good-quality stone can present a seismic behavior similar to that of clay brick churches, while weaker rubble stone masonry lacks interlocking and disaggregates, even for low PGA values. Redefining the thresholds is not a solution, and it is suggested that the stone church typology should be divided into subcategories according to more specific construction details. Similar to that of the clay brick churches, there is better agreement with the threshold of index 3 if cohesion is not taken into consideration (Lourenço et al. 2013).

FIGURE 3.6. Scatterplots showing the relationship between in-plane indexes and PGA for clay brick churches: (a) index 1, direction x; (b) index 1, direction y; (c) index 2, direction x; (d) index 2, direction y; (e) index 3, direction x, with zero cohesion; and (f) index 3, direction y, with zero cohesion. Source: Lourenço et al. 2013.

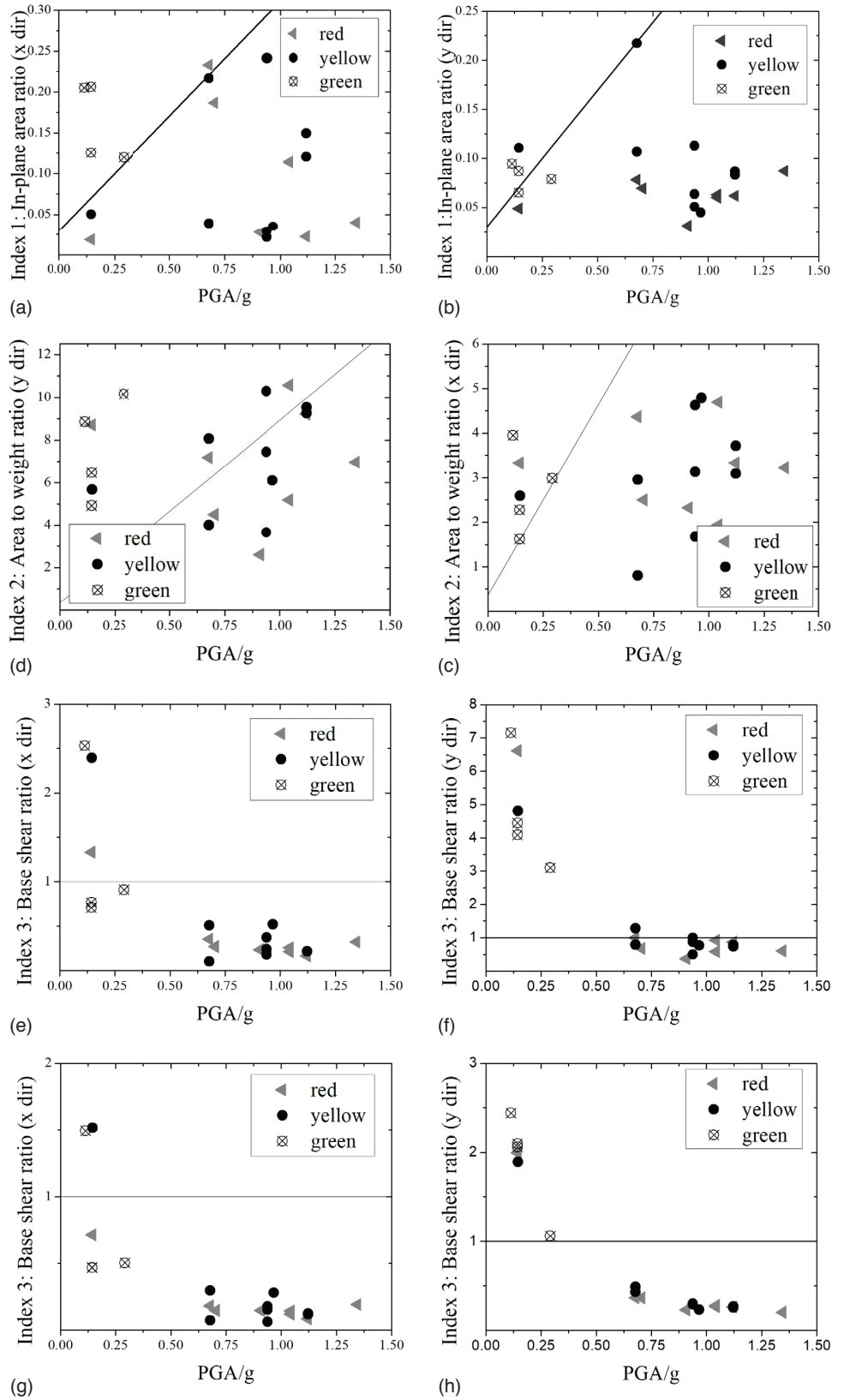
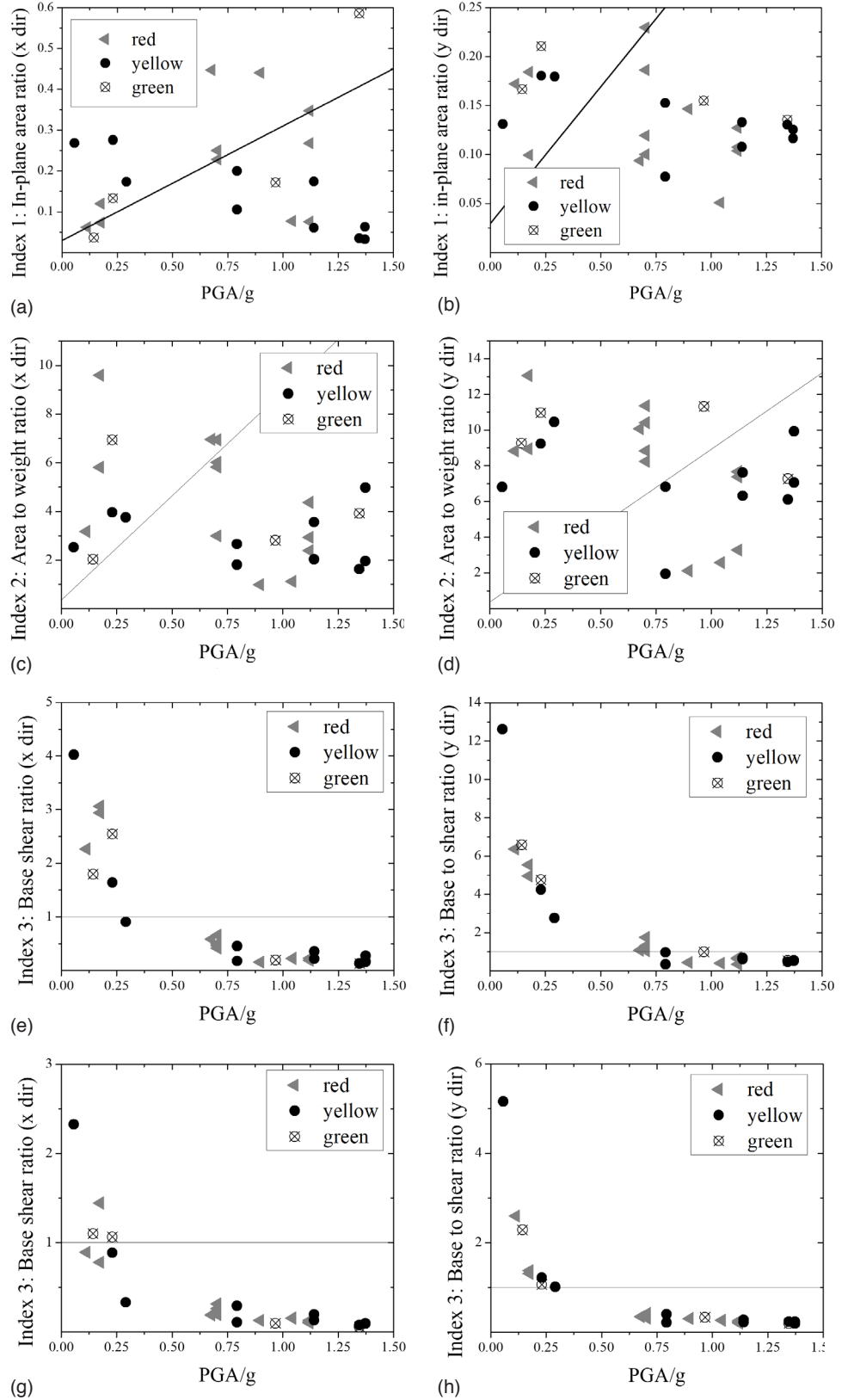


FIGURE 3.7. Scatterplots showing the relationship between in-plane indexes and PGA for stone churches: (a) index 1, direction x; (b) index 1, direction y; (c) index 2, direction x; (d) index 2, direction y; (e) index 3, direction x; (f) index 3, direction y; (g) index 3, direction x, with zero cohesion; and (h) index 3, direction y, with zero cohesion. Source: Lourenço et al. 2013.



Limit Macro-Block Assessment

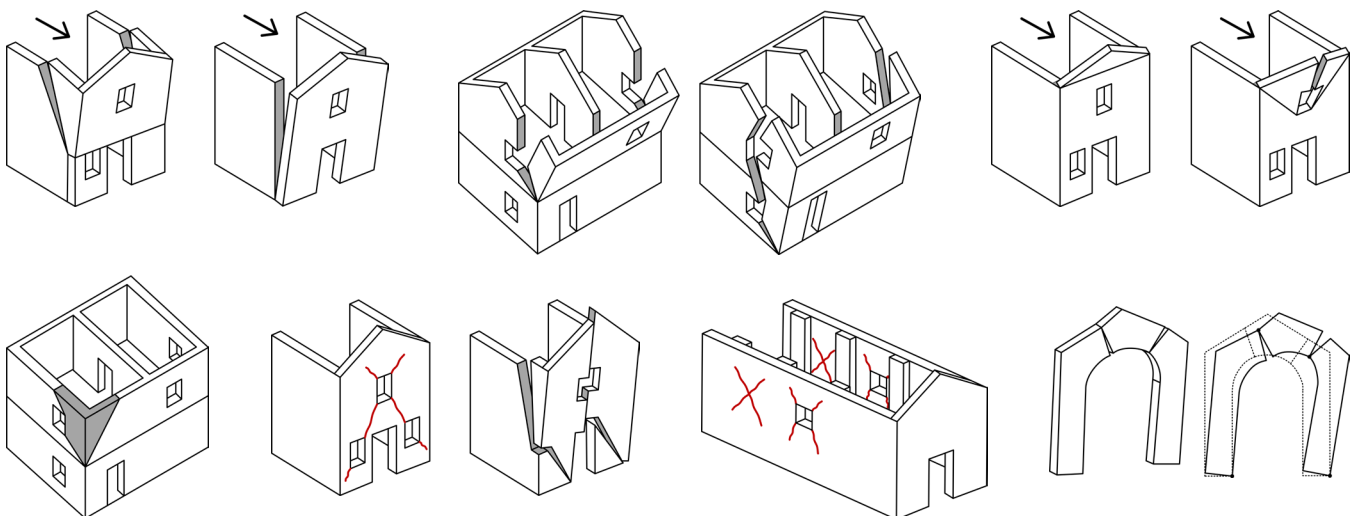
Masonry buildings are composed of three-dimensional assemblies of walls, with the out-of-plane behavior of each wall highly influenced by the type and strength of its connection to the other walls. However, when a global box (or structural integral) behavior is not guaranteed, the walls—especially peripheral ones, due to their lack of external bracing and the low tensile strength of masonry—become more vulnerable to out-of-plane overturning. During an earthquake, out-of-plane overturning is one of the main causes of damage or collapse in existing masonry structures (Casapulla, Giresini, and Lourenço 2017).

If a monolithic behavior can be assured for each wall, all walls can be regarded as rigid blocks at collapse, and their out-of-plane seismic response can be addressed through kinematic analysis. Smaller portions of wall, defined by cracks and fragmentations, may also be considered. The kinematic approach includes static force-based and displacement-based approaches using standard and nonstandard limit analysis methods and considering the evolution of motion over time through incremental kinematic analysis. Dynamic effects are more appropriately considered by means of the dynamic approach, since this accounts for energy dissipation in the evolution of motion (Casapulla, Giresini, and Lourenço 2017).

Limit Equilibrium Analysis

FIGURE 4.1. Examples of collapse mechanisms in facades, corners, and arch systems of existing masonry structures. Source: Adapted from DPCM February 9, 2011.

Partial collapses due to earthquakes often occur in existing masonry buildings and are generally caused by the loss of equilibrium in portions of the masonry. Local mechanisms in masonry walls are mostly caused by forces perpendicular to their plane; in the case of arch systems, these mechanisms can even be caused by in-plane forces (fig. 4.1).



Verifications of damage and collapse (in-plane and out-of-plane) with reference to local mechanisms can be carried out through limit equilibrium analysis, based on a linear kinematic approach based on selection of the collapse mechanism and evaluation of the horizontal forces that activate the kinematic mechanism (NTC 2018).

The nonlinear kinematic approach allows the determination of the horizontal forces that the structure is progressively capable of supporting with the development of the mechanism. This can be expressed in a diagram in terms of a multiplier a , the ratio between the applied horizontal forces and the corresponding weights of the masses (fig. 4.2), represented as a function of the displacement d_c of a reference point (or control point) of the system (fig. 4.3). The diagram is determined from the initiation of the kinematic mechanism ($a = a_0$) until the loss of capacity to support horizontal actions ($a = 0$). Such a diagram can be transformed into the capacity curve of an equivalent single degree of freedom system, where the displacement capacity of the local mechanism can be compared with the displacement demand from the seismic action.

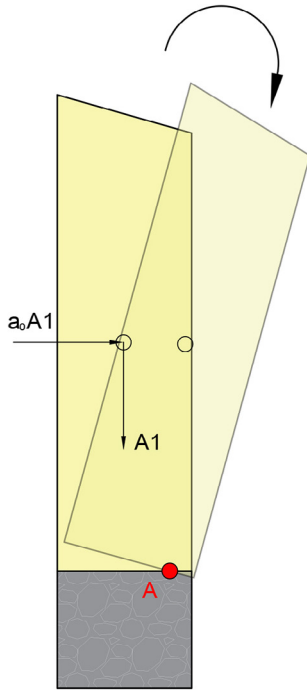


FIGURE 4.2.
Rotation of the block around the hinge line at collapse. Source: Karanikouloudis and Lourenço 2015.

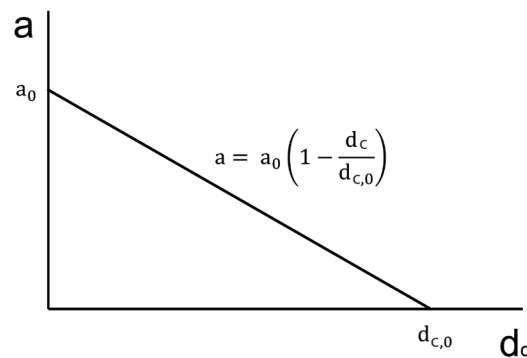


FIGURE 4.3.
Generic capacity spectrum of the rigid-block mechanism in terms of horizontal load multiplier a vs. horizontal displacement of the control point d_c .

For every possible local mechanism considered significant for the building, the method can be subdivided into the following five steps (NTC 2018):

1. Transformation of one part of the construction into a determinate system (kinematic chain) by identification of rigid bodies. These bodies are defined by fracture planes, assumed due to the low tensile strength of the masonry, that are capable of rotating or sliding (mechanism of damage and collapse).
2. Estimation of the horizontal load multiplier a_0 that causes activation of the mechanism (limit state of damage).
3. Estimation of the evolution of the horizontal load multiplier a with increasing displacements d_c of a control point of the kinematic chain, usually chosen close to the center of gravity, until total loss of horizontal seismic force capacity.
4. Transformation of the obtained diagram, into the capacity curve, in terms of spectral accelerations a^* and spectral displacements d^* , of an equivalent single degree of freedom (SDOF) oscillator, with the estimation of the ultimate displacement for the collapse mechanism (ultimate limit state).
5. Safety verification by checking compatibility of the demand displacements and/or of the demand forces with the structure.

In applying this method of analysis, the following assumptions may be made for simplification: (a) masonry withstands no tensile stresses, (b) there is no sliding between

blocks in the mechanism, and (c) compressive strength is infinite. Note that the last assumption is not recommended for earthen construction.

For a more realistic simulation of the behavior, the following assumptions are recommended: (a) sliding between blocks considering the presence of friction; (b) connections between the masonry walls of limited strength; (c) presence of metallic tie rods; (d) limited compressive strength of masonry by adequately moving the hinges from the edge of the section toward the center; and (e) presence of walls with separated leaves (NTC 2018).

Linear Kinematic Analysis

To obtain the horizontal load multiplier a_0 that activates the local damage mechanism, it is necessary to apply the following forces to the kinematic chain composed of the rigid blocks:

- the dead load of the blocks applied at their center of gravity;
- the vertical loads carried by the blocks (quasi-permanent due to the dead loads and relevant fraction of the live loads of the floors and roof, as well as other masonry elements not considered in the structural model);
- a system of horizontal forces proportional to the applied vertical loads, if these are not efficiently transmitted to the other parts of the building;
- possible external forces (e.g., those transmitted by metallic tie rods); and
- possible internal forces (e.g., those related to interlocking of masonry units) (NTC, 2018).

By assigning a virtual rotation θ_c to the generic block, it is possible to determine the displacements as a function of the rotation and the geometry of the structure due to the various forces applied in the respective directions. The load multiplier a_0 is obtained in terms of displacements, applying the virtual work principle (VWP) by equating the total work done by the external forces to the internal forces applied to the system, which corresponds to the virtual work (NTC 2018) as shown in equation 4.1:

$$a_0 \left(\sum_{i=1}^n P_i \delta_{x,i} + \sum_{j=n+1}^{n+m} Q_j \delta_{x,j} \right) - \sum_{i=1}^n P_i \delta_{y,i} - \sum_{h=1}^o F_h \delta_h = L_{fi} \quad (4.1)$$

where

- n is the total number of quasi-permanent loads (weights, vertical forces) applied to the different rigid blocks of the kinematic chain;
- m is the number of weight forces not directly acting on the blocks but whose mass, because of seismic action, generates horizontal forces on the elements of the kinematic chain and is not efficiently transmitted to the other parts of the building;
- o is the number of the external forces applied to the blocks but not related to mass;
- P_i is the generic quasi-permanent force (dead weight of the block applied at its center of gravity, or a fraction of relevant live loads);
- Q_j is the generic weight force not directly applied to the blocks, but whose mass, because of seismic action, generates horizontal forces on the elements of the kinematic chain and is not efficiently transmitted to the other parts of the building;
- $\delta_{x,i}$ is the virtual horizontal displacement of the point of application of the i^{th} quasi-permanent force P_i , assumed positive in the direction of the seismic action that activates the mechanism;

- $\delta_{x,j}$ is the virtual horizontal displacement of the point of application of the j^{th} weight force Q_j , assumed as positive in the direction of the seismic action that activates the mechanism;
- $\delta_{y,i}$ is the virtual vertical displacement of the point of application of the i^{th} quasi-permanent force P_i , assumed positive if upward;
- F_h is the generic external force (absolute value) applied to the block; these forces can favor the activation of the mechanism (e.g., thrust from vaults, roofs, etc.) or oppose it (e.g., tie beams);
- δ_h is the virtual displacement of the point of application of h^{th} external force F_h in the direction of the force and positive if in the opposite direction; and
- L_{fi} is the work done by the internal forces.

Nonlinear Kinematic Analysis

To define the displacement capacity of the structure until collapse using the mechanism considered, the horizontal load multiplier a can be estimated based not only on the initial configuration but also on variations of the kinematic chain, representative of the evolution of the mechanism and described by displacement of the control point d_c . The analysis must be performed until the corresponding multiplier $a = 0$, and the respective displacement $d_{c,0}$ is reached (NTC 2018).

For every configuration of the kinematic mechanism of the rigid blocks, the value of the multiplier a can be determined using equation 4.1 with reference to the varied geometry. The analysis can be performed either graphically, by identifying the geometry of the system in the different configurations until overturn, or analytically, by considering a sequence of virtual finite rotations and progressively updating the system's geometry.

If the various acting forces (weight, external and internal actions) are constant as the mechanism evolves, the curve obtained is almost linear. The displacement $d_{c,0}$ (corresponding to the $a = 0$ condition) can be derived from the simplified expression (eq. 4.2):

$$a = a_0 (1 - d_c / d_{c,0}) \quad (4.2)$$

The unknown collapse rotation $\theta_{c,0}$ can be estimated by expressing the evolution of the mechanism as a function of its rotation θ and by applying VWP using equation 4.1, and imposing $a = 0$.

Estimation of the Capacity Curve (SDOF)

With the horizontal load multiplier a as a function of the displacement d_c of the known control point of the structure, the capacity curve of the equivalent SDOF oscillator must be defined as a relationship between the spectral acceleration and displacement, a^* and d^* . The participating mass of the kinematic mechanism M^* can be evaluated by considering the virtual displacements of the various forces associated with the mechanism, such as a mode shape of vibration, at the points of application (eq. 4.3):

$$M^* = \frac{\left(\sum_{i=1}^n P_i \delta_{x,i} + \sum_{j=n+1}^{n+m} Q_j \delta_{x,j} \right)^2}{g \left(\sum_{i=1}^n P_i \delta_{x,i}^2 + \sum_{j=n+1}^{n+m} Q_j \delta_{x,j}^2 \right)} \quad (4.3)$$

where

- $n+m$ is the number of applied weight forces P_i and Q_j whose mass, due to seismic action, generates horizontal forces on the elements of the kinematic chain;
- $\delta_{x,i}$ is the virtual horizontal displacement of the point of application of the i^{th} force P_i ;
- $\delta_{x,j}$ is the virtual horizontal displacement of the point of application of the j^{th} force Q_j ;
- and
- g is the acceleration due to gravity.

The seismic spectral acceleration a^* is obtained by multiplying the load multiplier a by the acceleration due to gravity and dividing it by the fraction of participating mass of the kinematic mechanism. Therefore, as shown in equation 4.4, the spectral acceleration that activates the mechanism is equal to:

$$a_0^* = \frac{a_0 \left(\sum_{i=1}^n P_i + \sum_{j=n+1}^{n+m} Q_j \right)}{M^* FC} = \frac{a_0 g}{e^* FC} \quad (4.4)$$

where FC is the confidence factor and, as shown in equation 4.5, the fraction of participating mass of the structure is equal to:

$$e^* = \frac{g M^*}{\sum_{i=1}^n P_i + \sum_{j=n+1}^{n+m} Q_j} \quad (4.5)$$

The spectral displacement d^* of the equivalent SDOF oscillator can be obtained as the average displacement of the various points at which the forces P_i and Q_j are applied and weighted over the same. As an approximation, with the displacement of the control point d_c known, the equivalent spectral displacement d^* can be derived with reference to the virtual displacements evaluated on the initial configuration (eq. 4.6):

$$d^* = d_c \frac{\sum_{i=1}^n P_i \delta_{x,i}^2 + \sum_{j=n+1}^{n+m} Q_j \delta_{x,j}^2}{\delta_{x,c} \left(\sum_{i=1}^n P_i \delta_{x,i} + \sum_{j=n+1}^{n+m} Q_j \delta_{x,j} \right)} \quad (4.6)$$

where

- $\delta_{x,c}$ is the virtual horizontal displacement of the point c , assumed as reference to determine the displacement d_c .

If the capacity curve is linear (eq. 4.2) with constant forces, it assumes the following expression (eq. 4.7):

$$a^* = a_0^* \left(1 - d^* / d_0^* \right) \quad (4.7)$$

where

- d_0^* is the equivalent spectral displacement corresponding to the displacement $d_{c,0}$.

Here, it is noted that the behavior of the equivalent SDOF oscillator, constrained within transversal walls, is assumed as infinitely rigid prior to the activation of the mechanism (a_0^* for d^* equal to zero). For free-vibrating elements, the elastic dynamic response should be accounted for, with the period T_0 that defines a first linear branch (fig. 4.4) according to the following expressions (eq. 4.8):

$$a^* = \frac{4\pi^2}{T_0^2} d^* \quad (4.8)$$

where T_0 can be derived from the theory of elasticity for beams of distributed mass (eq. 4.9):

$$T_0 = \kappa \lambda h \sqrt{\frac{w}{Eg}} \quad (4.9)$$

and

h is the height of the element;

κ is a coefficient equal to 6.2 for a cantilever response and 2.2 for a flexural response, that of a simply supported beam;

λ is the slenderness ratio of the height h to the thickness t of the element;

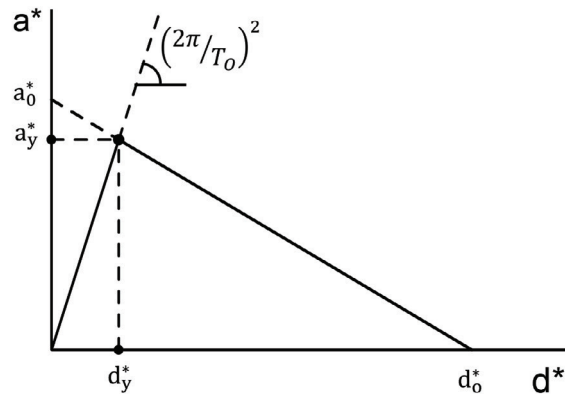
w is the specific mass of the masonry;

E is Young's modulus; and

g is the acceleration of gravity.

FIGURE 4.4.

Generic capacity spectrum of a corresponding SDOF oscillator system of a rigid-block mechanism not restrained within transversal walls.



The strength and displacement capacity for the damage limit state and ultimate limit state is derived from the capacity curve based on the following conditions (NTC 2018):

- damage limit state (DLS): from the spectral acceleration a_0^* , corresponding to the activation of the damage mechanism.
- ultimate limit state (ULS): from the spectral displacement d_u^* , corresponding to the minimum of the following displacements: (a) 40% of the displacement at which the multiplier $a = 0$, evaluated from a curve in which only those forces occur that are present until collapse; and (b) the displacement corresponding to the breakage of links and kinematic chains, but with no instability issues, which in acceleration terms causes more than 50% reduction of the maximum capacity.
- collapse limit state (CLS): from the spectral displacement d_u^* , corresponding to the minimum of the following displacements: (a) 60% of the displacement at which the multiplier $a = 0$, evaluated from a curve in which only those forces occur that are present until collapse; and (b) the displacement corresponding to a local instability in the structural elements (e.g., slipping of beams, collapse of vaults, etc.).

Safety Verification

Safety for the DLS is verified when the spectral acceleration of mechanism activation is higher than the demand acceleration derived from the elastic response spectrum. Here,

NTC (2018) distinguishes between elements or portions of the structures in contact with the ground and at a certain height while considering the acceleration amplifications. For elements or portions that are or can be assumed to be in contact with the ground, the safety verification can be determined using equation 4.10:

$$\dot{a}_o \geq a_g(P_{VR}) \cdot S \quad (4.10)$$

where

$a_g(P_{VR})$ is PGA for the specific region as a function of the probability of exceeding the selected limit state (NTC 2018); and

S considers the type of soil.

For elements or portions of the structure at a certain height, for which the kinematic response can be amplified with respect to the ground, the safety verification can be determined as follows (NTC 2018):

$$\dot{a}_o \geq S_e(0, \xi, z) = a_g(P_{VR}) \cdot S \cdot \Psi(z) \cdot \gamma \cdot \sqrt{1 + 0.0004 \cdot \xi^2} \quad (4.11)$$

where

$S_e(0, \xi, z)$ is the ordinate from the elastic spectral acceleration, determined for a period equal to zero in the considered height, for a viscous damping ξ of 5%;

$\Psi(z)$ can be assumed as z/H , z being the height from the building foundation to the barycenter of the restraint lines, assumed to be between the blocks considered in the mechanism and the rest of the structure, and H the total height of the building from the foundation; and

γ is the coefficient of modal participation, which—for structures with masses evenly distributed along the height (e.g., lumped masses in floors)—can be assumed equal to $3N/(2N+1)$, where N is the number of stories of the building.

In the case of local mechanisms, the DLS corresponds to the formation of cracks that affect only part of the building and not the entire structure; therefore, in existing masonry buildings, considering the justified requirements of conservation, verification of the DLS is desirable but not required (NTC 2018).

Verification for the ULS, which is necessary for guaranteeing safety with respect to structural failure, can be performed according to one of the following criteria: (a) simplified verification with q factor (linear kinematic analysis) or (b) verification by means of the capacity spectrum (nonlinear kinematic analysis) (NTC 2018).

Linear Kinematic Analysis (Force Control)

For elements or portions of the structure that are or can be assumed to be in contact with the ground, safety for the ULS is verified when the spectral acceleration \dot{a}_o^* that activates the mechanism satisfies the following inequality (eq. 4.12):

$$\dot{a}_o^* \geq \frac{a_g(P_{VR}) \cdot S}{q} \quad (4.12)$$

where

q is the behavior factor, which can be assumed equivalent to 2.0.

For elements or portions of the structure at a certain height, the safety verification can be determined as shown in equation 4.13 (NTC 2018):

$$\ddot{a}_0 \geq \frac{S_e(0, \xi, z)}{q} = \frac{a_g(P_{Ri}) \cdot S \cdot \psi(z) \cdot \gamma \cdot \sqrt{1 + 0.0004 \cdot \xi^2}}{q} \quad (4.13)$$

Nonlinear Kinematic Analysis (Displacement Control)

Safety verification for local mechanisms for the ULS involves the comparison of the displacement capacity d_{ULS}^* of the local mechanism and the displacement demand $\Delta_d(T_{ULS})$, evaluated by means of a response spectrum, estimated with respect to the equivalent period T_{ULS} . Here, the corresponding period for the ULS, based on the secant period, is further reduced to account for dispersion of the dynamic properties at the ULS (NTC 2018).

Once the displacement $d_{ULS}^* = 0.4 \cdot d_0^*$ is estimated and the acceleration a_{ULS}^* corresponding to the displacement d_{ULS}^* is identified on the capacity curve (fig. 4.5), the equivalent period is calculated (eq. 4.14):

$$T_{ULS} = 1.68\pi \sqrt{\frac{d_{ULS}^*}{a_{ULS}^*}} \quad (4.14)$$

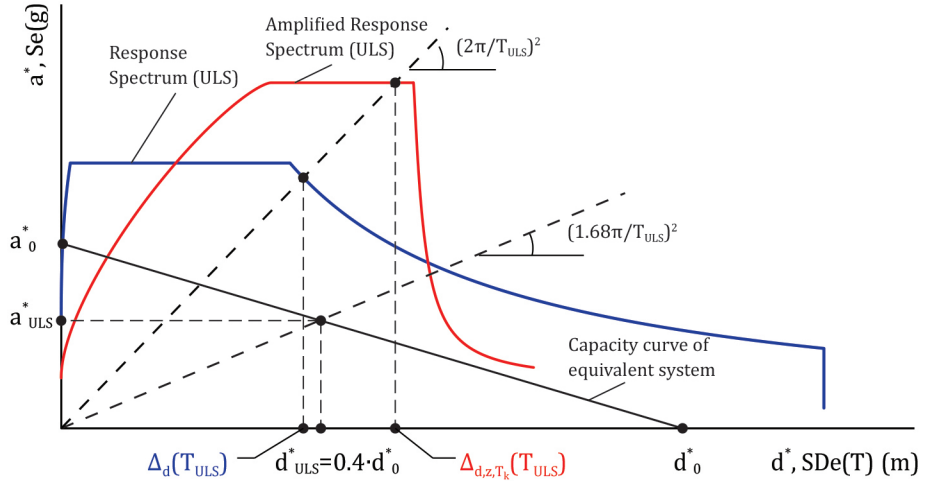
The displacement demand $\Delta_d(T_{ULS})$ can be obtained by determining the elastic spectral acceleration for the equivalent period and then converting it into displacement using equation 4.15:

$$\Delta_d(T_{ULS}) = S_e(T_{ULS}) \cdot \left(\frac{T_{ULS}}{2\pi}\right)^2 \quad (4.15)$$

Safety for the ULS is verified when the ultimate displacement demand respects the relationship with the displacement capacity of the ULS: $\Delta_d(T_{ULS}) \leq d_{ULS}^*$.

FIGURE 4.5.

Graphic verification of nonlinear kinematic analysis in displacement control for the response of the kinematic mechanism at the foundation base (in blue) and at a height z above the foundation base (in red).



For elements or portions of the structure at a certain height, the displacement demand is obtained from the updated, amplified response spectrum, according to the main period of the structure (T_k) and the height from the foundation base, by the following relationships (NTC 2018):

$$\Delta_d(T_{ULS}) = S_e(T_{ULS}, \xi, z) \cdot \left(\frac{T_{ULS}}{2\pi}\right)^2 \quad (4.16)$$

$$S_{ez,k}(T,\xi,z) = \begin{cases} \frac{1.1 \cdot \xi^{-0.5} \cdot \eta(\xi) \cdot a_{z,k}(z)}{1 + [1.1 \cdot \xi^{-0.5} \cdot \eta(\xi) - 1] \cdot \left(1 - \frac{T}{a \cdot T_k}\right)^{1.6}} & , T < a \cdot T_k \\ 1.1 \cdot \xi^{-0.5} \cdot \eta(\xi) \cdot a_{z,k}(z) & , a \cdot T_k \leq T < b \cdot T_k \\ \frac{1.1 \cdot \xi^{-0.5} \cdot \eta(\xi) \cdot a_{z,k}(z)}{1 + [1.1 \cdot \xi^{-0.5} \cdot \eta(\xi) - 1] \cdot \left(\frac{T}{b \cdot T_k} - 1\right)^{1.2}} & , T \geq b \cdot T_k \end{cases} \quad (4.17)$$

$$a_{z,k}(z) = S_e(T_k, \xi) \cdot \Psi(z) \cdot \gamma \cdot \sqrt{1 + 0.0004 \cdot \xi_k^2} \quad (4.18)$$

$$\eta(\xi) = \sqrt{\frac{10}{5 + \xi}} \quad (4.19)$$

where

- $a_{z,k}(z)$ is the acceleration contribution of the k -mode at a height z from the foundation base;
- $S_e(T_k, \xi)$ is the ordinate from the elastic spectral acceleration, determined for a period equal to T_k , for a viscous damping ξ of 5%;
- T_k is the principal period of the structure at the direction in which the most significant displacement demand is produced. If response spectra from many modes are to be used, the overall response can be obtained through the SRSS rule. It is advised that the natural periods are obtained from in situ ambient vibration tests. Alternatively, analytical formulas can be used, such as in equation 4.9;
- a, b are coefficients that define the range of the amplification spectrum, equal to 0.8 and 1.1, respectively;
- $\eta(\xi)$ is a scale factor for the response spectrum, if a value from the viscous damping ξ , different than 5%, is used;
- $\Psi(z)$ can be assumed as z/H , z being the height from the building foundation to the barycenter of the restraint lines, assumed to be between the blocks considered in the mechanism and the rest of the structure, and H the total height of the building from the foundation; and
- γ is the coefficient of modal participation, which—for structures with masses evenly distributed along the height (e.g., lumped masses in floors)—can be assumed equal to $3N/(2N+1)$, where N is the number of stories of the building.

Graphic verification of the capacity response for the SDOF oscillator system and the spectrum demand at the foundation base and at a certain height is presented in figure 4.5.

Application Example: Design of Buttresses for the Church of Kuñotambo, Peru

An investigation was conducted into the addition of buttresses to the south lateral wall of the church of Santiago Apóstol de Kuñotambo, in Acomayo, Cusco, as part of a strengthening

proposal (Karanikoloudis and Lourenço 2015). The design of the buttresses is described below.

The collapse mechanisms occur with out-of-plane overturning of individual large wall portions. The failure mode with the lowest lateral capacity is the out-of-plane overturning of the church's south lateral wall (fig. 4.6), with corresponding lateral capacity of 0.19 g. Design verification of the buttresses was conducted through limit analysis, following a kinematic approach and specifying out-of-plane mechanisms, according to the results of a previous numerical analysis (Lourenço et al. 2019). General design recommendations for buttresses in adobe buildings were accounted for, based on Indian norms (IS 13827 1993); the lateral capacity was based on Italian standards (OPCM 3431 2005; NTC 2018). Through a simplified linear kinematic approach, lateral forces and displacements were checked for the DLS and ULS. Nonlinear behavior was also considered by checking the ultimate displacement capacity of walls, with the displacement obtained from the Peruvian design response spectrum (NTE-0.30 2018).

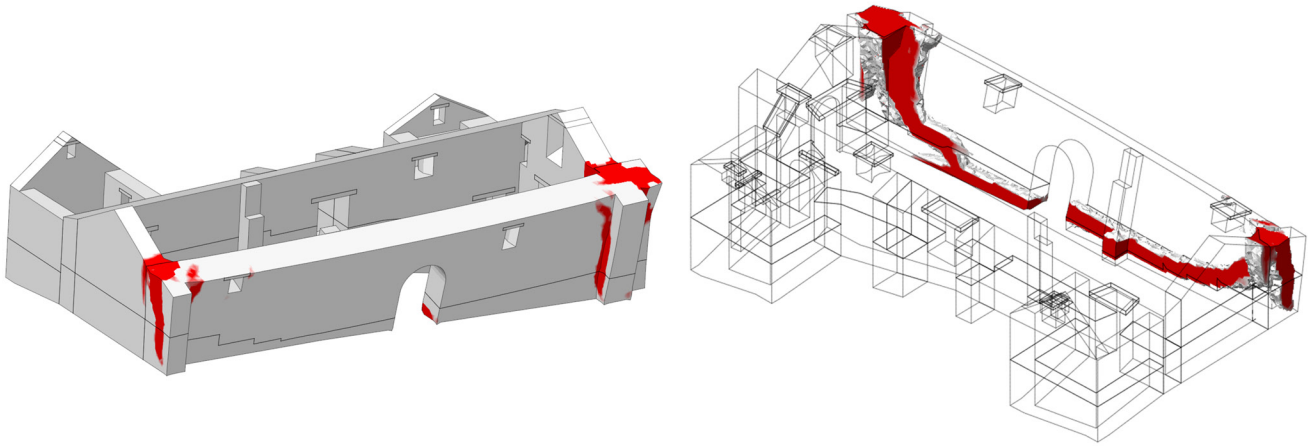


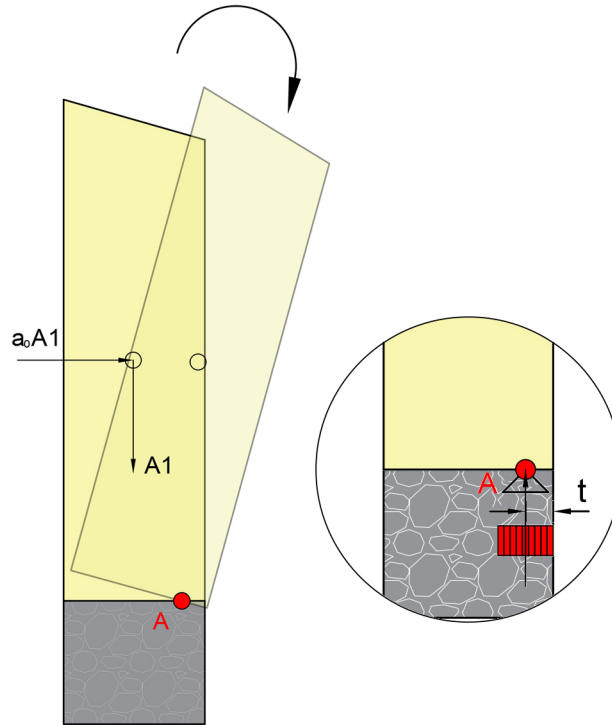
FIGURE 4.6. Diagrams showing distribution of maximum principal tensile strains near collapse for a pushover +y-y direction in the south lateral wall of the church of Kuñotambo, Peru. Source: Lourenço et al. 2019.

For the application of this limit analysis, several assumptions were considered: (a) the wall and the adjoining buttresses are monolithically connected, and the system rotates around the lower boundary of the adobe masonry; (b) the masonry has zero tensile strength; (c) there is unlimited friction between blocks (sliding not allowed); and (d) the design compressive strength of adobe is accounted for in order to place the rotating hinge line inside the thickness of the elements (Karanikoloudis and Lourenço 2015). According to NTC (2018, §8.7.1), a partial seismic coefficient γ_s of 2.0 is chosen. Although the Italian code indicates a triangular distribution of the compressive stresses at the base, alternatively a uniform stress distribution equal to 80% of the compressive strength was adopted. The corresponding plastic hinge position is given in equation 4.20, where $\sum_i W_i$ is the result of the vertical forces, σ_c is the average compressive strength of the material, and l is the transversal length of the effective area. As shown in figure 4.7, the block adopts a uniform stress distribution at the base, similar to the triangular distribution in the case of rectangular cross sections but conceptually more appealing. The average compressive strength of adobe masonry is taken equal to 0.45 MPa (Lourenço and Pereira 2018). Therefore, the distance of the hinge from the edge t can be determined as follows:

$$t = \frac{\sum_i W_i}{2 \times 0.8 \times \frac{\sigma_c}{\gamma_s} \times l} \quad (4.20)$$

The self-weight of the blocks is applied at the center of mass, and the assigned specific weight of adobe masonry is 19 kN/m^3 . The action from the roof in the wall is assumed as a uniform line load in the position of the wall plates, with a vertical component of 10.52 kN/m and a horizontal component of 5.32 kN/m , uniformly distributed across the thickness of the wall (Karanikoloudis and Lourenço 2015).

FIGURE 4.7. Rotation of the block around the hinge line, considering a rectangular distribution of compressive stresses, church of Kuñotambo, Peru. Source: Karanikoloudis and Lourenço 2015.



The horizontal equivalent seismic forces are proportional to the self-weight loads, with a load multiplier of a_o , and are applied in the center of mass of the blocks. The seismic coefficient is determined by equating the total work of internal and external forces and by assigning a virtual out-of-plane rotation θ_c to the blocks, with corresponding virtual displacements δ_c for the applied forces. The capacity curve of the generic blocks will contain pairs of lateral seismic loads and lateral displacements until collapse, with the load multiplier a_o obtained at the onset of movement. Transforming the macro-blocks formed into an SDOF system, nonlinear behavior is considered and displacement-based safety verifications are possible. Thus, performance is evaluated by checking compatibility in terms of spectral accelerations and displacements from the Peruvian elastic response spectrum (NTE-0.30 2018). To account for the ductility of the structure, a behavior factor q of 2.0 is considered if the structure is cracked and assuming the corresponding secant period T_s (NTC 2018).

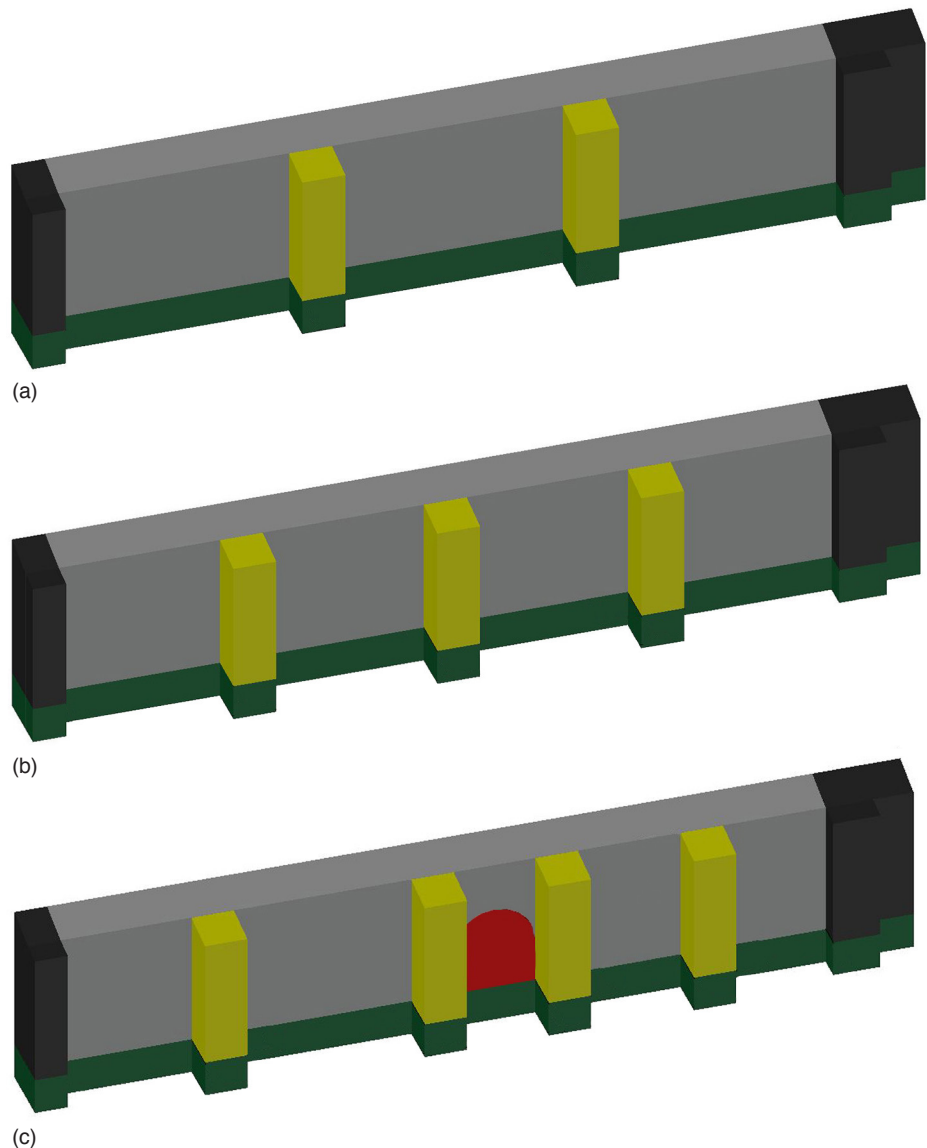
Complementary with the results of nonlinear pushover analysis and considering only average values, limit analysis regarding loading and material properties can be performed to obtain unreduced values of lateral capacity. As demonstrated in Lourenço et al. (2019) and in Karanikoloudis and Lourenço (2015), the differences in lateral capacity between limit analysis and nonlinear pushover analysis vary from 5% to 15%.

The church's south lateral wall has a large free span of around 31 m. The out-of-plane failure covers almost the entire wall, with separation at the corners. At an average height

of 1.5 m, the horizontal hinge line that formed mostly in the adobe base course interface is thus considered the rotation plane for all of the kinematic mechanisms that follow. In the original structure, two buttresses were already extant on either side of an arched opening (see red area in fig. 4.8c). Taking this into account in addition to the wall's large span and the low mechanical properties of adobe masonry, more buttresses may need to be added. Three proposals were considered: (a) two buttresses, evenly distributed along the free span of the wall; (b) three buttresses, evenly distributed along the free span; and (c) four buttresses, two in their original positions and two evenly distributed (see fig. 4.8). The entire free span of the wall is considered to interact with the proposed system of buttresses, and the rest of the wall is accounted for at the corners. Given the out-of-plane failure mode of the wall obtained in the pushover analysis and the cracks observed, the entire south wall is considered in the kinematic mechanism (Karanikoloudis and Lourenço 2015). To define the thickness and the length of the buttresses, the Indian code was used (IS 13827 1993). The code states that both the thickness and length of the buttresses (b_{but}) should be at least the same as the thickness of the transversal adjoining wall (1.72 m), which was the value adopted.

FIGURE 4.8.

Diagrams of strengthening proposals investigated for the south lateral wall, church of Kuñotambo, Peru: (a) two buttresses, evenly distributed along the free span of the wall; (b) three buttresses, evenly distributed along the free span; and (c) four buttresses, two in their original positions and two evenly distributed. Source: Karanikoloudis and Lourenço 2015.



Since the south lateral wall rests on a rubble stone base course of approximately 1.5 m in height, with the rotation plane assigned within their common interface, the possibility of an amplified response for the nonlinear kinematic analysis should be investigated for both unstrengthened and strengthened states. The response of the wall, as defined by the amplified design response spectrum (see eqs. 4.16–4.19), is a function of the principal natural period of the structure in the direction of the out-of-plane response. Ambient vibration tests, conducted in both unstrengthened and strengthened states—involving the addition of buttresses according to proposal (c) (see fig. 4.8)—defined the first period of the out-of-plane bending mode of single curvature as equal to 0.63 s and 0.27 s, respectively (Karanikoloudis and Lourenço 2018; Karanikoloudis and Lourenço 2020).

FIGURE 4.9.

Diagrams showing geometric configurations of the generic block in the unrestrained wall, church of Kuñotambo, Peru: (a) three-dimensional view, and (b) out-of-plane rotation in section. Dimensions in m. Source: Karanikoloudis and Lourenço 2015.

Kinematic Mechanism 1: Unstrengthened State

A portion 1 m long of the unrestrained, free-standing wall was considered. The geometric characteristics of the generic block and the kinematic chain configuration under a virtual rotation θ_c are shown in figure 4.9. The force control and displacement control kinematic analysis followed the process specified in NTC (2018). The applied forces and the center of mass are given in table 4.1.

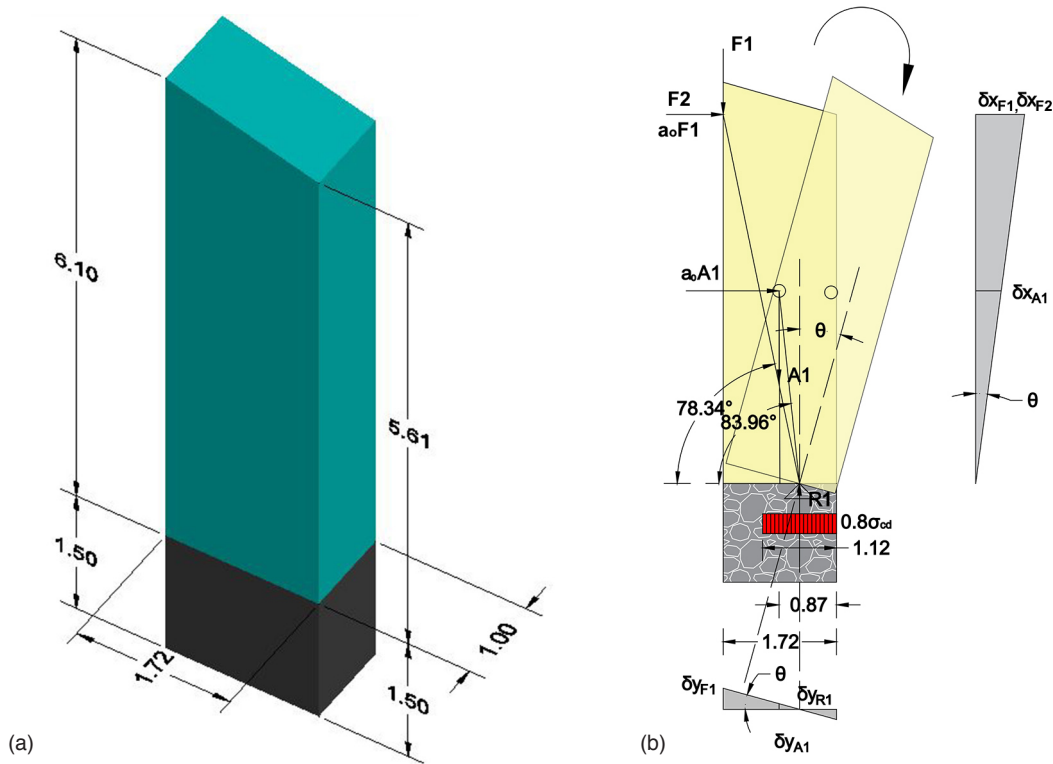


TABLE 4.1.

Load calculation in generic block (Karanikoloudis and Lourenço 2015).

	Area (m ²)	Length (m)	Volume (m ³)	F_i (kN)	$x_{Gi}^{[2]}$ (m)	$y_{Gi}^{[2]}$ (m)	$\delta_{x,i}$	$P_i * \delta_{x,i}$	$P_i * \delta_{x,i}^2$	β_{Gi}°	R_i	$F_i * R_i$
A1	10.07	1.00	10.07	191.33 ^[1]	0.87	2.93	0.52	99.49	51.74	83.96	2.99	572.08
F1	-	1.00	-	10.52	1.72	5.61	1.00	10.52	10.52	78.34	5.79	60.91
F2	-	1.00	-	5.32	1.72	5.61	-	-	-	-	-	-

^[1] For the weight forces, a mass density for adobe masonry of 19 kN/m³ is assumed.

^[2] Measured from the right bottom corner.

Considering a uniform stress distribution, the location of the rotating hinge can be calculated using equation 4.20 as follows:

$$t = \frac{\sum F_i}{2 \cdot 0.8 \cdot \frac{\sigma_c}{\gamma_s} \cdot I} = 0.56 \text{ m}$$

The vertical and horizontal displacements, corresponding to the applied loads at a given rotation angle θ , are:

$$\delta_{yF1} = (x_{Gi} - t) \cdot \theta = (1.72 - 0.56) \cdot \theta$$

$$\delta_{yA1} = (x_{Gi} - t) \cdot \theta = (0.87 - 0.56) \cdot \theta$$

$$\delta_{xF2} = y_{Gi} \cdot \theta = 5.61 \cdot \theta$$

$$\delta_{xA1} = y_{Gi} \cdot \theta = 2.93 \cdot \theta$$

Applying the VWP—the angle θ for which the work of the internal and external forces is equal—provides the solution. The load multiplier needed for the activation of the mechanism reads:

$$a_o (A_1 \cdot \delta_{xA1} + F_1 \cdot \delta_{xF1}) + F_2 \cdot \delta_{xF2} - F_1 \cdot \delta_{yF1} - A_1 \cdot \delta_{yA1} = 0 \Rightarrow a_o (g) = 0.068$$

To obtain the capacity curve of an equivalent system of one degree of freedom, equivalent values of the acceleration and displacements must be calculated. The transformation into an SDOF system provides the following (FC being equal to 1.0, corresponding to a level of confidence (LC3) [NTC 2018]):

$$\text{Corresponding equivalent mass: } M^* = \frac{(\sum_i P_i \cdot \delta_{xi})^2}{g \cdot \sum_i P_i \cdot \delta_{xi}^2} = 19.82 \text{ Ton}$$

$$\text{Fraction of participating mass: } e^* = \frac{g \cdot M^*}{\sum_i P_i} = 0.96$$

$$\text{Corresponding equivalent acceleration: } a_o^* = \frac{g \cdot a_o}{e^* FC} = 0.070 \cdot g$$

For the DLS verification, safety is achieved when the acceleration for the activation of the mechanism a_o^* is greater than that specified from the elastic spectrum evaluated for $T = 0$ sec, where $a_g(P_{VR})$ is the PGA for the Cusco region for the selected limit state, in this case the DLS. According to Eurocode 8 (EC8 EN 1998-1 2004, §2.1[4]), the PGA of the elastic response spectrum for the DLS can be derived from one of the reference ULS, multiplied by the importance factor γ_I , under the defined reliability levels. Under the same probability of exceedance equal to 10%, over 95 years (DLS) and 475 years (ULS), the reference PGA is scaled by a reduction factor, here equal to 0.58. The elastic response spectrum for the ULS has a PGA equal to 0.25 g, and S accounts for the type of soil, which is assumed with a value of 1.20 (NTE-0.30 2018):

$$a_o^* = 0.070 \text{ g} \not\geq a_g(P_{VR}) \cdot S = 0.174 \text{ g}$$

Thus, the unrestrained south lateral wall for the DLS is not verified. The addition of transversal buttressing is needed.

Since the rotating plane for the adobe wall is at an average height of 1.5 m from the foundation base, the elastic spectral acceleration of the amplified spectrum for a period T equal to zero should also be checked for the DLS (NTC 2018):

$$\Psi(z) = \frac{z}{H_{total}} = \frac{1.5}{1.5 + 5.86} = 0.20, \quad \gamma = 1 \text{ and } \xi = 5\%$$

$$a_o^* = 0.070 g > S_\theta(0, \xi, z) = a_g(P_{V_h}) \cdot S \cdot \Psi(z) \cdot \gamma \cdot \sqrt{1 + 0.0004 \cdot \xi^2} = 0.035 g$$

Verification for the ULS determines the safety margin with respect to collapse. Two different methods were considered: (a) a linear kinematic analysis with use of the behavior factor q , related to ductility; and (b) a nonlinear kinematic analysis through the capacity spectrum.

The first method (force control) can be verified through the following equation:

$$a_o^* = 0.070 g \not\geq \frac{a_g(P_{V_h}) \cdot S}{q} = 0.15 g, \quad q = 2$$

Accounting for the possibility of amplification at a certain height from the foundation base, the force control method forms:

$$a_o^* = 0.070 g > \frac{a_g(P_{V_h}) \cdot S \cdot \Psi(z) \cdot \gamma \cdot \sqrt{1 + 0.0004 \cdot \xi^2}}{q} = 0.031 g, \quad q = 2$$

The displacement control (nonlinear kinematic analysis) is conducted by comparing the displacement demand from the design spectrum $\Delta_d(T_{ULS})$ with the displacement capacity of the system from the ULS, here d_{ULS}^* . The verification is satisfied if $\Delta_d(T_{ULS}) \leq d_{ULS}^*$. The required finite rotation θ that zeroes the moment M_s is:

$$M_s = \sum_i P_i \cdot R_i \cdot \cos(\beta_i + \theta) = 0 \Rightarrow \theta = 6.49^\circ$$

$$d_{ko} = y_G \cdot \sin \theta = 0.35 \text{ m}$$

where y_G is the barycenter of all masses (wall system and roof mass).

The corresponding displacement of the center of mass for a unit top displacement is:

$$\delta_{x,k} = \frac{y_G}{H} = 0.50 \text{ m}$$

The maximum corresponding displacement d_o^* is:

$$d_o^* = d_{ko} \cdot \frac{\sum_i P_i \cdot \delta_{x,i}^2}{\delta_{x,k} \cdot \sum_i P_i \cdot \delta_{x,ii}} = 0.39 \text{ m}$$

The maximum allowable displacement for the ULS is defined as:

$$d_{ULS}^* = 0.4 \cdot d_o^* = 0.16 \text{ m}$$

The corresponding displacement of the SDOF system, with an equivalent period T_{ULS} , is determined by the following equation and fig. 4.10:

$$T_{ULS} = 1.68\pi \sqrt{\frac{d_{ULS}^*}{a_{ULS}}} = 3.25 \text{ s}$$

$$a_s(T_{ULS}) = a_o^* \cdot \left(1 - \frac{d_{ULS}^*}{d_o^*}\right) = 0.04 g$$

Finally, the displacement demand as derived from the design spectrum of the Peruvian seismic code (NTE-0.30 2018) is depicted in figure 4.10 and given in the following equation:

$$\Delta_d(T_{ULS}) = \left(\frac{T_{ULS}}{2\pi}\right)^2 \cdot 2.5 \cdot Z \cdot U \cdot S \cdot \left(\frac{T_P \cdot T_L}{T_{ULS}^2}\right) = 0.22 \text{ m} \not\leq d_{ULS}^* = 0.16 \text{ m}$$

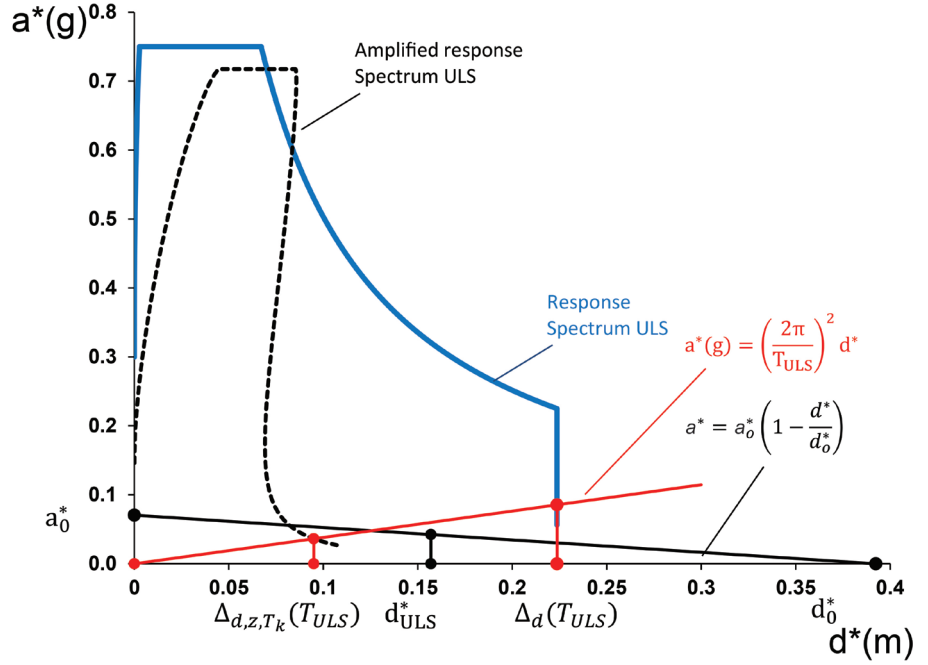
where

$$\begin{aligned} Z &= 0.25 \text{ g,} \\ U &= 1.0, \\ S &= 1.20, \\ T_p &= 0.6 \text{ s, and} \\ T_L &= 2.0 \text{ s.} \end{aligned}$$

Thus, the structure is not verified for the ULS.

FIGURE 4.10.

Graphic verification of nonlinear kinematic analysis in displacement control, at foundation base and at a height z above the foundation base, for the unstrengthened state of the south lateral wall, church of Kuñotambo, Peru. Note the first linear part of the design spectrum (NTE-030 2018, §30.1).



Addressing the possibility of amplification, due to the height z of the rotation plane, from the foundation base, the same displacement verification is performed with the amplified response spectrum of figure 4.10, given by equations 4.16–4.19:

$$\Delta_{d,z,T_k}(T_{ULS}) = \left(\frac{T_{ULS}}{2\pi}\right)^2 \cdot \frac{1.1 \cdot \xi^{-0.5} \cdot \eta(\xi) \cdot a_{z,k}(z)}{1 + [1.1 \cdot \xi^{-0.5} \cdot \eta(\xi) - 1] \cdot \left(\frac{T_{ULS}}{b \cdot T_k} - 1\right)^{1.2}} = 0.10 \text{ m} < d_{ULS}^* = 0.16 \text{ m}$$

where

$$\xi = 5\%, \quad \eta(\xi) = 1.0, \quad \Psi(z) = \frac{1.5}{5.86 + 1.5} = 0.20, \quad \gamma = 1.0, \quad b = 1.1, \quad T_k = 0.63 \text{ s}$$

$$a_{z,k}(z) = S_\theta(T_k, \xi) \cdot \Psi(z) \cdot \gamma \cdot \sqrt{1 + 0.0004 \cdot \xi^2} = 0.15 \text{ g}$$

The maximum of the spectral demand is chosen for the ULS; thus the structure is not verified for the ULS and the addition of transversal buttressing is necessary.

Kinematic Mechanism 2: Strengthened State

Three different strengthening proposals were examined: the placement of four, three, and two buttresses, respectively, with initial dimensions and location (see fig. 4.8). The generic block includes a portion 31 m long of the free span of the south lateral wall of the church of

Kuñotambo. Dimensions and corresponding applied forces for the four-buttress proposal are depicted in figure 4.11 and table 4.2.

FIGURE 4.11.

Geometric configuration of the generic block, church of Kuñotambo, Peru: (a) out-of-plane rotation in section, and (b) three-dimensional view showing placement of four buttresses. Source: Karanikoloudis and Lourenço 2015.

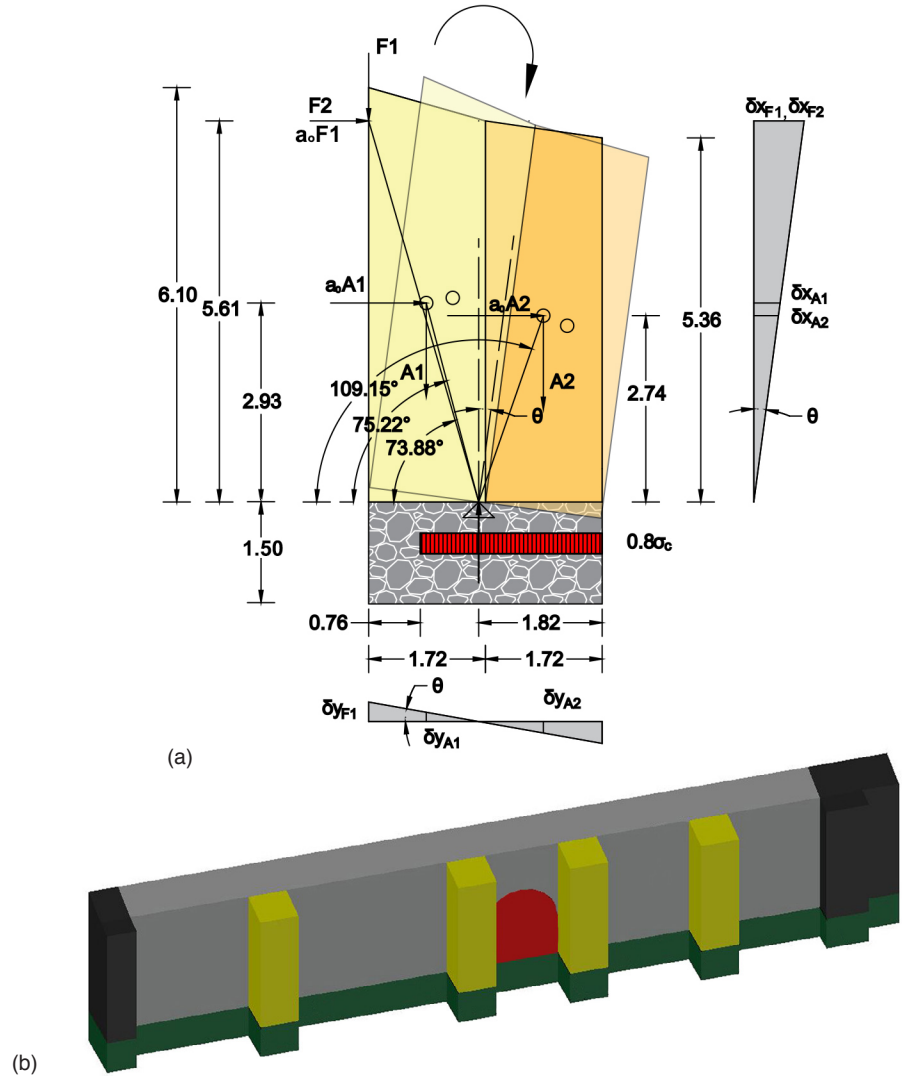


TABLE 4.2.

Load calculation in generic block, with values rounded to two decimal points (Karanikoloudis and Lourenço 2015).

	Area (m ²)	Length (m)	Volume (m ³)	F_i (kN)	$x_{Gi}^{[1]}$ (m)	$y_{Gi}^{[1]}$ (m)	$\delta_{x,i}^{[2]}$	$\delta_{y,i}^{[2]}$	$F_i \cdot \delta_{x,i}$	$F_i \cdot \delta_{x,i}^2$	β_{Gi}^0	R_i	$F_i \cdot R_i$
A1	10.07	31.00	312.17	5931.23	2.59	2.93	0.52	0.14	3097.77	1617.91	75.22	3.03	17968.66
A2	9.43	6.88 ^[3]	64.88	1232.69	0.87	2.74	0.49	0.17	602.06	294.06	109.15	2.90	3579.24
F1	-	31.00	-	326.12	3.44	5.61	1.0	0.29	326.12	326.12	73.88	5.84	1904.38
F2	-	31.00	-	164.92	3.44	5.61	1.0	0.29	-	-	-	-	-

^[1] Measured from the right bottom corner.

^[2] Displacements normalized according to $\delta_{x,i}(F2)$.

^[3] Total length of buttresses 4×1.72 m.

The rotating hinge is located at the barycenter of the effective area. Taking into consideration the uniform stress distribution (see eq. 4.20), the complex area of the base, and the fact that the base area of the buttresses (A_{but}) is under compressive stresses, the total length of the effective area under compression is equal to:

$$l = b_{but} + \frac{\sum F_i - 0.8 \cdot \frac{\sigma_c}{\gamma_s} \cdot A_{but}}{0.8 \cdot \frac{\sigma_c}{\gamma_s} \cdot l_{wall}} = 2.68 \text{ m}$$

resulting in the hinge being located 1.82 m from the exterior corner. The vertical and horizontal displacements, corresponding to the applied loads, at a given rotation angle θ are:

$$\delta_{yF1} = (2 \cdot 1,72 - t) \cdot \theta$$

$$\delta_{yA1} = (x_{GA1} - t) \cdot \theta$$

$$\delta_{yA2} = (t - x_{GA2}) \cdot \theta$$

$$\delta_{xF2} = 5.61 \cdot \theta$$

$$\delta_{xA2} = y_{GA2} \cdot \theta$$

$$\delta_{xA1} = y_{GA1} \cdot \theta$$

The acceleration for the activation of the mechanism by applying the VWP is:

$$a_o(A_1 \cdot \delta_{xA1} + A_2 \cdot \delta_{xA2} + F_1 \cdot \delta_{xF1}) + F_2 \cdot \delta_{xF2} - F_1 \cdot \delta_{yF1} - A_1 \cdot \delta_{yA1} + A_2 \cdot \delta_{yA2} = 0$$

$$\Rightarrow a_o(g) = 0.13$$

To obtain the capacity curve of an equivalent system of SDOF, equivalent values of the acceleration and displacements must be calculated. The transformation into this system provides:

$$\text{Corresponding equivalent mass: } M^* = \frac{(\sum_i P_i \cdot \delta_{xi})^2}{g \cdot \sum_i P_i \cdot \delta_{xi}^2} = 737.23 \text{ Ton}$$

$$\text{Fraction of participating mass: } e^* = \frac{g \cdot M^*}{\sum_i P_i} = 0.97$$

$$\text{Corresponding equivalent acceleration: } a_o^* = \frac{g \cdot a_o}{e^* FC} = 0.14 \cdot g$$

For the DLS, safety is achieved when the acceleration for the activation of the mechanism a_o^* is greater than the one specified from the elastic spectrum evaluated for $T = 0$ sec, where $a_g(P_{VR})$ is 0.25 g and S is equal to 1.20 (NTE-0.30 2018), with a reduction factor of 0.58, as explained in the previous section:

$$a_o^* = 0.14 \text{ g} \not\geq a_g(P_{VR}) \cdot S = 0.174 \text{ g}$$

Thus, the safety of the specific buttressing solution in the south lateral wall for the DLS is not verified.

As discussed in the previous section, since the level of the rotating plane for the adobe wall is at a height of 1.5 m from the foundation base, the elastic spectral acceleration of the amplified spectrum for a period T equal to zero should also be checked for the DLS (NTC 2018). With average height accounted for, the check reads:

$$\Psi(z) = \frac{z}{H_{total}} = \frac{1.5}{1.5 + 5.73} = 0.21, \gamma = 1 \text{ and } \xi = 5\%$$

$$a_o^* = 0.14 \text{ g} > S_e(0, \xi, z) = a_g(P_{VR}) \cdot S \cdot \Psi(z) \cdot \gamma \cdot \sqrt{1 + 0.0004 \cdot \xi^2} = 0.036 \text{ g}$$

Regarding verification for the ULS, the force control method, with the use of the behavior factor q , is given through the following equation:

$$a_0^* = 0.14 \text{ g} \not\geq \frac{a_g(P_{V_r}) \cdot S}{q} = 0.15 \text{ g}, q = 2$$

Accounting for the possibility of amplification at a certain height from the foundation base, the force control method provides:

$$a_0^* = 0.14 \text{ g} > \frac{a_g(P_{V_r}) \cdot S \cdot \Psi(z) \cdot \gamma \cdot \sqrt{1 + 0.0004 \cdot \xi^2}}{q} = 0.031 \text{ g}, q = 2$$

For nonlinear kinematic analysis through the capacity spectrum (NTE-0.30 2018), the displacement demand from the design spectrum, here $\Delta_d(T_{ULS})$, is compared with the displacement capacity of the system from the ULS, here d_{ULS}^* , under the condition $\Delta_d(T_{ULS}) \leq d_{ULS}^*$.

The required finite rotation θ that zeroes the moment M_s is:

$$M_s = \sum_i P_i \cdot R_i \cdot \cos(\beta_i + \theta) = 0 \Rightarrow \theta = 15.72^\circ$$

$$d_{ko} = y_G \cdot \sin \theta = 0.82 \text{ m}$$

where y_G is the barycenter of all masses (wall system and roof mass).

The corresponding displacement of the center of mass for a unit top displacement is:

$$\delta_{x,k} = \frac{y_G}{H} = 0.51 \text{ m}$$

The maximum corresponding displacement d_o^* is:

$$d_o^* = d_{ko} \cdot \frac{\sum_i P_i \cdot \delta_{x,i}^2}{\delta_{x,k} \cdot \sum_i P_i \cdot \delta_{x,ii}} = 0.90 \text{ m}$$

The maximum allowable displacement for the ULS is defined as:

$$d_{ULS}^* = 0.4 \cdot d_o^* = 0.36 \text{ m}$$

The corresponding displacement of the SDOF system with an equivalent period T_{ULS} is shown in the following equation and figure 4.12:

$$T_{ULS} = 1.68\pi \sqrt{\frac{d_{ULS}^*}{a_{ULS}^*}} = 3.52 \text{ s}$$

$$a_s(T_{ULS}) = a_0^* \cdot \left(1 - \frac{d_{ULS}^*}{d_o^*}\right) = 0.08 \text{ g}$$

Finally, the displacement demand as derived from the design spectrum of the Peruvian seismic code (NTE-0.30 2018) is depicted above (see fig. 4.12) and is given by the equation:

$$\Delta_d(T_{ULS}) = \left(\frac{T_{ULS}}{2\pi}\right)^2 \cdot 2.5 \cdot Z \cdot U \cdot S \cdot \left(\frac{T_p \cdot T_L}{T_{ULS}^2}\right) = 0.22 \text{ m} < d_{ULS}^* = 0.36 \text{ m}$$

where

$$Z = 0.25 \text{ g},$$

$$U = 1.0,$$

$$S = 1.20,$$

$$T_p = 0.6 \text{ s, and}$$

$$T_L = 2.0 \text{ s.}$$

Addressing the possibility of amplification due to the height z of the rotation plane from the foundation base, the same displacement verification is performed with the amplified response spectrum (fig. 4.12), given by equations 4.16–4.19:

$$\Delta_{d,z,T_k}(T_{ULS}) = \left(\frac{T_{ULS}}{2\pi}\right)^2 \cdot \frac{1.1 \cdot \xi^{-0.5} \cdot \eta(\xi) \cdot a_{z,k}(z)}{1 + [1.1 \cdot \xi^{-0.5} \cdot \eta(\xi) - 1] \cdot \left(\frac{T_{ULS}}{b \cdot T_k} - 1\right)^{1.2}} = 0.03 \text{ m} < d_{ULS}^* = 0.34 \text{ m}$$

where

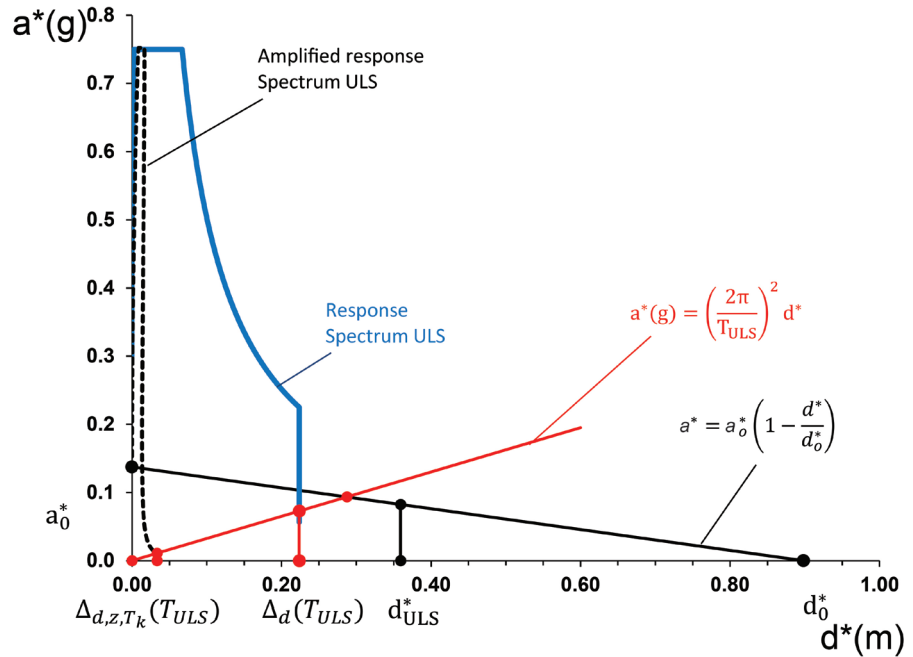
$$\xi = 5\%, \quad \eta(\xi) = 1.0, \quad \Psi(z) = \frac{1.5}{5.61 + 1.5} = 0.21, \quad \gamma = 1.0, \quad b = 1.1, \quad T_k = 0.27 \text{ s}$$

$$a_{z,k}(z) = S_e(T_k, \xi) \cdot \Psi(z) \cdot \gamma \cdot \sqrt{1 + 0.0004 \cdot \xi_k^2} = 0.15 \text{ g}$$

The maximum of the spectral demand is chosen for the ULS; thus the structure is verified for the ULS under the displacement control method.

FIGURE 4.12.

Graphic verification of nonlinear kinematic analysis in displacement control at foundation base and at a height z above the foundation base, for the strengthened state of the south lateral wall of the church of Kuñotambo, Peru, with four additional buttresses. Note the first linear part of the design spectrum (NTE-0.30 2018, §30.1).



This means the structure is safe under structural failure (ULS) only for the displacement control method. It must be noted that given the presence of wall paintings in the interior surfaces of the church, the verification of the strengthened wall for the DLS is essential and the possibility of cracking under lower-intensity earthquakes is not acceptable. Additional performance criteria on material properties are required. Note also that a seismic safety coefficient of 2 provides additional margin.

This procedure for four buttresses was followed for the remaining two strengthening proposals (three buttresses and two buttresses, evenly spaced). Yet, the design verifications for the DLS and the force control for the ULS are not fulfilled for all three proposals (table 4.3). The key factor appears to be the low compressive strength of adobe masonry, which affects the rotation line of the substructure. Increased performance criteria are required in a zone of interest located on the lower half of the new adobe buttresses, together with the lower external portion of the current adobe wall.

TABLE 4.3.

Results of kinematic analysis for unstrengthened and strengthened conditions of the DLS and ULS (Karanikoloudis and Lourenço 2015).

		DLS				ULS			
Increased performance criteria at the base of new adobe masonry ^[1]		×		↙		×		↙	
Unstrengthened conditions		$a_o^* = 0.07 \text{ g}$ $< \frac{a_g(P_{V_R}) \cdot S}{q} = 0.17 \text{ g}$	×	-	-	$a_o^* = 0.07 \text{ g}$ $< \frac{a_g(P_{V_R}) \cdot S}{q} = 0.15 \text{ g}$ $\Delta_d(T_{ULS}) = 22.4 \text{ cm}$ $< d_{ULS}^* = 15.7 \text{ cm}$	×	-	-
Strengthened conditions	4 Buttresses	$a_o^* = 0.14 \text{ g}$ $< \frac{a_g(P_{V_R}) \cdot S}{q} = 0.17 \text{ g}$	×	$a_o^* = 0.34 \text{ g}$ $> \frac{a_g(P_{V_R}) \cdot S}{q} = 0.17 \text{ g}$	↙	$a_o^* = 0.14 \text{ g}$ $< \frac{a_g(P_{V_R}) \cdot S}{q} = 0.15 \text{ g}$ $\Delta_d(T_{ULS}) = 22.4 \text{ cm}$ $< d_{ULS}^* = 39.5 \text{ cm}$	×	$a_o^* = 0.34 \text{ g}$ $> \frac{a_g(P_{V_R}) \cdot S}{q} = 0.15 \text{ g}$ $\Delta_d(T_{ULS}) = 22.4 \text{ cm}$ $< d_{ULS}^* = 52.8 \text{ cm}$	↙
	3 Buttresses	$a_o^* = 0.12 \text{ g}$ $< \frac{a_g(P_{V_R}) \cdot S}{q} = 0.17 \text{ g}$	×	$a_o^* = 0.31 \text{ g}$ $> \frac{a_g(P_{V_R}) \cdot S}{q} = 0.17 \text{ g}$	↙	$a_o^* = 0.12 \text{ g}$ $< \frac{a_g(P_{V_R}) \cdot S}{q} = 0.15 \text{ g}$ $\Delta_d(T_{ULS}) = 22.4 \text{ cm}$ $< d_{ULS}^* = 40.1 \text{ cm}$	×	$a_o^* = 0.31 \text{ g}$ $> \frac{a_g(P_{V_R}) \cdot S}{q} = 0.15 \text{ g}$ $\Delta_d(T_{ULS}) = 22.4 \text{ cm}$ $< d_{ULS}^* = 46.7 \text{ cm}$	↙
	2 Buttresses	$a_o^* = 0.11 \text{ g}$ $< \frac{a_g(P_{V_R}) \cdot S}{q} = 0.17 \text{ g}$	×	$a_o^* = 0.27 \text{ g}$ $> \frac{a_g(P_{V_R}) \cdot S}{q} = 0.17 \text{ g}$	↙	$a_o^* = 0.11 \text{ g}$ $< \frac{a_g(P_{V_R}) \cdot S}{q} = 0.15 \text{ g}$ $\Delta_d(T_{ULS}) = 22.4 \text{ cm}$ $< d_{ULS}^* = 27.8 \text{ cm}$	×	$a_o^* = 0.27 \text{ g}$ $> \frac{a_g(P_{V_R}) \cdot S}{q} = 0.15 \text{ g}$ $\Delta_d(T_{ULS}) = 22.4 \text{ cm}$ $< d_{ULS}^* = 44.0 \text{ cm}$	↙

^[1] The performance criteria are set by locally increasing the average compressive strength of adobe masonry from 0.45 MPa to 1 MPa. The zone of interest is located on the lower half of the new adobe buttresses, together with the lower external portion of the current adobe wall.

A proposed solution is to introduce stabilized adobe blocks containing a certain percentage of lime and additives, such as fly ash, low-fired brick dust, or pozzolana, as well as the consolidation and partial replacement of existing adobe blocks. The performance criteria are set by locally increasing the average compressive strength of adobe masonry to 1 MPa, namely an increase of 120%. It is advisable to verify the performance criteria through material capacity testing. Under these new criteria, and with a partial seismic coefficient γ_s of 2.0 (NTC 2018, §8.7.1), the nonlinear kinematic analysis results for four, three, and two evenly spaced buttresses present a high capacity margin (see table 4.3).

In all the previously mentioned cases, extensive consideration was given to connecting the buttresses to the wall by installing timber beams at various levels. However, a more conservative approach can be taken with the buttresses separated from the south lateral

wall. Here, the separated buttresses, having the same configuration in terms of number, width, and spacing to the ones in the current section, experience a rocking effect from the adjoining wall. Because of friction along the interface, lateral forces from the lateral wall are transferred to the buttresses. Two hypotheses were considered for the south wall and the four buttresses of 1.72 m in length and an appropriate design width: for hypothesis A, in acting with the wall, the system of buttresses assumes all of the equivalent seismic load from the lateral wall (fig. 4.13a); for hypothesis B, in acting independently of the wall, the lateral wall counteracts the maximum lateral load in an unrestrained condition, similar to section “Kinematic Mechanism 1: Unstrengthened State,” equal to 0.07 g, and the system of buttresses acts independently from the wall by assuming the residual lateral load. Both hypotheses, as well as dimensions and applied forces, are diagrammed in figure 4.13.

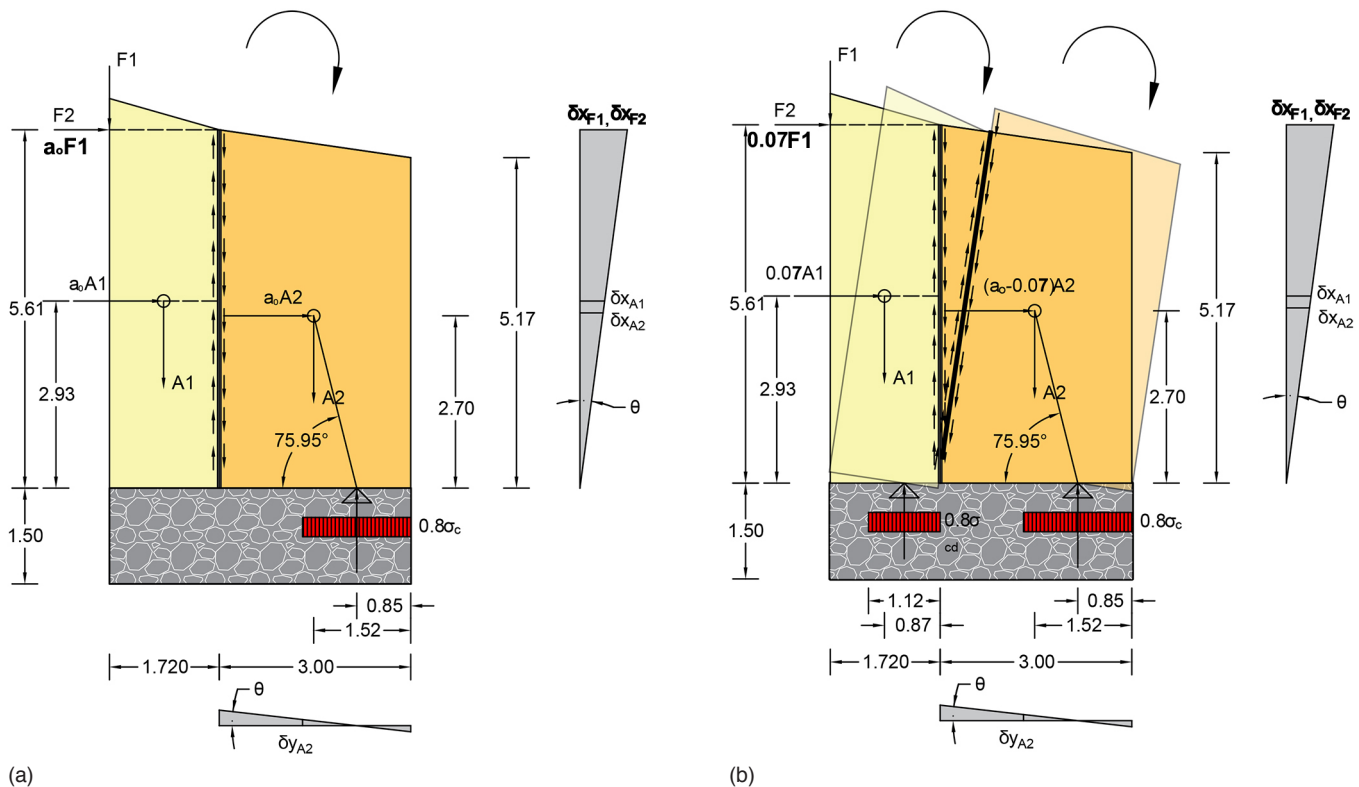


FIGURE 4.13. Geometric configurations of the generic block with separation of the buttresses from the church's south lateral wall: (a) in hypothesis A, the buttresses act together with the wall; and (b) in hypothesis B, the buttresses act independently of the wall. Note the indicative buttress width of 3.0 m. Source: Karanikoloudis and Lourenço 2015.

For both hypotheses, it was necessary to increase the dimensions of the buttresses. This was determined by progressively increasing the length of the buttresses until the DLS and ULS verifications were satisfied, the latter in both force control and displacement control. Here, it is noted that the higher capacity demand is from the DLS. Also, increased performance criteria were accounted for at the base of the new buttresses. The required length for the buttresses was 4.7 m for hypothesis A and 4.3 m for hypothesis B (Karanikoloudis and Lourenço 2015).

The hypothesis of buttresses disconnected from the system of walls proved to be undesirable, leading to large dimensions. Thus, proper connectivity is needed between the existing walls and the new buttresses, namely by inserting horizontal timber elements at various heights along the interfaces and extending the system of beams at the top eaves of the lateral walls and over the corner junctions (Karanikoloudis and Lourenço 2015).

Simplified Finite Element Modeling Approaches for Seismic Assessment

Although the use of finite element modeling (FEM) for the analysis of historic buildings can be demanding in both time and technical capacity, this technique is receiving increasing attention in spite of the uncertainties present in many historic structures.

Conventional contemporary structures are usually analyzed by FEM based on the following two hypotheses: linear elastic behavior and the use of one-dimensional (i.e., beam or truss) or two-dimensional (plate or membrane, slab or shell) elements. This is appropriate, since materials that resist tension, such as timber or steel, are adopted, or reinforcement is placed in areas where tension is expected, as in the case of reinforced concrete, and structural elements can be properly modeled using linear (one-dimensional) elements and plate-type (two-dimensional) elements.

The two hypotheses usually are not applied in analyzing historic buildings due to the mechanical characteristics of the materials, which are mostly masonry-based. These characteristics result in recurring cracking, which limits the use of linear elastic behavior, and the need to use tri-dimensional elements to represent the large dimensions of the structural elements (walls and vaults) and the buildings' geometric complexity. Nevertheless, it is expected that FEM can be applied and the obtained results used in the diagnosis process, safety assessment, and strengthening design of historic buildings. In order to accomplish this, a well-calibrated model must compare the observed structural damage with the analytical stress concentration in the model to be used as a tool to evaluate the soundness of the possible strengthening interventions.

Summary of Types of Finite Element Analysis

This section describes the different types of finite element analysis (FEA) available. These methods are related to material behavior (table 5.1), structural elements (table 5.2), information needed (table 5.3), and expected results (table 5.4). From these alternatives, a strategy for a simplified seismic analysis for historic buildings can be established.

TABLE 5.1.
Methods of FEA related to linear elastic and nonlinear material behavior.

Method of analysis	Material behavior	
	Linear elastic	Nonlinear
Static (linear)	Yes	No
Pushover (nonlinear)	No	Yes
Response spectrum (dynamic)	Yes	No
Linear time history analysis (dynamic)	Yes	No
Nonlinear time history analysis (dynamic)	No	Yes

TABLE 5.2.

Methods of FEA related to structural elements.

Method of analysis	Structural element		
	Linear 1D	Plane 2D	Solid 3D
Static (linear)	Yes	Yes	Yes
Pushover (nonlinear)	Yes	Yes	No
Response spectrum (dynamic)	Yes	Yes	Yes
Linear time history analysis (dynamic)	Yes	Yes	No
Nonlinear time history analysis (dynamic)	Yes	Yes	No

TABLE 5.3.

Methods of FEA related to required information.

Method of analysis	Information required	
	Linear elastic	Nonlinear
Static (linear)	<ul style="list-style-type: none"> • Geometry • Loads: vertical and horizontal • External constraints • Connections between elements • Young's modulus • Ultimate strength • Limit strain or displacement 	No
Pushover (nonlinear)	• As for static (linear)	• Material and joints inelastic behavior
Response spectrum (dynamic)	<ul style="list-style-type: none"> • As for static (linear) • Mass distribution • Design spectrum 	No
Linear time history analysis (dynamic)	<ul style="list-style-type: none"> • As for static (linear) • Mass distribution • Seismic acceleration signal • Damping 	No
Nonlinear time history analysis (dynamic)	• As for linear time history analysis	• Material and joints inelastic behavior

TABLE 5.4.

Methods of FEA related to expected results.

Method of analysis	Expected result	
	Linear elastic	Nonlinear
Static (linear)	<ul style="list-style-type: none"> • Elastic stresses and strains • Areas of stress and strain concentration 	No
Pushover (nonlinear)	No	<ul style="list-style-type: none"> • Inelastic capacity curve (force vs. displacement) • Cracking and crushing areas • Failure mechanism
Response spectrum (dynamic)	<ul style="list-style-type: none"> • Natural frequencies and vibration modes (allowing to calculate stress, strain, and displacement envelopes) • Elastic stresses and strains • Areas of stress concentration 	No
Linear time history analysis (dynamic)	<ul style="list-style-type: none"> • Dynamic elastic stresses and strains • Dynamic areas of stress and strain concentration 	No
Nonlinear time history analysis (dynamic)	No	<ul style="list-style-type: none"> • Dynamic inelastic behavior of the structure, elements, and joints, including energy dissipation and global hysteresis • Cracking and crushing areas • Failure mechanism

According to the type of analysis adopted, different information regarding the material behavior/properties is required. Static linear analysis and response spectrum analysis only require linear elastic information, while pushover analysis requires nonlinear information regarding material properties (table 5.1). Time history analysis can be carried out in either the linear or nonlinear material state. Note that geometric nonlinear analysis is not consid-

ered, as it usually is not relevant for historic structures. This might not be the case in, for example, flat vaults, thin and long vaults, or in heavily compressed and slender columns.

The same process is reflected in tables 5.2, 5.3, and 5.4 regarding structural elements type, general information required, and expected results, respectively. In table 5.2, linear 1D indicates a linear-type element in which one dimension is much larger than the other two (beam or truss); plane 2D indicates a plane-type element in which one dimension is much smaller than the other two (wall, slab, or shell); and solid 3D indicates a fully three-dimensional element (often denoted as volume element or brick). Note that solid 3D is shown for static linear and response spectrum analysis only from the perspective of current applications and limiting analysis time, as there is no restriction from using solid 3D for the other methods of analysis.

Simplified Finite Element Analysis

In order to have a simplified FEA, the following assumptions can be made: (a) the material behavior is elastic and remains in the linear range; (b) the structural components are modeled using one-dimensional (linear) and two-dimensional (usually shell) elements; and (c) the type of analysis can be static (linear) or response spectrum (dynamic).

Based on these assumptions, the information requested for the simplified analysis in either format is quite similar (see table 5.3) and varies only in requiring the loads for the static method and the design spectrum for the response spectrum method. The expected results are also similar (see table 5.4). Both methods are able to determine the elastic strains and stresses as well as the areas of stress concentration. With the response spectrum method, additional information regarding natural frequencies and vibration modes can be obtained.

It is well known that the accuracy and confidence of the results of a structural analysis are highly dependent on the confidence of the information given to the numerical program as input data. Regarding the information needed for the analysis and the expected results, table 5.5 provides a ranking of confidence level: low, medium, high. Young's modulus has a low level of confidence, since this variable is highly dependent on the moisture in the

TABLE 5.5.

Level of confidence (low, medium, high) regarding structural analysis input and output.

Information required	Geometry	High
	Vertical loads	High
	Horizontal loads	Medium
	Mass distribution	High
	Connection between elements	Medium
	Design spectrum	High
	Young's modulus	Low
	Ultimate strength	Medium
	Limit strain/displacement	Low
Expected results	Elastic stresses	Medium-low
	Elastic strains	Low
	Natural frequencies	Low
	Modes of vibration	Medium
	Stress concentration	Medium-high

walls and the natural dispersion of results due to other factors. On the other hand, the highest level of confidence would be on the geometry of the structure and vertical loads, since these are variables that normally can be determined very accurately.

Regarding the expected results, those that depend on Young's modulus, including strains and frequencies, have the lowest level of confidence. On the other hand, stresses have a medium-high confidence level because the stresses due to vertical loads can be computed very accurately, but when combined with seismic stresses, the confidence level is lower. The concentration of stresses can be accurately predicted even with linear elastic analysis; this has been corroborated in several analyses of structures when compared with visual inspection of the stress concentration locations.

Traditional code requirements for structural safety verification follow either the strength criteria—in which the requested strength is compared with the ultimate strength given by the code—or the displacement criteria—in which the computed lateral maximum displacement is compared with the limit lateral displacement given by the code. In the case of historic buildings, both approaches have medium to low accuracy confidence. The computed values of stress and strains, as well as the input material stress and strain properties, have medium to low confidence; therefore, the code safety verification must be used with caution; also, the areas of stress concentration and the vibration modes have the highest degree of confidence (see table 5.5). It is possible to have reasonable confidence in the strength capacity of the walls if they are free of deterioration or if conservation actions have been carried out or planned. Note that structural analysis is only one component of safety assessment per the 2001 International Scientific Committee on the Analysis and Restoration of Structures of Architectural Heritage (ISCARSAH) recommendations, and should be combined with historical, inductive, and experimental approaches.

Verification of Structural Safety Using the Areas of Stress Concentration

The areas of stress concentration in a historic building depend on the material properties, such as Young's modulus and strength capacity. They also depend on the geometry and the type of connections between elements, both variables with a medium to high level of confidence. Therefore, it is reasonable to expect a sound degree of confidence in this result. The areas of stress concentration can be used to validate the structural model of the building in its actual condition by comparing the numerical analysis with the damage that occurred to the building in the past. If the evidence of damage coincides with the area of stress concentration in the model, a good representation of the structural behavior can be expected.

Once the structural model of the building in its actual condition is validated, the structural interventions can be included in the original model to obtain the retrofitted model. This new model can be used to verify that the stress concentration has spread in a wider area and with lesser stress and strain values and, in turn, to validate the proposed structural intervention. In the section "Examples of simplified FEA," an example is given to illustrate this procedure.

Verification of Structural Safety Using the Vibration Modes

The use of the vibration mode is another way to determine the more vulnerable areas of the building that, in this case, are related to the amplitude of displacements. Since the analysis is linear and elastic, the displacements are proportional to the stresses and the area of maximum stresses usually coincides with the area of maximum amplitude of displacements.

Here, the objective is similar to that of the verification using stress concentration as described above. By comparing the results before and after the structural intervention, it

is possible to ascertain whether the proposed intervention lowers the natural period of the structure, which means the structure is stiffer and therefore lower displacements are expected for the same level of input. Note also that a stiffer structure usually has a higher elastic seismic demand than a slender one. For historic masonry buildings, this is often not the case, because the periods of the unstrengthened structure are already rather low.

This criterion is more qualitative than quantitative and is particularly useful to understanding the effect of the retrofitting when showing the modes in motion. Again, the section “Examples of simplified FEA” provides an example.

Examples of Simplified Finite Element Analysis

This section presents two examples of simplified FEA of historic masonry structures and shows how these analyses can be used to assess the current behavior of a structure and to measure the impact and effectiveness of a proposed intervention.

Application Example: The Church of Kuñotambo, Peru

A model of the adobe church of Kuñotambo in its actual condition is shown in figure 5.1a. Because of deterioration and lack of maintenance, the north wall is now a long, unsupported wall with no buttresses. However, the sacristy and the baptistery, along with two remaining buttresses, provide lateral support to the south wall. A seismic response spectrum analysis performed in the north–south direction shows a very high tensile stress concentration in the north wall (see fig. 5.1b). The roof of the church, constructed with A-type wooden truss, is not included in the model because it has minimal interaction with the adobe walls. The mass of the roof is distributed along the top of the north and south walls.

The initial structural intervention proposed for the church would provide lateral support to the north wall. It comprises the inclusion of four buttresses in the north wall and thirteen wooden tie beams anchored in the north and south walls, as shown in figure 5.2a.

FIGURE 5.1. Model of the church of Kuñotambo, Peru, in its actual condition: (a) model showing the thickness of the walls, and (b) model showing seismic analysis in the north–south direction for a shell element model in SAP2000. Note the tensile stress concentration in the north wall (maximum stress level 0.85 MPa).

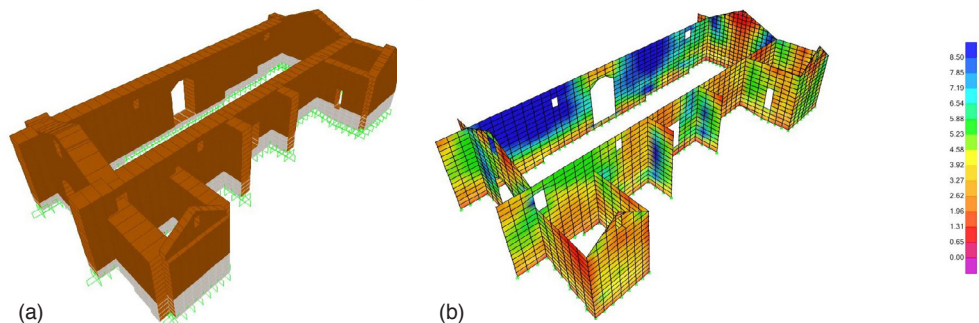
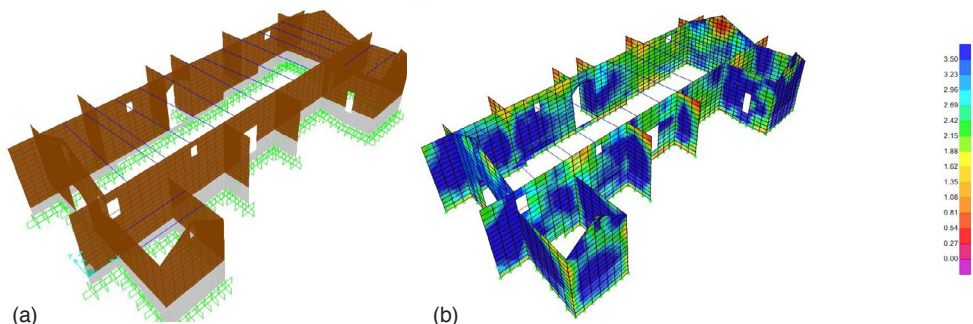


FIGURE 5.2. Model of the initial structural intervention for the church of Kuñotambo, Peru: (a) model of the proposed retrofit, and (b) model showing seismic analysis in the north–south direction for a shell element model in SAP2000. Note the tensile stress concentration in the north wall (maximum stress level 0.35 MPa, less than half of the actual condition model).



The retrofitted model was then subjected to a seismic analysis in the north–south direction with the same PGA as in the initial model. This resulted in a wider distribution of stresses due to the action of the buttresses and the wooden tie beams. The maximum stresses are in the order of 40% compared with the initial unreinforced model.

Vibration mode is another way to determine the more vulnerable areas of the building, as stated above. In figure 5.3, the first and second modes of vibration show that the north wall is the one with greater displacements and coincide with the areas of maximum stresses from the previous analysis. The first mode has a period of 0.5 s and the second mode has a period of 0.32 s. The two more important modes (with higher participant mass) for the retrofitted model are shown in figure 5.4; these are the second and twelfth modes, respectively. The second mode (fig. 5.4a) has a vibration period of 0.41 s and corresponds to the north–south direction, and the twelfth mode (fig. 5.4b), with a vibration period of 0.23 s, corresponds to the east–west direction. A reduction in the period of vibration is observed, meaning that the structure is stiffer. Therefore, a lower displacement is expected for the same input signal, even though the north wall is still the most demanding in displacement with respect to the rest of the building.

FIGURE 5.3. Model showing actual condition of the church of Kuñotambo, Peru: (a) first vibration mode, $T = 0.5$ s; and (b) second vibration mode, $T = 0.32$ s.

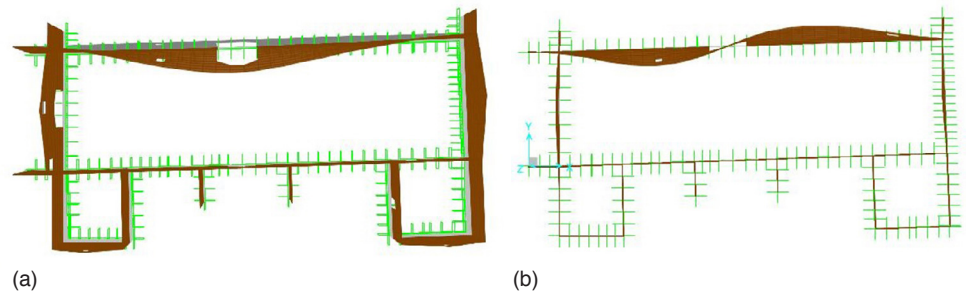
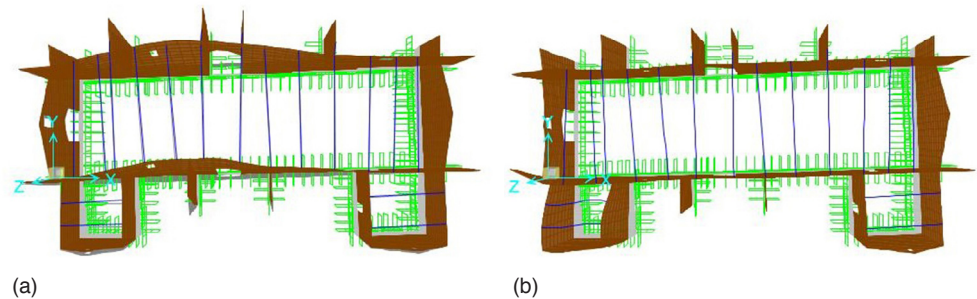


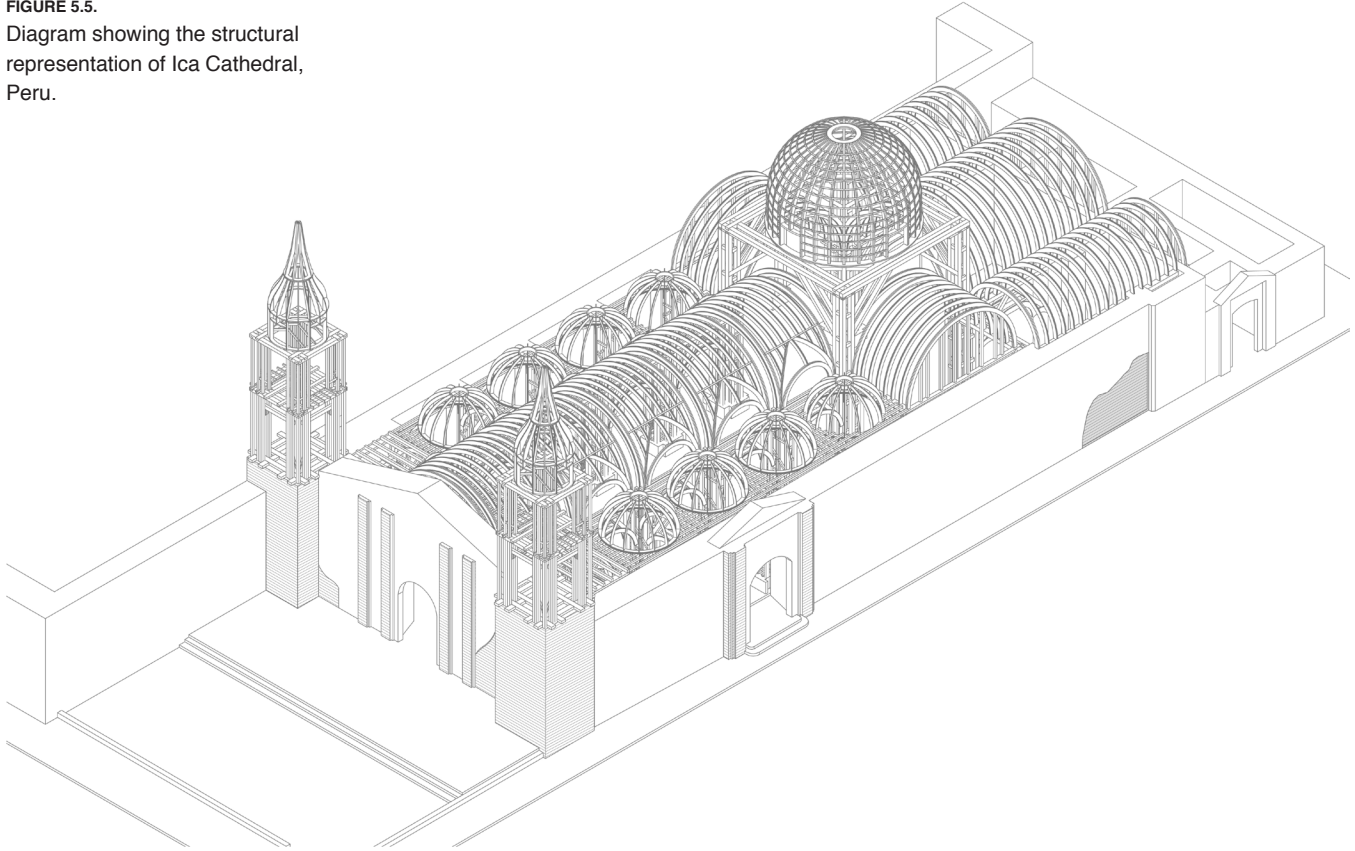
FIGURE 5.4. Model of retrofit proposal for the church of Kuñotambo, Peru, showing the modes with higher participant mass: (a) second vibration mode, $T = 0.41$ s; and (b) twelfth vibration mode, $T = 0.23$ s.



Application Example: Partial Substructure Analysis of Ica Cathedral, Peru

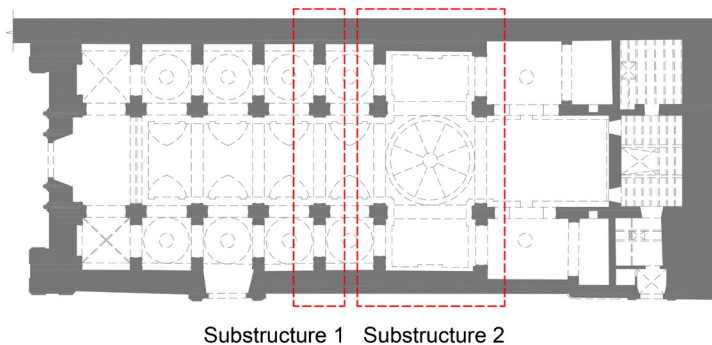
As part of the strengthening proposal of Ica Cathedral, the analysis of the building in subportions was necessary. Its design is presented in figure 5.5. The cathedral is a combination of a timber structure with adobe, brick, and rubble stone. The external envelope of the building is composed of masonry walls and the internal structure is completely made up of timber elements. The roof of the building is supported by the timber structure, and the lateral walls are believed to be connected to the structure by timber elements embedded in the walls. Ica Cathedral's global seismic behavior is governed by the capacity of the walls to resist lateral forces. As long as the walls remain standing, the only possibility of damage is a local collapse of the timber structure—which, in fact, occurred during the Pisco earthquake in August 2007.

FIGURE 5.5.
Diagram showing the structural representation of Ica Cathedral, Peru.



A simplified analysis requires the modeling of the cathedral's portions in substructures, each representing one particular aspect of the seismic behavior of the building. Therefore, it was decided to model two transversal portions of the structure: the transept and one bay of the main nave, known as substructure 1 and substructure 2, respectively (fig. 5.6). This was possible because the roof of the building did not act as a rigid diaphragm.

FIGURE 5.6.
Plan view of Ica Cathedral, Peru, showing the two modeled substructures, each representing an aspect of the seismic behavior of the building: substructure 1 = the transept; substructure 2 = bay of the main nave.



Substructure 1 includes two types of elements (fig. 5.7): a shell element for the portion of lateral walls, and beam elements (straight and curved) for the timber elements. All timber elements are connected by pinned connections. The timber elements support the weight of the tributary area of the roof, while the wall elements bear their own weight.

The analysis can be static (and linear here), assuming a distribution of lateral forces proportional to the mass of the structure. As shown in figure 5.8, the lateral displacement of the substructure is controlled by the interaction between the timber elements and the wall up to its top level, and the timber arch is free to laterally displace. In this model, the mechanical properties of the wall can be improved to an acceptable level of displacement and stress.

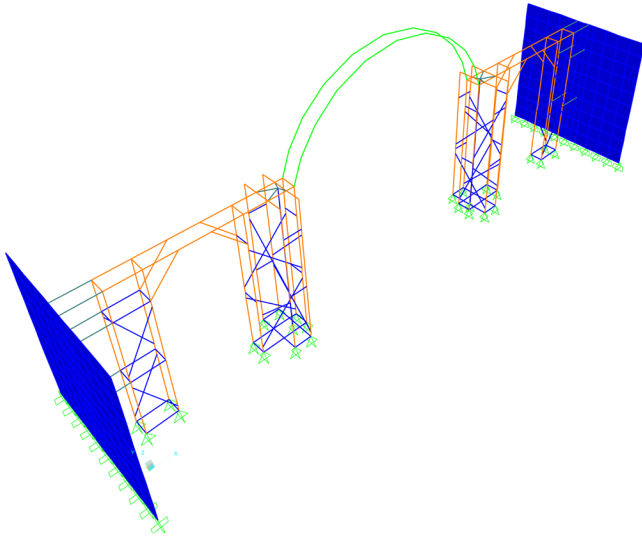


FIGURE 5.7. Isometric view of the model of substructure 1 of Ica Cathedral, Peru; substructure 1 corresponds to the transept.

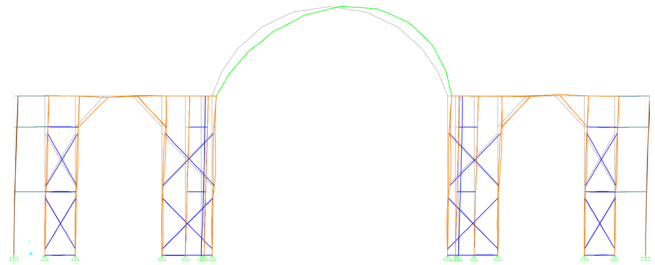


FIGURE 5.8. View of the model of Ica Cathedral, Peru, showing the displacement of substructure 1 due to lateral equivalent seismic force.

Substructure 2 is more complex because of the inclusion of the transept dome and the lateral vaults (fig. 5.9). As in substructure 1, the timber elements are linear with pinned connections and the lateral walls are shell elements. The weight of the roof is entirely supported by the timber structure.

The analysis can be static, assuming a distribution of lateral forces proportional to the mass of the structure. As shown in figure 5.10, the lateral displacement of the substructure is controlled by the interaction between the timber elements and the wall up to its top level, whereas the vaults and dome are free to move laterally.

In this model, for the lower part, the mechanical properties of the wall can be improved to an acceptable level of displacement and stress. For the upper timber structure, timber elements or connectors can be added to control the lateral displacement. In general, timber structures are able to stand larger lateral displacements without losing their load capacity, and the critical points are the connections.

Other substructures of Ica Cathedral that can be studied include the lateral masonry envelope isolated from the timber structure, the facade wall, and the timber structure of the cathedral's towers.

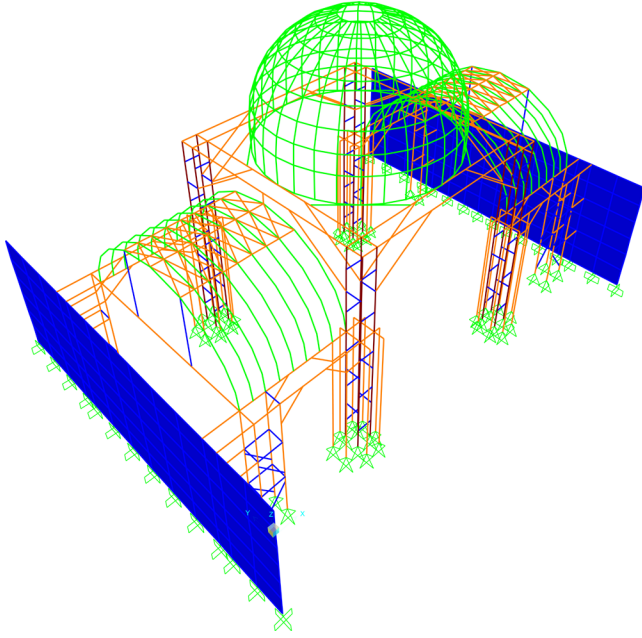


FIGURE 5.9. Isometric view of the model of substructure 2 of Ica Cathedral, Peru; substructure 2 corresponds to the bay of the main nave.

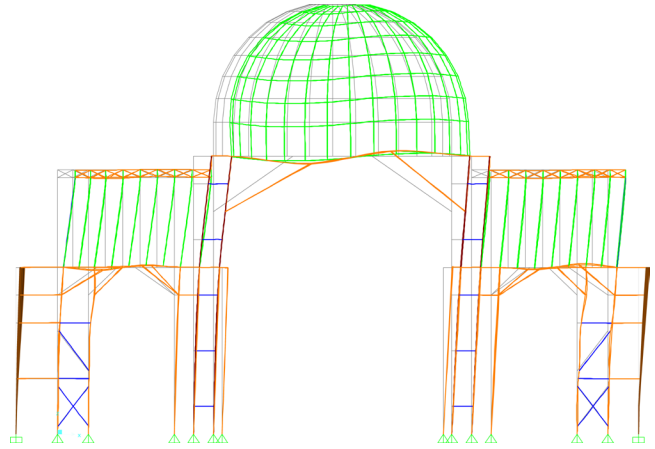


FIGURE 5.10. View of the model of Ica Cathedral, Peru, showing the displacement of substructure 2 due to lateral equivalent seismic force.

Examples of Design Calculations

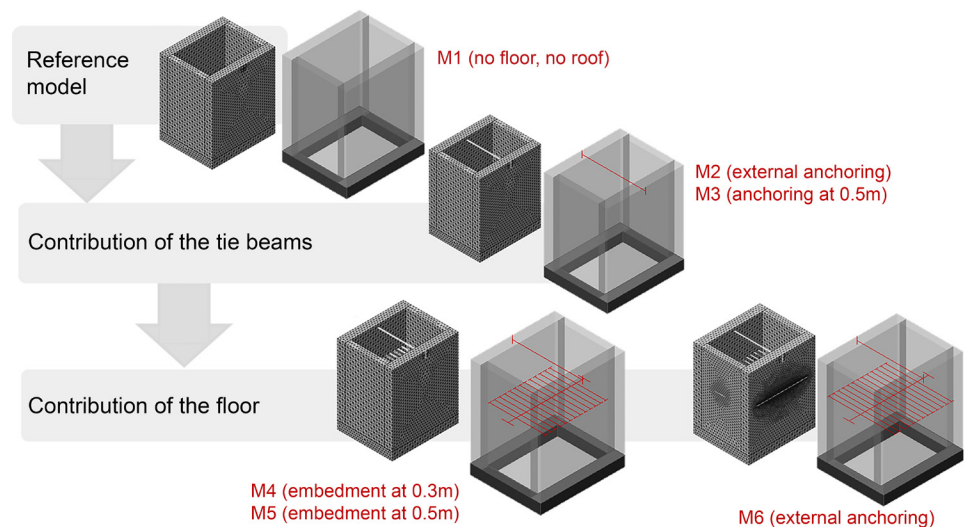
Chapter 6 presents examples of design calculations and prescribed interventions, considering the techniques and methods of analysis described in chapters 3–5. The examples involve two Peruvian case studies: the seismic assessment of Casa Arones in Cusco and the strengthening proposal for Ica Cathedral. It must be emphasized that these are presented as case studies of the application of simple calculations. They are not intended as a strict course of action to be followed; instead, it is recommended that professionals consult this methodology in designing their own interventions.

Seismic Assessment of Casa Arones, Cusco, Peru

This section addresses part of the structural performance and the seismic assessment of Casa Arones, one of four building prototypes studied during the Seismic Retrofitting Project (SRP) (Cancino et al. 2012) under the auspices of the GCI. Casa Arones is a representative example of a traditional house, or *casa cuzqueña*, located in the historic center of Cusco. A full and detailed structural assessment is in Lourenço et al. (2019).

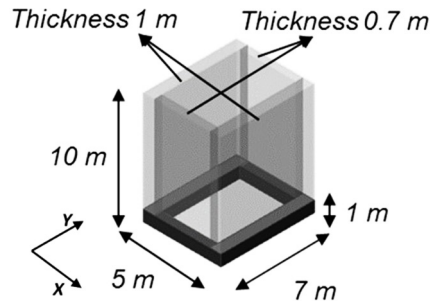
Several possible configurations were tested using a set of representative models with dimensions and material properties referring to Casa Arones. Starting from a reference model, other models were created and considered for the study, both with and without floor and roof ties (fig. 6.1). Limit macro-block analysis was carried out to assess the seismic performance of the building without horizontal diaphragms.

FIGURE 6.1. Examples of reference models created and considered in the study of Casa Arones, Peru. Source: Lourenço et al. 2019.



Dimensions of reference model 1 are presented in figure 6.2. Model 1 consists of a two-story building 9 m tall with a rubble stone masonry foundation 1 m high. The adobe walls—whose thickness corresponds to 1 m for longitudinal and 0.7 m for transversal—define a plan space of 5 × 7 m. The roof is assumed to transfer loads to the longitudinal walls and is defined in the form of a vertical pressure assumed equal to 5.6 kN/m² and a horizontal thrust of 3 kN/m² (Lourenço et al. 2019).

FIGURE 6.2.
Dimensions of reference model 1, Casa Arones, Peru, including wall thickness and plan space. Source: Lourenço et al. 2019.



Limit equilibrium analysis with macro-blocks was used to assess the response of the building, following the kinematic approach (chap. 4). This method allows the evaluation of the horizontal action that activates the collapse mechanism, assuming the following: (a) no tensile capacity of the masonry, (b) infinite compressive capacity of the masonry, and (c) no sliding between the blocks. The hypothesized mechanism is given by a rotation of the entire wall around a hinge. A horizontal loading in the x positive direction of model 1 will result in the out-of-plane failure of the longitudinal wall. The characteristics of this failure mechanism depend on the quality of the connection between the walls. When a good connection between the perpendicular walls is ensured, the out-of-plane movement of the longitudinal wall will involve the stabilizing contribution of the transversal walls. The amount of this contribution depends on the geometric features and on the mechanical properties of the masonry. On the other hand, if a good connection is not guaranteed, the out-of-plane failure will involve only the longitudinal wall, with crack formation in the connection (Lourenço et al. 2019).

The compressive strength of masonry was considered for the definition of the position of the hinge. The distance of the hinge from the edge t can be determined by equation 4.20 (chap. 4), assuming a rectangular distribution of stresses.

If the material is continuous along the entire height, the failure should appear at the base, and the position of the hinge is ruled by the compressive capacity of the material. At Casa Arones, the wall is composed of a foundation and a wall of different materials, therefore both the level of the foundation and the level of the interface between the two materials should be verified. In fact, due to the lower compressive capacity of the adobe masonry, the hinge shifts inward to a larger extent, resulting in a more unfavorable configuration for this material (Lourenço et al. 2019).

Based on these considerations, four cases of out-of-plane mechanisms were considered (fig. 6.3). The first two cases consider no connection between the two walls with the hinge formation at the base (LA_1) or at the lowest adobe section (LA_2); the last two cases consider the contribution of the transversal wall, again with the hinge forming at the base (LA_3) and at the lowest adobe section (LA_4).

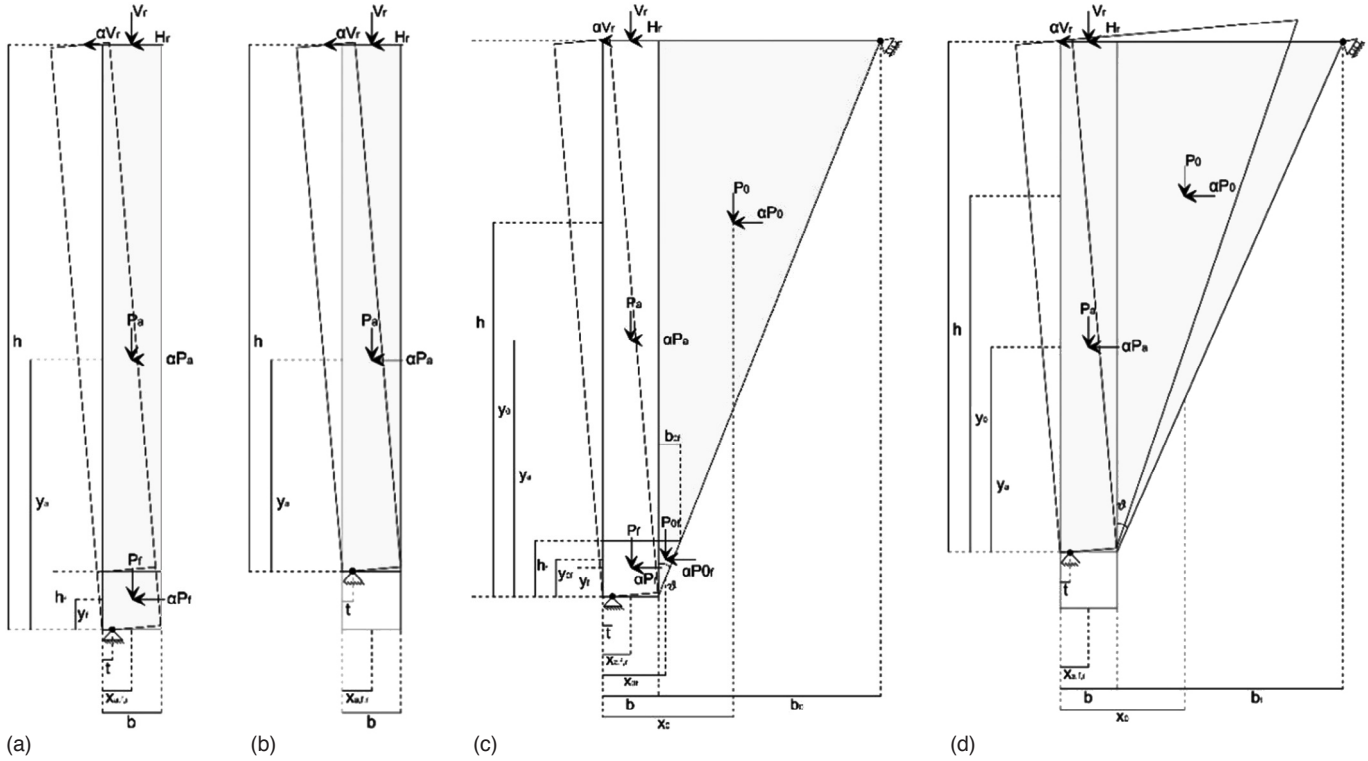


FIGURE 6.3. Four out-of-plane mechanisms considered in the macro-block analysis of the longitudinal wall at Casa Arones, Peru: (a) LA_1 has no connection between the two walls and a hinge formation at the foundation level; (b) LA_2 has no connection between walls and a hinge formation at the lowest adobe masonry section; (c) LA_3 has a connection and a hinge formation at the foundation level; and (d) LA_4 has a connection and a hinge formation at the lowest adobe masonry section. Source: Lourenço et al. 2019.

The multiplier a_0 was obtained applying the VWP. Because the kinematics is a simple rotation, the VWP is reduced to the equilibrium of the horizontal and vertical forces around the hinge (eq. 4.1, chap. 4). After the evaluation of the collapse multiplier a_0 , the corresponding seismic spectral acceleration a_0^* can be calculated according to equation 4.4 (chap. 4).

The results of the calculations for the four out-of-plane mechanisms evaluated are presented in terms of position of the hinge t and spectral acceleration of the activation of the mechanism, a_0^* (table 6.1). The maximum lateral load that can be applied to model 1 in the x direction is 0.02 g and 0.03 g in the models without connections between transversal walls. When a good connection is ensured, the capacity of the wall increases enormously, with a spectral acceleration of 0.16 g (fig. 6.4). The contribution of the transversal walls is fundamental in terms of capacity of the structure. It should be noted that the interlocking of the adobes is ruled by the low strength of the material, and therefore the adobe will break without providing the connection needed. To avoid this failure mechanism in such structures, additional elements should be inserted into the masonry in the form of stones or timber keys in the corners of walls.

FIGURE 6.4. Comparison between the capacities of the four mechanisms considered for model 1, Casa Arones, Peru, for a wall with a thickness of 1 m and a total height of 10 m. Source: Lourenço et al. 2019.

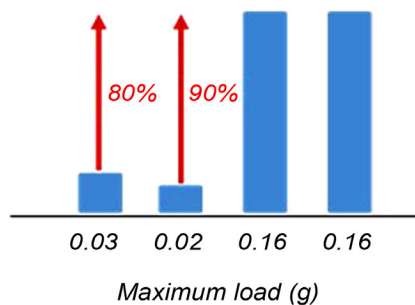


TABLE 6.1. Results of the limit equilibrium analysis for the four out-of-plane mechanisms, model 1, Casa Arones, Peru (Lourenço et al. 2019).

Model	t (m)	a_0^* (g)
LA_1	0.20	0.03
LA_2	0.24	0.02
LA_3	0.20	0.16
LA_4	0.24	0.16

Also of importance is the fact that this method of limit equilibrium analysis with macro-blocks, following the kinematic approach without the need for any software, is able to provide valuable information on the structural assessment of existing buildings and on the design of strengthening solutions. Steel ties could be added to the mechanism to assess the improvement of the overall seismic response of the structure.

Strengthening Proposal for Ica Cathedral, Peru

Ica Cathedral is an eighteenth-century church that was heavily damaged by the earthquakes that struck Peru in 2007 (see chaps. 1 and 5) and 2009. Considered representative of religious buildings erected in the country's coastal cities, the cathedral, along with Casa Arones, is one of four building prototypes studied as part of the SRP (Lourenço et al. 2019). The complex historic building is characterized by an external masonry envelope made of rubble stone, brick, and adobe, and an internal timber framing system constructed using the quincha technique.

The safety assessment of the cathedral in its current condition has been addressed (Lourenço et al. 2019; Ciocci, Sharma, and Lourenço 2018) and will not be covered here. Several analyses, including linear elastic, eigenvalue, nonlinear static under self-weight, pushover, and nonlinear dynamic loading, were performed. The results pointed out the need to address the most vulnerable regions of the structure identified by the pushover analyses; that is, the northwestern corner and other out-of-plane mechanisms (Lourenço et al. 2019). This section presents the proposed strengthening solutions.

A global strengthening of the structure is proposed guaranteeing the principles of minimum intervention and reversibility as well as the use of technologies that are easy to implement in future conservation and strengthening projects for similar constructions. Here, only the steel anchoring systems are considered to address the out-of-plane mechanism of the front facade by improving its connection with the internal timber structure. Limit analysis was used to assess the front facade under out-of-plane actions. Afterward, implementation of steel anchoring systems was carried out according to the criteria specified by Eurocode 3 (EN 1993-1-1 2005; EN 1993-1-8 2005) and the recommendations provided by Ciocci, Sharma, and Lourenço (2016).

Following the method described in chapter 4, the fired brick front facade was represented as an assembly of rigid bodies subjected to permanent actions and to horizontal inertial actions proportional to the mass through a seismic multiplier. The out-of-plane rotation of the front facade was considered, assuming no influence from the bell towers and accounting for the strengthening that already had been carried out on the pediment (fig. 6.5a). The mechanism was hypothesized as a simple rotation around a plastic hinge located at the point where the resulting compression force is applied. Compression was calculated assuming a triangular distribution of stresses and limiting the maximum stress in the most compressed edge to the value of compressive strength of fired brick masonry. This is likely to be a conservative approach, given the presence of the towers.

The load multiplier that induces the onset of rocking was calculated by simple rotational equilibrium of vertical and horizontal forces—self-weight and inertial forces, respectively. This calculation was 0.15 for the out-of-plane mechanism of the front facade. Since the obtained value of 0.24 g—calculated according to equation 4.10 (chap. 4) for the region of Ica—is lower than the demand, steel strengthening systems were proposed for the front facade.

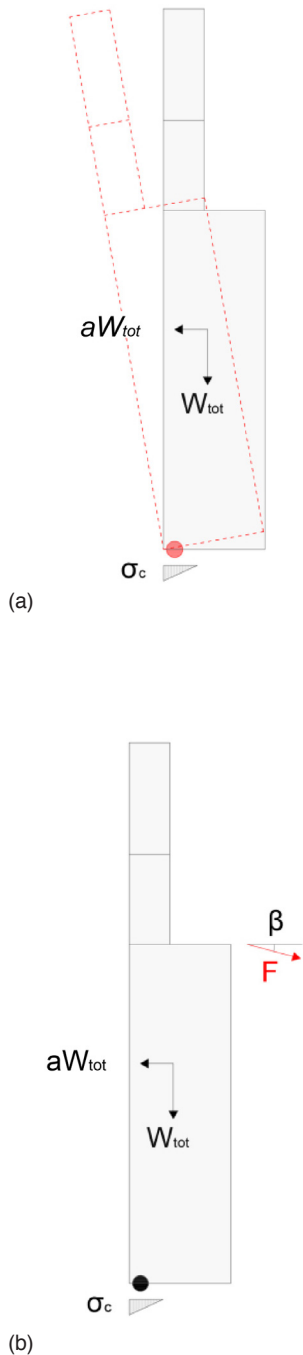


FIGURE 6.5. Failure mechanisms considered for Ica Cathedral, Peru: (a) out-of-plane mechanism of the front facade; and (b) failure mechanism of the strengthened front facade. Source: Ciocci, Sharma, and Lourenço 2016.

To calculate the minimum resisting action that must be provided by the strengthening system, limit analysis was applied assuming a new failure mechanism, as shown in figure 6.5b. The calculations were carried out assuming the angle β between the inclined strengthening ties and the horizontal plane equal to 10° , and the resisting action obtained was equal to 176 kN.

Assuming four steel anchoring systems—two for each pillar, located between the cathedral's choir loft and its lateral naves—each system must be designed to carry 44 kN. Each is composed of an external and internal steel anchoring system connected by steel ties through the thickness of the brick front facade. The external system consists of a square steel plate with stiffening elements that can be embedded for a maximum of about 0.12 m in the front facade. The internal system comprises steel profiles with bolts to assure connection with the internal timber structure. Elevation and plan for both systems are shown in figure 6.6.

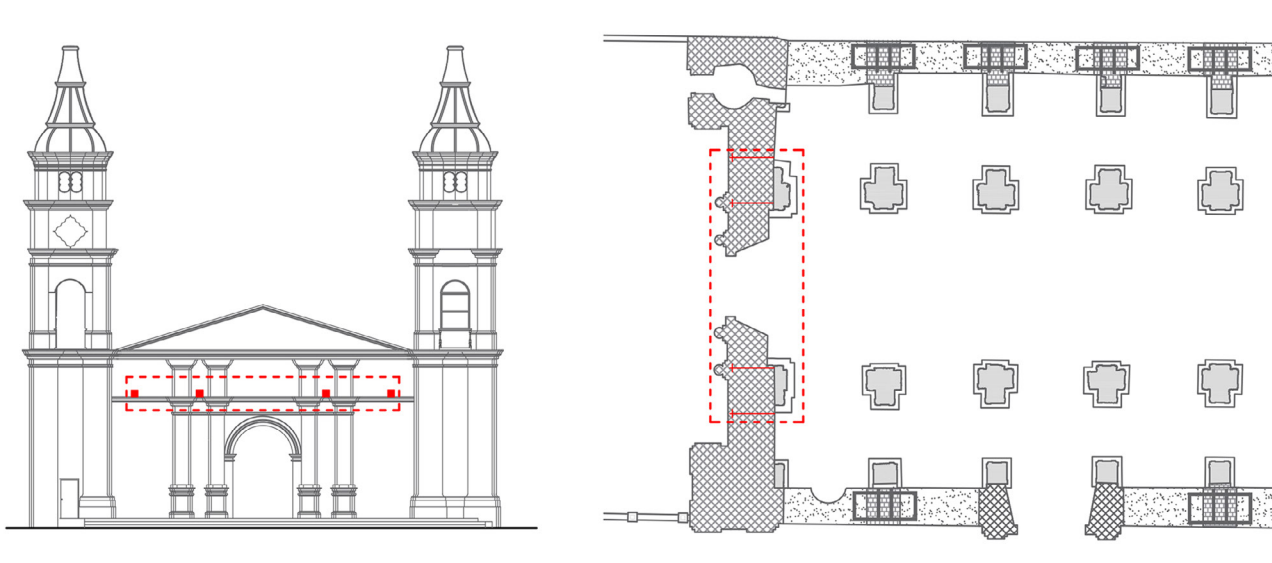


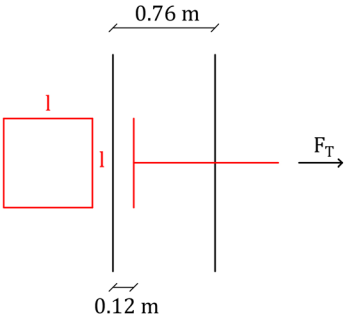
FIGURE 6.6. Elevation (left) and plan (right) of the steel anchoring systems for the front façade of Ica Cathedral, Peru; red dashed margins identify the location of proposed interventions, while continuous red lines identify the position of the steel anchoring system. Source: Ciocci, Sharma, and Lourenço 2016.

Design and verification of these steel elements were carried out according to Eurocode 3 (EN 1993-1-1 2005; EN 1993-1-8 2005). The pullout of steel plates due to tensile failure, as well as the shear failure of the masonry, the failure of the steel tie, and the crushing of masonry, was considered in the design of the external anchoring system. The diameter of the tie was defined considering the yielding of the steel according to the diagram in equation 6.1, where F_T is the force in the tie (44 kN), f_{yd} is the design value of the steel strength, and \varnothing is the diameter of the steel tie. Assuming a steel grade of S355 and $\gamma_m = 1.05$, f_{yd} is calculated to be equal to 338 MPa.

$$F_T = f_{yd} \cdot \pi \frac{\varnothing^2}{4} \Leftrightarrow \varnothing = \sqrt{\frac{4F_T}{\pi f_{yd}}} \quad (6.1)$$

$$\varnothing \geq 13 \text{ mm} \rightarrow \varnothing = 25 \text{ mm}$$

The dimensions of the steel plate were defined considering the crushing of the masonry (eq. 6.2), where f_{cd} is the design compressive capacity of brick masonry and l is the length of the squared plate. Assuming an average value of 1.70 MPa for the compressive strength of brick masonry (Ciocchi, Sharma, and Lourenço 2018), $FC = 1.0$, and $\gamma_m = 2.0$, f_{cd} is evaluated to be equal to 0.85 MPa.



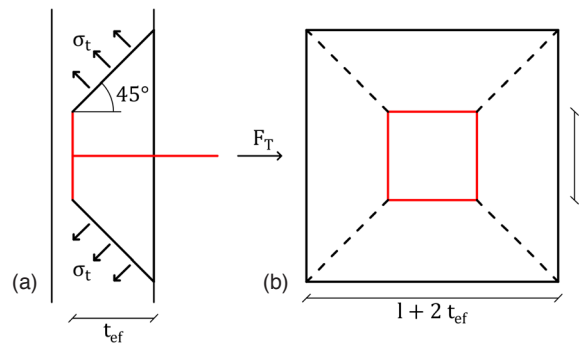
$$F_T \cdot f_{cd} \cdot l^2 \Leftrightarrow l = \sqrt{\frac{F_T}{f_{cd}}} \quad (6.2)$$

$$l \geq 0.23 \text{ m} \rightarrow l = 0.30 \text{ m}$$

Tensile failure of the masonry was verified by comparing the tensile stresses imposed by the plate and the steel tie with the design tensile strength of masonry. Figure 6.7 shows a diagram of the tensile failure considered and equation 6.3 shows the verification, where σ_t is the tensile stress imposed by the tie in the masonry, A_{ef} is the effective area of the tensile surface (corresponding to the four sides of the truncated pyramid), t_{ef} is the effective thickness of the wall (0.64 m), and f_{ctd} is the design tensile capacity of brick masonry. Assuming an average value of 0.1 MPa for the tensile strength of brick masonry (Ciocchi, Sharma, and Lourenço 2018), $FC = 1.0$, and $\gamma_m = 2.0$, f_{ctd} is calculated to be equal to 0.05 MPa.

FIGURE 6.7.

Schematic of the tensile failure of the masonry considered in the design of the steel tie for Ica Cathedral, Peru, in plan (a) and elevation (b) view.



$$\sigma_t \leq f_{ctd}$$

$$F_T = \frac{\sqrt{2}}{2} \sigma_t A_{ef} \Leftrightarrow \sigma_t = \sqrt{2} \frac{F_T}{A_{ef}} \quad (6.3)$$

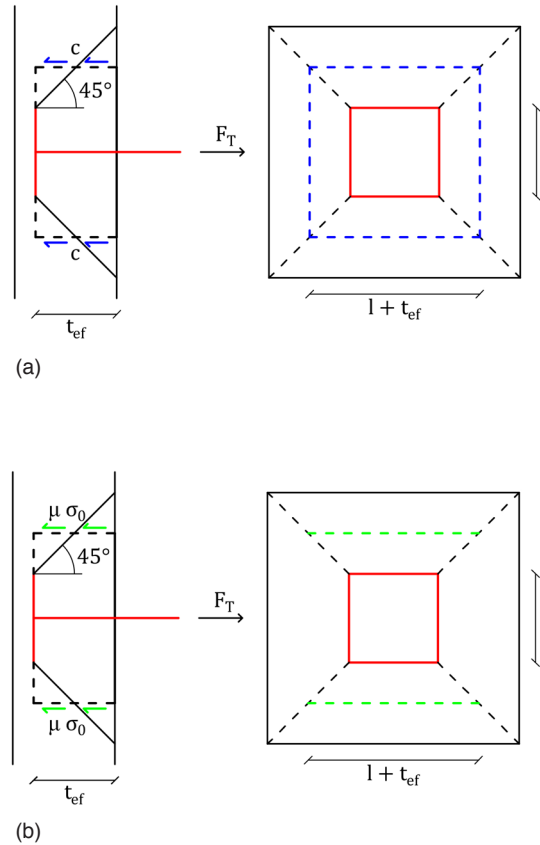
$$A_{ef} = 2\sqrt{2} \cdot t_{ef} (2l + 2t_{ef})$$

$$\sigma_t = 0.02 \text{ MPa} \leq 0.05 \text{ MPa} \rightarrow \text{OK!}$$

The shear failure of the masonry was verified considering both the cohesion and the friction at the middle plane of the truncated pyramid (fig. 6.8). Equation 6.4 shows the safety verification, where c is the cohesion of the masonry, μ is the friction coefficient (0.4), f_{vd0} is the design shear capacity of brick masonry in the absence of normal stresses (0.071 MPa), $A_{ef,c}$ is the effective area for the cohesion mechanism, $A_{ef,f}$ is the effective area for the fric-

FIGURE 6.8.

Schematic of the shear failure of the masonry considered in the design of the steel tie for Ica Cathedral, Peru: (a) cohesion mechanism; (b) friction mechanism.



tion mechanism (top and bottom surfaces only), and σ_0 is the normal stress due to the weight of the pediment (0.054 MPa):

$$c \leq f_{vd0}$$

$$F_T = c \cdot A_{ef,c} + \mu \cdot \sigma_0 \cdot A_{ef,f} \quad c = \frac{F_T - \mu \cdot \sigma_0 \cdot A_{ef,f}}{A_{ef,c}}$$

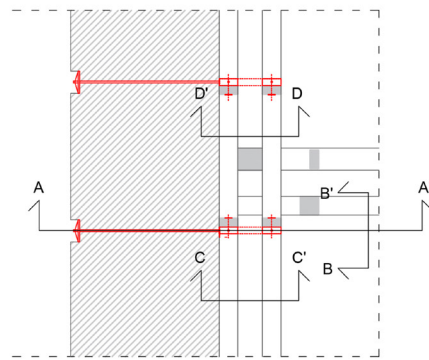
$$A_{ef,c} = 2t_{ef}(2l + 2t_{ef})$$

$$A_{ef,f} = 2t_{ef}(l + t_{ef})$$
(6.4)

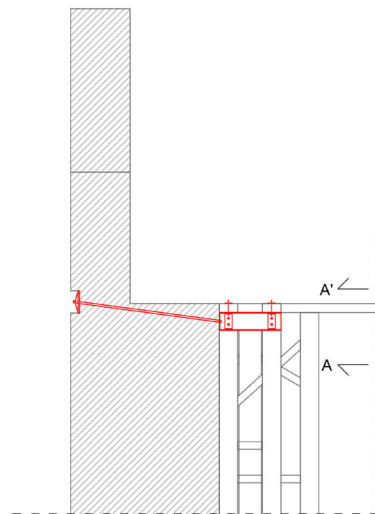
$$c = 0.007 \text{ MPa} \leq 0.071 \text{ MPa} \rightarrow \text{OK!}$$

Regarding the internal anchoring system, normal and tangential stresses were verified for the steel elements and bolts, and compression stresses perpendicular to the grain were checked to avoid the failure of timber under these steel elements. The elements of the final proposed solution are shown in figure 6.9. To implement this anchoring system, it is important to ensure the durability of these steel elements in resisting corrosion, as well as the proper tightening of bolts to prevent loosening under seismic action. In addition, injections of lime-based grout are recommended for filling the holes created to anchor the steel ties to the front facade (Ciocci, Sharma, and Lourenço 2016).

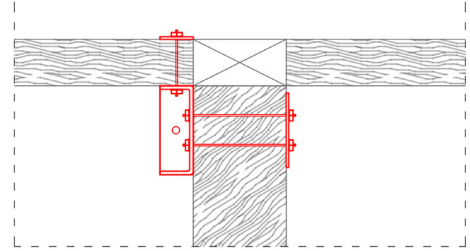
FIGURE 6.9. Elements (in red) of the internal steel anchoring system proposed for the front facade of Ica Cathedral, Peru. Source: Ciocci, Sharma, and Lourenço 2016.



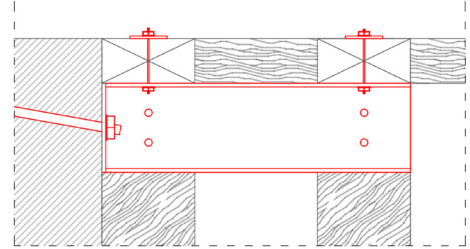
PLAN



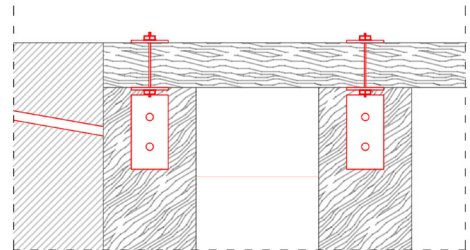
SECTION A - A'



SECTION B - B'



SECTION C - C'



SECTION D - D'



Conclusions and Recommendations

This publication is the final installment in a series on safety assessment of historic earthen sites as part of the Seismic Retrofitting Project (SRP) of the Getty Conservation Institute. It is intended to help engineering professionals whose work involves the assessment and analysis of historic earthen structures using simplified calculations.

The mechanical properties of masonry have a wide variation that depends mostly on properties of constituent materials (such as strength) and unit arrangement, shape, and dimension. Although there are normative documents with reference values for mechanical properties of masonry, in most cases historic earthen masonry is less prescribed. Still, from the available literature it is possible to provide sound estimates of the mechanical properties to be adopted, as provided in this publication. Also discussed here is a qualitative method in the form of a quality index, using only visual inspection (without the need for destructive tests), which can be related to the mechanical properties. This method is adequate only for brick and stone masonry, which often appears in earthen construction.

A blueprint assessment approach described in this document aims at providing a simpler, fast, and low-cost analysis, being based on a simplified geometric approach that allows immediate screening of the large number of buildings at risk. The objective is to adopt simple indexes (a numerical indicator deduced from observations and used as an indicator of a process or condition) related to geometric data as a first (very fast) screening technique to help prioritize further studies with respect to seismic vulnerability. It is expected that the geometric indexes could detect cases of serious vulnerability and can define priority of study.

The limit macro-block assessment allows verifications of damage and collapse (in-plane and out-of-plane) with reference to local mechanisms by means of limit equilibrium analysis, based on a kinematics approach that depends on the selection of the collapse mechanism and the evaluation of the horizontal forces that activate that kinematic mechanism. This method appears to be a valid solution when simplified assessment tools are needed, allowing verification of safety in terms of both linear kinematic analysis (force control) and nonlinear kinematic analysis (displacement control).

Simplified finite element analysis (FEA), based on linear static analysis and response spectrum analysis, is still a useful tool for professionals as shown in chapter 5. FEA contributes to the assessment of the overall behavior of the masonry structure, as well as the assessment of the effectiveness of strengthening solutions. Safety considerations can be made using areas of stress concentration and modes of vibration.

Often, the assessment of a masonry structure determines that the actual state of the building is insufficient, requiring interventions in terms of both repair and retrofitting/strengthening actions. These actions fall into two main categories: (a) interventions aimed at improving the connections between the elements of the building, and (b) interventions aimed at avoiding disintegration of the masonry elements. Best practices interventions should guarantee the principles of minimum intervention and efficiency.

As the final outcome of the SRP, a series of guidelines will be developed. These guidelines will include a number of appropriate techniques for repair and retrofitting as part of a publication from the Ministry of Culture of Peru in the near future.

The application examples of the various analysis methods given in this document highlight the possibilities for the structural assessment of masonry buildings, the design of strengthening elements, and the combination of different strengthening techniques into a complete proposal.

As its final objective, this publication is intended to guide professionals in performing the assessment of existing buildings and the design of strengthening solutions using simplified methods of analysis. Other publications in this series address the complex task of using advanced FEA for historic earthen structures and provide detailed examples of modeling results.

References

- Angelillo, M., P. B. Lourenço, and G. Milani. 2014. Masonry behavior and modeling. In *Mechanics of Masonry Structures*, edited by M. Angelillo, 1–26. CISM International Centre for Mechanical Sciences 551. Vienna: Springer.
- ASCE 41-06. 2006. *Seismic Rehabilitation of Existing Buildings*. Reston, VA: American Society of Civil Engineers.
- ATC-20. 1989. *Procedures for Post-Earthquake Safety Evaluation of Buildings*. Redwood City, CA: Applied Technology Council.
- ATC-20-2. 1995. *Addendum to the ATC-20 Post-Earthquake Building Safety Procedures*. Redwood City, CA: Applied Technology Council.
- Borri, A., G. Castori, and M. Corradi. 2014. Determination of shear strength of masonry panels through different tests. *International Journal of Architectural Heritage* 8: 913–27.
- Borri, A., G. Castori, M. Corradi, and E. Speranzini. 2011. Shear behavior of unreinforced and reinforced masonry panels subjected to in-situ diagonal compression tests. *Construction and Building Materials* 25 (12): 4403–14.
- Borri, A., M. Corradi, G. Castori, and A. De Maria. 2015. A method for the analysis and classification of historic masonry. *Bulletin of Earthquake Engineering* 13: 2647–65.
- Borri, A., and A. De Maria. 2009. L'indice di Qualità Muraria (IQM): Evoluzione ed Applicazione nell'Ambito delle Norme Tecniche per le Costruzioni del 2008. In *XIII Convegno ANIDIS "L'ingegneria Sismica in Italia,"* Bologna: ANIDIS.
- Cancino, C. 2011. *Damage Assessment of Historic Earthen Buildings after the August 15, 2007, Pisco Earthquake*. Los Angeles: Getty Conservation Institute.
- Cancino, C., S. Lardinois, D. D'Ayala, C. F. Ferreira, D. T. Dávila, E. V. Meléndez, and L. V. Santamato. 2012. *Seismic Retrofitting Project: Assessment of Prototype Buildings*. Los Angeles: Getty Conservation Institute.
- Casapulla, C., L. Giresini, and P. B. Lourenço. 2017. Rocking and kinematic approaches for rigid block analysis of masonry walls: State of the art and recent developments. *Buildings* 7 (3): 69–87.
- Chiostrini, S., L. Galano, and A. Vignoli. 2003. In situ shear and compression tests in ancient stone masonry walls of Tuscany, Italy. *Journal of Testing and Evaluation* 31 (4): 289–304.
- Ciocchi, M. P., S. Sharma, and P. B. Lourenço. 2016. *Assessment of the Strengthening Proposal for Ica Cathedral, Peru*. Report 2016-DEC/E-11. Guimarães: TecMinho – University of Minho.
- Ciocchi, M. P., S. Sharma, and P. B. Lourenço. 2018. Engineering simulations of a super-complex cultural heritage building: Ica Cathedral in Peru. *Meccanica* 53 (7): 1931–58.
- Corradi, M., A. Borri, G. Castori, and R. Sisti. 2014. Shear strengthening of wall panels through jacketing with cement mortar reinforced by GFRP grids. *Composite part B* 64 (6): 33–42.
- CRSMN. 2003. *Canterbury Regional Strong-Motion Network*. Christchurch: Canterbury Seismic Instruments. <http://www.csi.net.nz/>.

- DPCM February 9. 2011. *Valutazione e riduzione del rischio sismico del patrimonio culturale con riferimento alle norme tecniche per le costruzioni di cui al Decreto Ministeriale 14 gennaio 2008*. Rome: Presidenza del Consiglio dei Ministri.
- EC6 (EN 1996-1-1). 2005. *Eurocode 6: Design of Masonry Structures. Part 1-1: General Rules for Reinforced and Unreinforced Masonry Structures*. Brussels: European Committee for Standardization.
- EC8 (EN 1998-1). 2004. *Eurocode 8: Design of Structures for Earthquake Resistance. Part 1: General Rules, Seismic Actions and Rules for Buildings (EN 1998-1)*. Brussels: European Committee for Standardization.
- EN 1993-1-1. 2005. *Eurocode 3: Design of Steel Structures. Part 1-1: General Rules and Rules for Buildings*. Brussels: European Committee for Standardization.
- EN 1993-1-8. 2005. *Eurocode 3: Design of Steel Structures. Part 1-8: Design of Joints*. Brussels: European Committee for Standardization.
- Giuffrè, A. 1999. *Lecture sulla meccanica delle murature storiche*. Rome: Kappa.
- Hardy, M., C. Cancino, and G. Ostergren, eds. 2009. *Proceedings of the Getty Seismic Adobe Project 2006 Colloquium: Getty Center, Los Angeles, April 11–13, 2006*. Los Angeles: Getty Conservation Institute.
- IS 13827. 1993. *Improving Earthquake Resistance of Earthen Buildings: Guidelines*. New Delhi: Bureau of Indian Standards.
- Karanikoloudis, G., and P. B. Lourenço. 2015. *Analysis of Local Collapse Mechanisms and Design of Buttresses in Kuño Tambo Church, Peru*. Report 2015-DEC/E- 44. Guimarães: TecMinho – University of Minho.
- Karanikoloudis, G., and P. B. Lourenço. 2018. Structural assessment and seismic vulnerability of earthen historic structures. Application of sophisticated numerical and simple analytical models. *Journal of Engineering Structures* 160: 488–509.
- Karanikoloudis, G., and P. B. Lourenço. 2020. *Experimental In situ Testing and Visual Inspection of a Retrofitted Adobe Historic Structure, within the Getty Seismic Retrofitting Project. The Church of Kuñotambo, in Peru*. Report 2020-DEC/E-03. Guimarães: TecMinho – University of Minho.
- Lourenço, P. B., F. Greco, A. Barontini, M. P. Ciocci, and G. Karanikoloudis. 2019. *Seismic Retrofitting Project: Modeling of Prototype Buildings*. Los Angeles: Getty Conservation Institute; Guimarães: TecMinho – University of Minho.
- Lourenço, P. B., D. V. Oliveira, J. C. Leite, J. M. Ingham, C. Modena, and F. da Porto. 2013. Simplified indexes for the seismic assessment of masonry buildings: International database and validation. *Engineering Failure Analysis* 34: 585–605.
- Lourenço, P. B., and J. M. Pereira. 2018. *Seismic Retrofitting Project: Recommendations for Advanced Modeling of Historic Earthen Sites*. Los Angeles: Getty Conservation Institute; Guimarães: TecMinho – University of Minho.
- Lourenço, P. B., and J. A. Roque. 2006. Simplified indexes for the seismic vulnerability of ancient masonry buildings. *Construction and Building Materials* 20: 200–208.
- Magenes, G., and A. Penna. 2009. Existing Masonry Buildings: General Code Issues and Methods of Analysis and Assessment. In *Eurocode 8 Perspectives from the Italian Standpoint Workshop*, edited by E. Cosenza. Naples: Doppiavoce.
- Mastrodicasa, S. 1978. *Dissesti statici delle strutture edilizie: Diagnosi, consolidamento, istituzioni teoriche*. Milan: Hoepli.
- Meli, R. 1998. *Structural Engineering of Historical Buildings*. Mexico City: Fundación ICA.
- NTC. 2018. *Norme tecniche per le costruzioni. With Circolare from January 21, no. 7 (2019)*. Rome: Ministero delle Infrastrutture e dei Trasporti.

- NTE-0.30. 2018. *Modifican la norma técnica e.030 diseño sismorresistente del reglamento nacional de edificaciones*. Lima: Ministerio de Vivienda y Saneamiento.
- NZSEE. 2009. *Building Safety Evaluation during a State of Emergency: Guidelines for Territorial Authorities*. Wellington: New Zealand Society for Earthquake Engineering.
- NZSEE. 2017. *The Seismic Assessment of Existing Buildings: Technical Guidelines for Engineering Assessment*. Wellington: New Zealand Society for Earthquake Engineering.
- OPCM 3431. 2005. Ordinanza 3431. *Norme tecniche per il progetto, la valutazione e l'adeguamento sismico degli edifici*. Rome: Presidenza del Consiglio dei Ministri.
- Regione dell'Umbria. 2003. *Norme tecniche per la progettazione degli interventi e la realizzazione delle opere di cui alla L.R. 23.10.2002 no. 18 finalizzate alla riduzione della vulnerabilità sísmica*. Perugia: Regione dell'Umbria.
- Sheppard, P. F. 1985. In-situ test of the shear strength and deformability of an 18th century stone-and-brick masonry wall. In *Proceedings of the 7th International Brick/Block Masonry Conference*, Melbourne, Australia, vol. 1, 149–60.
- Tolles, E. L., E. E. Kimbro, and W. S. Ginell. 2002. *Planning and Engineering Guidelines for the Seismic Retrofitting of Historic Adobe Structures*. Los Angeles: Getty Conservation Institute.
- Tomazevic, M. 1999. *Earthquake-Resistant Design of Masonry Buildings*. London: Imperial College Press.
- Vitruvius, I. D. Rowland, T. N. Howe, M. Dewar. 2005. *Vitruvius: Ten books on architecture*. Cambridge: Cambridge University Press.
- Zilch, K., and M. Schatz. 2001. *Masonry Construction Manual*. Munich: Institute fur International Architektur documentation GmbH.

